Université de Sherbrooke

Monte Carlo Simulation of the Radiolysis of Water by Fast Neutrons at Elevated Temperatures up to 350 ^{o}C

Par
Sofia Loren BUTARBUTAR
Département de médecine nucléaire et radiobiologie

Mémoire présenté à la Faculté de médecine et des sciences de la santé
en vue de l'obtention du grade de maître ès sciences (M. Sc.)
en sciences des radiations et imagerie biomédicale

Sherbrooke, Québec, Canada
Septembre, 2014

Jury

Pr Abdelouahed Khalil	*Examinateur*, Département de médecine, Service de gériatrie, Faculté de médecine et des sciences de la santé
Pr M'hamed Bentourkia	*Examinateur*, Département de médecine nucléaire et radiobiologie, Faculté de médecine et des sciences de la santé
P^{r} Jean-Paul Jay-Gerin	*Directeur de recherche*, Département de médecine nucléaire et de radiobiologie, Faculté de médecine et des sciences de la santé

RESUME

SIMULATION MONTE CARLO DE LA RADIOLYSE DE L'EAU PAR DES NEUTRONS RAPIDES À TEMPÉRATURES ÉLEVÉES ALLANT JUSQU'À 350 °C

Sofia Loren BUTARBUTAR
Département de médecine nucléaire et radiobiologie

Mémoire présenté à la Faculté de médecine et des sciences de la santé en vue de l'obtention du diplôme de maître ès sciences (M.Sc.) en sciences des radiations et imagerie biomédicale, Faculté de médecine et des sciences de la santé, Université de Sherbrooke, Sherbrooke, Québec, Canada, J1H 5N4

Le contrôle de la chimie de l'eau dans un réacteur nucléaire refroidi à l'eau nécessite une compréhension détaillée des effets de la radiolyse de l'eau afin de limiter la corrosion et la dégradation des matériaux par oxydation générée par les produits de cette radiolyse. Toutefois, la mesure directe de la chimie dans le cœur des réacteurs est extrêmement difficile, sinon impossible, en raison des conditions extrêmes de haute température et haute pression, et les champs d'irradiation mixtes neutrons/γ, qui ne sont pas compatibles avec l'instrumentation chimique normale. Pour ces raisons, des modèles théoriques et des simulations sur ordinateur sont essentielles pour la prédiction de la chimie sous rayonnement de l'eau de refroidissement dans le cœur et son impact sur les matériaux. Dans ce travail, des simulations Monte Carlo ont été utilisées pour calculer les rendements des principales espèces (e^-_{aq}, $H^\bullet$, H_2, $^\bullet OH$ et H_2O_2) formées lors de la radiolyse de l'eau liquide neutre par des neutrons mono-énergétiques de 2 MeV à des températures entre 25 et 350 °C. Le choix des neutrons de 2 MeV comme énergie d'intérêt est représentatif du flux de neutrons rapides dans un réacteur. Pour l'eau légère, la contribution la plus significative à la radiolyse vient des quatre premières collisions des neutrons qui produisent, dans la majorité des cas, des protons avec des énergies de recul de ~1.264, 0.465, 0.171 et 0.063 MeV et des transferts d'énergie linéique (TEL) moyens respectivement de ~22, 43, 69 et 76 keV/μm. Par ailleurs, nous avons négligé les effets des radiations dus aux ions de recul de l'oxygène. Les rendements moyens finaux peuvent alors être estimés comme étant la somme des rendements résultant de l'action de ces protons après pondérations en fonction de l'énergie déposée. Les rendements ont été calculés à 10^{-7}, 10^{-6} et 10^{-5} s. Les valeurs obtenues sont en accord avec les données expérimentales disponibles. En comparant nos résultats avec les données obtenues pour les rayonnements à faible TEL (rayons γ de ^{60}Co ou électrons rapides), nos rendements calculés pour les neutrons rapides ont montré une dépendance en température essentiellement similaire, mais avec des valeurs plus faibles pour les rendements en radicaux libres et des valeurs plus élevées pour les rendements moléculaires. Nous avons également utilisé les simulations Monte Carlo pour étudier l'existence de la chute rapide de la constante de vitesse de réaction de l'électron hydraté (e^-_{aq}) sur lui-même – l'une des principales sources de formation de H_2 – au-dessus de 150 °C. Cette dépendance en température a été observée expérimentalement en milieu *alcalin* par divers auteurs, mais jamais en milieu neutre. Lorsque cette baisse de la constante de vitesse d'auto-réaction de e^-_{aq} est incluse dans nos codes de simulation, tant pour des rayonnements de bas TEL (grappes isolés) que de haut TEL (trajectoires cylindriques), $g(H_2)$ montre une discontinuité marquée à la baisse à ~150°C, *ce qui n'est pas observée expérimentalement*. Les conséquences de la présence de cette discontinuité dans le rendement en H_2 pour les rayonnements à bas et haut TEL sont discutées. Enfin, nous avons tenté d'expliquer l'augmentation – considérée comme anormale – du rendement en H_2 en fonction de la température au-dessus de 200 °C par l'intervention de la réaction des atomes $H^\bullet$ avec l'eau, préalablement proposée par Swiatła-Wojcik et Buxton en 2005. La constante de vitesse de cette réaction est toujours controversée.

Mots-clés: radiolyse de l'eau, neutrons rapides, protons de recul, transfert d'énergie linéaire (TEL), haute température, rendements de radiolyse, auto-réaction de l'électron hydraté, constante de vitesse, rendement de H_2, simulation Monte Carlo.

ABSTRACT

MONTE CARLO SIMULATION OF THE RADIOLYSIS OF WATER BY FAST NEUTRONS AT ELEVATED TEMPERATURES UP TO 350 °C

Sofia Loren BUTARBUTAR
Département de médecine nucléaire et radiobiologie

Thesis presented at Faculty of Medicine and Health Sciences in order to obtain the Master degree of Sciences (M.Sc.) in Radiation Sciences and Biomedical Imaging, Faculty of Medicine and Health Sciences, Université de Sherbrooke, Sherbrooke, Québec, Canada, J1H 5N4

Controlling the water chemistry in a water-cooled nuclear power reactor requires understanding and mitigating the effects of water radiolysis to limit the corrosion and degradation of materials by oxidizing radiolysis products. However, direct measurement of the chemistry in reactor cores is extremely difficult due to the extreme conditions of high temperature, pressure, and mixed neutron/γ-radiation fields, which are not compatible with normal chemical instrumentation. For these reasons, theoretical models and computer simulations are essential for predicting the detailed radiation chemistry of the cooling water in the core and the impact on materials. Monte Carlo simulations were used to calculate the yields for the primary species (e^-_{aq}, $H^\bullet$, H_2, $^\bullet OH$, and H_2O_2) formed from the radiolysis of neutral liquid water by mono-energetic 2-MeV neutrons and the mechanisms involved at temperatures between 25 and 350 °C. In this work, we chose 2-MeV neutron as our energy of interest since it is known as representative of a fast neutron flux in a nuclear reactor. For light water, for that chosen energy, the most significant contribution to the radiolysis comes from the first four neutron collisions that generate mostly ejected protons with energies of ~1.264, 0.465, 0.171, and 0.063 MeV, which had, at 25 °C, mean linear energy transfers (LETs) of ~22, 43, 69, and 76 keV/μm, respectively. In this work, we simply neglected the radiation effects due to oxygen ion recoils. The average final fast neutron yields could be estimated as the sum of the yields for these protons after allowance was made for the appropriate weightings (by using the Eq (2) in Chapter 4) according to their deposited energy. Yields were calculated at 10^{-7}, 10^{-6} and 10^{-5} s. Our computed yield agreed reasonably well with the available experimental data. By comparing our results with data obtained for low-LET radiation (^{60}Co γ-rays or fast electrons), our computed yields for fast neutron radiation showed essentially similar temperature dependences over the range of temperature studied, but with lower values for yields of free radicals and higher values for molecular yields. In this work, we also used our Monte Carlo simulation to investigate the existence of drop of hydrated electron (e^-_{aq}) self-reaction rate constant at 150 °C. One of the main sources of H_2 formation is the self-reaction of hydrated electrons. The temperature dependence of the rate constant of this reaction (k_1), measured under *alkaline* conditions, reveals that the rate constant drops abruptly above ~150 °C. However, when this drop in the e^-_{aq} self-reaction rate constant is included in our code for low (isolated spurs) and high (cylindrical tracks) linear energy transfer (LET), $g(H_2)$ shows a marked downward discontinuity at ~150 °C which is *not* observed experimentally. The consequences of the presence of this discontinuity in H_2 yield for both low and high LET radiation are discussed. Another reaction that might explain the anomalous increasing of H_2 yield with temperature is the reaction of $H^\bullet$ atoms with water previously proposed by Swiatla-Wojcik and Buxton (2005) whose rate constant is still in controversial.

Keywords: Water radiolysis, fast neutrons, recoil protons, linear energy transfer (LET), high temperature, radiolytic yields, self-reaction of the hydrated electron, rate constant, yield of H_2, Monte Carlo.

TABLE OF CONTENTS

LIST OF FIGURES

Chapter I

Chapter 3 – Article No. 1

Chapter 4 – Article No. 2

average LET: 40 keV/μm), *(14)* (●) (2-MeV neutron *G*-values estimated from the ~23 MeV $^{2}H^{+}$ and 157 MeV $^{7}Li^{3+}$ ion radiolysis of water using a weighting procedure), *(1, 25-28)* (■) (from combined measurements and computer modeling; irradiations carried out using the YAYOI fast-neutron source reactor at the University of Tokyo, with an average energy for fast neutrons of ~0.8 MeV), *(29)* (◊), *(30)* (□), *(31)* (▲) (mean *G*-values from different research groups calculated by disregarding the highest and lowest value for each species; according to the author, these values are probably correct within about 25%), and *(32)* (Δ). The purple dash-dot lines show the fast neutron *G*-values estimated in *(10)* for natural uranium (for which most of the in-reactor fast neutron flux spectrum falls into the 0.5 to 6 MeV energy range with a peak of about 2 MeV). The olive dash-dot-dot lines show the *G*-values for 2-MeV neutron radiolysis calculated by Swiatla-Wojcik and Buxton *(15)* at 10^{-6} s after the ionization event. The primary (or "escape") yields for the low-LET (~0.3 keV/μm) radiolysis of water *(18)* obtained using our previously calculated spur lifetimes between 25 and 350 °C *(33)* are also shown (blue dotted lines) for the sake of comparison. The reaction of the $H^{\bullet}$ atom with water was assumed to follow an Arrhenius temperature dependence over the 25-350 °C range studied, with a rate constant of ~4.6 × $10^{-5}M^{-1}$ s^{-1} at 25 °C *(10)* and $10^{4}M^{-1}$ s^{-1} at 300 °C, in agreement with recent muon spin spectroscopy experiments using muonium as an analogue of a hydrogen atom *(34)*.

Chapter 5

temperature in the range of 25-350 °C: (a) $G(e^-_{aq})$, (b) $G(^{\bullet}OH)$, (c) $G(H^{\bullet})$, (d) $G(H_2O_2)$, and (e) $G(H_2)$. Our simulated results, obtained at 10^{-7}, 10^{-6} and 10^{-5} s based on the radiation effects in 1.264, 0.465, 0.171, and 0.063 MeV recoil proton tracks, are shown as solid, dashed and dotted lines, respectively. To distinguish between one reaction and another reaction, we lead the eyes by matching the color of lines where the reactions equations belong to. The reactions are laid above zero value correspond to reactions that form species while under zero value correspond to the decay of species.

LIST OF TABLES

LIST OF ABBREVIATIONS

σ	Cross section
A	Mass number of nucleus
D	Diffusion coefficient
DEA	Dissociative electron attachment
DNA	Deoxyribonucleic acid
$\mathbf{e^-_{aq}}$	Hydrated electron
eV	Electronvolts
$\mathbf{E_0}$	Initial neutron kinetic energy
$\mathbf{E_n}$	Average energy of neutron after n collision
Ep	Energy of proton
$\boldsymbol{G_x}$ **or** ***g*****(X)**	Primary yield of the radiolytic species X
G**(X)**	Experimental 100-eV yield of the final product X
IRT	Independent reaction times
k	Reaction rate constant
keV	Kilo-electronvolts
LET	Linear energy transfer
MC	Monte-Carlo
MeV	Mega-electronvolts
molec./100 eV	Molecule/100 eV
Z	Atomic number

1. INTRODUCTION

Radiation chemistry is a mature branch of radiation science which is continually evolving and finding wider applications. This is particularly apparent in the study of the roles of free radicals in biology generally, and radiation biology specifically. The irradiation of water by fast neutrons is relevant to both radiation biology and nuclear technology. In radiation biology, where water is a major constituent of living cells, representing of about 70%-85% water by weight, fast neutrons produce high-LET radiations which can be used for treating cancer efficiently. In nuclear technology, fast neutrons (produced from fission process) decompose the water, which are used both as a moderator and as a heat transport medium circulating around the reactor core at operating temperatures ~ 250-310 ºC, results in radiolysis of water form radiolytic species (such as $^{\bullet}OH$, H_2O_2, O_2) which furthermore can interact with reactor components material. Hence, to suppress that effect, it is important to know how the radiation (i.e., fast neutrons) interacts with water and what the posterior products according to the quality of radiation (LET) and the irradiation conditions.

From the theoretical point of view, stochastic simulation methods employing Monte Carlo techniques have been used successfully to model the complex sequence of events that are produced by the interaction of ionizing radiation with pure liquid water. These simulation methods have permitted detailed studies of the relationship between track structure and radiation-induced chemical change. Monte Carlo code can model the entire water radiolysis process to simulate the primary interactions and to describe the fast kinetics of reactive radicals and ions as a function of the linear energy transfer (LET) of the ionizing radiation, pH, and temperature. For this reason Monte Carlo can be used to model the radiolysis of cooling water with mixed radiation filed in the reactor core such as neutrons, γ-rays, and fast electrons. It is well-known that experiment in and around reactor core are extremely difficult to perform, due to the high temperatures, high pressures and mixed radiation fields, thus computer simulations in this condition are an important investigation route to predict the detailed of radiation chemistry in the nuclear reactor core and the consequences to the reactor component materials.

In this work, Monte Carlo simulations were used to determine the radiolytic species yields (or *G*-values) for the radiolysis of pure liquid water at elevated temperature (25-350 ^{o}C) by high-LET fast neutrons radiation.

1.1 Interaction of ionizing radiation with matter

Ionizing radiation is composed of energetic particles and electromagnetic radiations that can cause direct or indirect ionization of a medium, by ejecting an electron if the energy is sufficient enough, from an atom, and leave a residual positive ion. However, if the energy of the ionization radiation is not sufficient enough to knock out an electron from its atom, the atom can be excited to the higher energy levels (see, for example: EVANS, 1955; ANDERSON, 1984; IAEA-TECDOC-799, 1995; MOZUMDER, 1999; TOBUREN, 2004). Directly ionizing radiations can ionize matter through the Coulomb interactions. They are fast moving charged particles such as electrons, protons, α-particles, stripped nuclei, or fission fragments. Indirectly ionizing radiations can secondarily ionize matter. They are electrically neutral; this includes energetic electromagnetic radiations such as X- or γ-rays or neutrons. The type of interaction of photons with matter can be classified into Compton Effect, photoelectric effect and pairs production (if the energy of incident photon energy is greater than 1.022 MeV). Neutrons are heavy-neutral particles, they interact primarily with matter through elastic nuclear scattering (it means that total kinetic energy of the neutron and nucleus is unchanged by the interaction) resulting in the production of energetic ejected protons or other positively charged nuclei (ions), characteristic of the irradiated medium, which can ionize and excite molecules along their paths. Regardless of the type of ionizing radiation, the final common result in all modes of absorption of ionizing radiation is thus the formation of tracks of physical energy-loss events in the form of ionization and excitation processes and in a geometrical pattern that depends on the type of involved radiation.

If the ejected electrons in the ionization event possess sufficient energy, they could further ionize one or more other molecules of the medium. According to this fact, the primary high-energy electron can produce a large number (~4×10^4 by a 1 MeV particle) of secondary electrons along its track as it gradually slows down (ICRU REPORT 31, 1979).

Electrons can lose their energy up to a half of their initial energy in individual ionizing collisions (PODGORSAK, 2006). Mostly these secondary electrons have low kinetic energies with a distribution that lies essentially below 100 eV, and a most probable energy below 10 eV (LAVERNE and PIMBLOTT, 1995; SANCHE, 2002; AUTSAVAPROMPORN, 2006). In most cases, they lose all their excess energy by multiple quasi-elastic (i.e., elastic plus phonon excitations) and inelastic interactions with their environment, including ionizations and/or excitations of electronic, intramolecular vibrational or rotational modes of the target molecules (MICHAUD *et al.*, 2003), and quickly reach thermal equilibrium (i.e., they are "thermalized") and then hydrated. Determining exactly which of these competing interaction types will take place is a complex function of the target medium and the energy range of the incident electron. By definition, a measure of the probability that any particular one of these interactions will occur is called the "cross section" (expressed in units of area) for that particular interaction type (see, for example: JOACHAIN, 1975). The total cross section σ, summed over all considered individual processes i, is used to determine the distance to the next interaction, and the relative contributions σ_i to σ are used to determine the type of interaction. Actually, the mean distance between two consecutive interactions or "mean free path" λ is defined by

$$\lambda = \frac{1}{N\sigma}, \qquad (1)$$

where N is the number of atoms or molecules per unit volume, and

$$\sigma = \sum_i \sigma_i \qquad (2)$$

In a dilute aqueous environment, thermalized electrons undergo trapping and hydration in quick succession (within ~10^{-12} s) as a result of the water electric dipoles rotating under the influence of the negative charge (BERNAS *et al.*, 1996). In course of thermalization, electrons that have kinetic energies lower than the first electronic excitation threshold of the medium, the so-called "subexcitation" electrons (PLATZMAN, 1955) may lead into prompt geminate ion recombination (FREEMAN, 1987) or may attach into the water surrounding. The last event yields in the production of energetic (~1-5 eV) anion

fragments via formation of dissociative negative ion states (resonances) (i.e., dissociative electron attachment, or DEA) (CHRISTOPHOROU *et al.*, 1984; BASS and SANCHE, 2003).

As a consequence of the energy gained by the medium which usually occurs within a few picoseconds, a sequence of very fast reactions and molecular rearrangements lead to the formation of new, highly nonhomogeneously distributed chemical species in the system, such as charged and/or neutral molecular fragments, reactive free radicals, and other excited chemical intermediates. The trail of the initial physical events, along with the chemical species, is generally referred to as the track of a charged particle, and its overall detailed spatial distribution, including contributions from secondary electrons, is commonly known as "track structure" (see for example: PARETZKE, 1987; MAGEE and CHATTERJEE, 1987; KRAFT and KRÄMER, 1993; PARETZKE *et al.*, 1995; MOZUMDER, 1999; LAVERNE, 2000, 2004). Any radiation induced chemistry is dependent on both the track structure and the time that the chemistry occurs in the evolution of the track. The initial formation of the track is governed by the physics of the energy deposition by the incident ion and the transport of that energy by secondary electrons.

1.2 Proton tracks structure in liquid water

1.2.1 Track structure in radiation chemistry and radiobiology

The distribution of spatial of the energy deposition events of a charged particle (e.g., proton) and their geometrical dispositions produced tracks. Track structure is a new tool to study the mechanisms of radiation effects. This charged particle loses its energy by Columbic interaction with the electrons of the medium. The amount of energy transfer by the charged particle into the matter is called the linear energy transfer (LET). Moreover, track-structure effects are usually called "LET effects" as most of the early studies used this parameter to characterize the different radiation chemical yields (or "*g*-values") for various irradiating ions in liquid water. However, radiation chemical yields are not strictly dependent on LET, but rather the localized track structure. The initial formation of the track is governed by the physics of the energy deposition by the incident ion and the transport of

that energy by secondary electrons. The radiation track structure is of crucial importance in specifying the precise spatial location and identity of all the radiolytic species and free-radical intermediates generated in the tracks, and their subsequent radiobiological action at the molecular and cellular levels. Radiation induced tracks are very dynamic and evolve from their initial geometry because of the reaction and diffusion of reactive species. Reaction and diffusion continue with the passage of time. Track structure, reaction scheme and yields of primary species, forms the fundamental of radiation-chemical theory (MOZUMDER, 1999). It is well accepted that differences in the biochemical and biological effects (e.g., damage to DNA, changes in cell signalling, etc.) of different qualities of radiation must be analyzed in terms of track structure (CHATTERJEE and HOLLEY, 1993; MUROYA et al., 2006).

1.2.2 *High-LET radiation*

Linear energy transfer (LET (keV/μm)) is defined as the rate at which energy is transferred from ionizing radiation to matter. Ionizing radiation such as electron generated from X-rays beams have high energy and low LET. The average LET of a 1-MeV electron in water is ~0.3 keV/μm. The track-averaged mean energy loss per collision event by such a fast electron is in the region ~48–65 eV (LAVERNE and PIMBLOTT, 1995; MOZUMDER, 1999; AUTSAVAPROMPORN, 2006). However, a heavy charged particle *(e.g.*, proton, deuteron, alpha) loses kinetic energy *via* a sequence of small energy transfers to atomic electrons in the medium. Those particles categorized as high-LET radiation. Protons have a higher LET than fast electrons and it is characterized by regions of high energy-deposition density thus higher concentration of water decomposition products as compared to fast electrons or γ-rays. High-LET radiation tracks effect differs from those of low-LET radiation. Low LET radiation will produce low concentrations of radicals that will most likely interact with the bulk water surroundings while high LET radiation will produce overlapping tracks to form a continuous cylinder that contain a higher concentration of radicals making second order favored radical-radical reactions. As LET increases, the distantly-spaced, nearly spherical spurs are formed closer together and eventually overlap (for LET greater than ~10–20 keV/μm) to form dense continuous columns. High-LET tracks produced by the heavy particles consist initially of a cylindrical

"core" and a surrounding region traversed by the emergent, comparatively low-LET secondary electrons, called the "penumbra" (MOZUMDER *et al.*, 1968; CHATTERJEE and SCHAEFER, 1976; FERRADINI, 1979; MAGEE and CHATTERJEE, 1980, 1987; MOZUMDER, 1999; LAVERNE, 2000, 2004).

Figure 1.1 shows typical two-dimensional representations of short (1–5 μm) track segments of $^{1}H^{+}$, $^{4}He^{2+}$, $^{12}C^{6+}$, and $^{20}Ne^{10+}$ ions (MUROYA *et al.*, 2006). These track segments are calculated using our Monte Carlo simulation code, called IONLYS, under the same LET conditions (~70 keV/μm). As it can be seen from the figure, these tracks can be considered as straight lines. It is also seen that the ejected high-energy secondary electrons travel to a farther distance away from the track core as the velocity of the incident ion increases, from protons to neon ions.

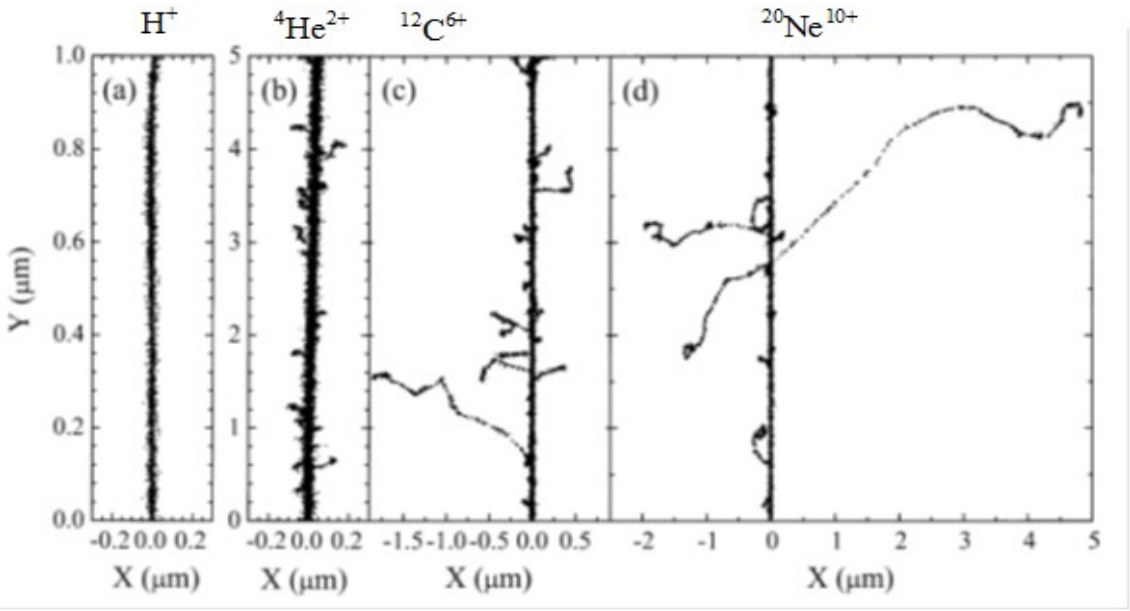

Figure 1.1 Projections over the *XY* plane of track segments calculated (at ~10^{-13} s) for (a) H^{+} (0.15 MeV), (b) $^{4}He^{2+}$ (1.75 MeV/nucleon), (c) $^{12}C^{6+}$ (25.5 MeV/nucleon), and (d) $^{20}Ne^{10+}$ (97.5 MeV/nucleon) impacting ions. Ions are generated at the origin and along the Y axis in liquid water under identical LET conditions (~70 keV/μm). Monte Carlo simulation can calculate the LET of charged particle. In order to calculate the LET, it needs energy,

charge and mass of that specific particle. In this case, we vary the energy of particle to get that specific LET.

The track segments for the different ions have been chosen equal to 5 μm, except for $^{1}H^{+}$, for which have adopted a track length of 1 μm. The penetration range of proton in liquid water at energy of 0.15 MeV is about 1 μm (Watt, 1996). This reduction in the track length for $^{1}H^{+}$ was dictated by the fact that the penetration range of this ion in liquid water, at the considered energy of 0.15 MeV, amounts to only ~2.3 μm. For the case of a 1-μm segment of 0.15 MeV proton track, the LET is nearly constant (~70 keV/μm) along the trajectory. Dots represent the energy deposited at points where an interaction occurred (MUROYA *et al.*, 2006).

In other words, although all the particles depositing the same amount of energy per unit path length, the energy is lost in a volume that increases in the order $^{1}H^{+}<^{4}He^{2+}<^{12}C^{6+}<^{20}Ne^{10+}$, indicating that the higher-Z particle has the lower mean density of reactive species. This irradiating-ion dependence of the track structure at a given LET (i.e., tracks of different ions with the same LET have different radial profiles) is in a good agreement with Bethe's theory of stopping power and indicates that LET is not a unique descriptor of the radiation chemical effects within heavy charged particle tracks (SCHULER and ALLEN, 1957; SAUER *et al.*, 1977; LAVERNE and SCHULER, 1987*a*; KAPLAN and MITEREV, 1987; FERRADINI and JAY-GERIN, 1999; LAVERNE, 2000, 2004). Some studies have focused to identify other comparative characteristics of radiation in place of LET, for instance the factor Z^2/β^2 (where Z is the charge number of the ion and β is the ratio of its velocity to that of light in vacuum) (KATZ, 1970) or, equivalently, the parameter MZ^2/E (where M is the heavy ion mass and $E = ½\ MV^2$ its kinetic energy) (PIMBLOTT and LAVERNE, 2002; LAVERNE, 2004). PIMBLOTT and LAVERNE (2002) suggested that no deterministic parameterization can realistically represent a phenomenon (namely, the effect of radiation quality on early radiation chemistry) that is *stochastic* in nature. KATZ (1978) also indicated that we need at least two parameters in order to speak of a track structure and that single parameter reductions do not fully describe

observed effects. Nevertheless, despite its limitations, LET still continues to be a dominant parameter in the radiation chemistry of heavy ions.

1.3. Water Radiolysis

Radiolysis of water is the dissociation of water molecules as a result of absorption of radiation energy such as neutrons, photons, and electrons by the water itself. The result of absorption of such radiation by water is the formation of a variety of excited and ionized water molecule. The overall process when water exposed to high-energy radiation until producing of primary species at ~10^{-6} s can be described successively into three stages as below (PLATZMAN, 1958):

Physical stage, consisting of deposition of radiant energy and formation of initial products in a specific, highly nonhomogeneous track structure geometry.

Physicochemical stage, is the stage leading to the establishment of thermal equilibrium in the bulk medium with reactions and reorganization of initial products to give stable molecules and chemically reactive species such as free atoms and radicals.

Chemical stage, is the stage where the various reactive species diffuse and react with one another (or with the environment).

It is well-known that the radiolysis of pure deaerated (air free) liquid water by low-LET radiation (such as ^{60}Co γ-rays, X-rays, fast electrons, or high-energy protons) mainly produce short-lived radicals species and long-lived molecular products e^-_{aq} (hydrated electron), $H^\bullet$ (hydrogen atom), H_2 (molecular hydrogen), $^\bullet OH$ (hydroxyl radical), H_2O_2 (hydrogen peroxide), $HO_2^\bullet/O_2^{\bullet-}$ (hydroperoxyl/superoxide anion radicals, pK_a = 4.8), H^+, OH^-. (for a review, see: SPINKS and WOODS, 1990). Under ordinary irradiation conditions, by about sub picosecond time scales, the ionized and excited water molecules have decomposed to give a number of reactive radical species (such as mentioned above), that concentrated in a small, spatially isolated regions of dense ionization and excitation events, referred to as "spurs" (MAGEE, 1953), along the track of the radiation. The self-diffusion of water occurs on about the 100 picosecond timescale so nothing can really move on shorter timescales. Some reactions occur between adjacent species, however by

the 10^{-9} s reaction and diffusion of reactive species has begun. New products are being formed and reactive radicals are being consumed. Owing to diffusion from their initial positions, the radiolytic products then either react within the spurs as they expand or escape into the bulk solution. Reaction and diffusion continue with the passage of time. At ambient temperature, this spur expansion is essentially complete by about 10^{-6}-10^{-7} s after the initial energy deposition. The so-called "primary" radical and molecular yields ("long-time" or "escape" yields) $g(e^-_{aq})$, $g(H^\bullet)$, $g(H_2)$, $g(^\bullet OH)$, $g(H_2O_2)$, represent the number of species formed or destroyed per 100 eV of absorbed energy that remains after spur expansion and becomes available to react with added solutes (treated as spatially homogeneous) in the bulk medium at moderate concentrations.

For low-LET radiation, following equation for the radiolysis of pure deaerated liquid water can be represented conceptually for an absorbed energy of 100 eV (FERRADINI and JAY-GERIN, 1999) (the symbol $\wwarrow$ is used to distinguish reactions brought about by the absorption of ionizing radiation):

$$G_{-H_2O}\, H_2O \wwarrow G e^-_{aq}\, e^-_{aq} + G_{H^\bullet}\, H^\bullet + G_{H_2} H_2 + G_{H^+} H^+ + G_{OH^-}\, OH^-$$
$$+ G_{^\bullet OH}\, {}^\bullet OH + G_{H_2O_2}\, H_2O_2 + G_{HO_2^\bullet/O_2^{\bullet-}}\, HO_2^\bullet/O_2^{\bullet-} + \ldots, \qquad (3)$$

Coefficients G_X in the above equation– also written as $g(X)$ – are the "primary" radical and molecular yields of the various radiolytic species X, and G_{-H_2O} denotes the corresponding yield for net water decomposition. Mechanism of radiolysis of pure liquid water by low LET radiation is well understood at room temperature. It is already summarized in several text books. For ^{60}Co γ-rays (photon energies of 1.17 and 1.33 MeV), hard X-rays or fast electrons of the same energies, at neutral pH and 25 ºC (average LET ~ 0.3 keV/μm), the most recently reported values of the primary yields are (LAVERNE, 2004) (in units of molecules per 100 eV):[1]

[1]These units (abbreviated as "molec./100 eV") for *g*-values are used throughout in this work. For conversion into SI units (mol J^{-1}): 1 molec./100 eV ≈1.0364 × 10^{-7} mol J^{-1}.

$$G e^-_{aq} = 2.50 \qquad G_{H\bullet} = 0.56 \qquad G_{H_2} = 0.45 \qquad G_{\bullet OH} = 2.50 \qquad G_{H_2O_2} = 0.70 \tag{4}$$

These primary yield values, include the small contribution of $HO_2^\bullet/O_2^{\bullet-}$ about less than 1% of the other primary radiolytic species. Equation (4) can be illustrated in a relation between species yield such following equations:

$$G e^-_{aq} + G_{OH^-} = G_{H^+}$$

$$G e^-_{aq} + G_{H\bullet} + 2\, G_{H_2} = G_{\bullet OH} + 2\, G_{H_2O_2} + 3\, G_{HO_2\bullet/O_2\bullet-}, \tag{5}$$

expressing the charge conservation and material balance of Eq. (3).

The yields of the free radical and molecular species formed in the radiolysis of water change with time, and also depend on the quality of radiation (refer to LET) and the concentration of additive or scavenger. One of the main goals in the study of the radiation chemistry of water is to determine the yields and their dependences on different parameters.

The series of complex events of decomposition of water by ionizing radiation can be divided consecutively into three stages (PLATZMAN, 1958; KUPPERMANN, 1959). The scheme of time scale of events that occur in the radiolysis of water is clearly shown in Figure. 1.2 while the detail explanation is given as below.

(i) The "*physical stage*" consists of the phenomena by which energy from the incident ionizing radiation (energetic photons, for example, γ-rays from ^{60}Co or X-ray photons, or charged particles, such as fast electrons, protons or heavy ions generated by a particle accelerator, or neutron radiation, or high-energy α-particles from suitable radioactive nuclides) is absorbed by the system. Its duration is less than ~10^{-16} s. The main consequences are the production of a large number of ionized and electronically excited water molecules, denoted $H_2O^{\bullet+}$ and $H_2O^*_{elec}$, respectively, along the path of the radiation. Note here that $H_2O^*_{elec}$ represents many excited states, including the so-called superexcitation states (PLATZMAN, 1962*a*) and the collective electronic oscillations of the "plasmon" type (HELLER *et al.*, 1974; KAPLAN and MITEREV, 1987; WILSON *et al.*, 2001). The ionization and excitation event, consecutively, as the earliest processes in the radiolysis of water can be expressed in the equations below,

$$H_2O \rightsquigarrow H_2O^{\bullet+} + e^- \quad (6)$$

$$H_2O \rightsquigarrow H_2O^*_{elec} \quad (7)$$

Generally, the electron ejected from water molecule in the ionization event has sufficient energy either to ionize or excite one or more other water molecules in the vicinity, and this leads, to the formation of track entities, or "spurs", that contain the products of the events. For low-LET radiation, the spurs are separated by large distances relative to their diameter and the track can be viewed, at this stage, as a random succession of isolated spherical spurs.

(ii) The "*physicochemical stage*" consists of the processes that lead to the establishment of thermal equilibrium in the system with reactions and reorganization of initial products to give stable molecules and chemically reactive species such as free atoms and radicals. Its duration is about 10^{-12} s for aqueous solutions. The ions and excited-state water molecules created during physical stage are highly unstable; they dissipate their excess energy by bond rupture, luminescence, energy transfer to neighboring molecules. They are allowed to undergo a random walk during their very short lifetime (~10^{-14} s) (MOZUMDER and MAGEE, 1975) via a sequence of electron transfers (about 20, on the average, over a few molecular diameters; COBUT *et al.*, 1998) from neighboring water molecules to the $H_2O^{\bullet+}$ hole (*i.e.*, electron-loss center) (OGURA and HAMILL, 1973). These short-lived $H_2O^{\bullet+}$ radical cations subsequently decompose to form $^{\bullet}OH$ radicals by proton transfer to a neighboring H_2O molecule:

$$H_2O^{\bullet+} + H_2O \rightarrow H_3O^+ + {}^{\bullet}OH \quad (8)$$

where H_3O^+ (or equivalently, H^+_{aq}) represents the hydrated hydrogen ion.

The energetic (or "dry") secondary electrons lose their kinetic energy via a sequence of interactions with the medium, such as further ionization and excitation until they eventually attain thermal energies (~0.025 eV at 25 ºC) after about 4×10^{-14} s (MEESUNGNOEN *et al.*, 2002*a*). In the course of their thermalization, "dry" electrons can

be recaptured by their parent ions due to the Coulomb attraction of the latter which tends to draw them back together to undergo electron-cation "geminate" recombination:

$$e^- + H_2O^{\bullet+} \rightarrow H_2O^*_{vib} \quad (9)$$

As the electron is recaptured, the parent ion is transformed into a (vibrationally) excited neutral molecule, and then decomposes to form radical species (see the detail description later).

The electron released in the ionization event (secondary electron) can cause further ionization and excitation if it has sufficient kinetic energy. Eventually, its energy falls below the first electronic excitation threshold of water (~7.3 eV; see: MICHAUD *et al.*, 1991), forming the so-called "subexcitation electron" (PLATZMAN, 1955). This latter loses the rest of its energy relatively slowly by exciting vibrational and rotational modes of water molecules. Once thermalized (e^-_{th}), it can be localized or "trapped" (e^-_{tr}) in a pre-existing potential energy well of appropriate depth in the liquid before it reaches a fully relaxed, hydrated state (e^-_{aq}) as the dipoles of the surrounding molecules orient under the influence of the negative charge of the electron. The e^-_{aq} behaves like chemical specie and it is of great importance in the radiolysis of water. In liquid water at 25 ºC, thermalization, trapping, and hydration can then follow in quick succession in less than ~10^{-12} s (for example, see: JAY-GERIN et al., 2008, and references therein):

$$e^- \rightarrow e^-_{th} \rightarrow e^-_{tr} \rightarrow e^-_{aq} \quad (10)$$

In the course of its thermalization, the ejected electron can also temporarily be captured by a water molecule to form a transient anion

$$e^- + H_2O \rightarrow H_2O^- \quad (11)$$

This anion then undergoes dissociation mainly into H^- and $^{\bullet}OH$ according to

$$H_2O^- \rightarrow H^- + {}^{\bullet}OH \quad (12)$$

followed by the reaction of the hydride anion with another water molecule through a fast proton transfer reaction:

$$H^- + H_2O \rightarrow H_2 + OH^- \qquad (13)$$

Reactions (11), (12) and (13) correspond to the so-called "dissociative electron attachment" (or DEA) process, which has been observed in amorphous solid water at ~20 K for electron energies between about 5 and 12 eV (ROWNTREE *et al.*, 1991). It has been suggested that DEA to water was responsible for the yield of "nonscavengeable" molecular hydrogen in the radiolysis of liquid water at early times (PLATZMAN, 1962*b*; FARAGGI and DÉSALOS, 1969; GOULET and JAY-GERIN, 1989; KIMMEL *et al.*, 1994; COBUT *et al.*, 1996). Experimental works have sustained this proposed mechanism, by showing that the previously accepted nonscavengeable yield of H_2 is due to precursors of e^-_{aq} and it can be lowered with appropriate (dry electron) scavengers at high concentration (PASTINA *et al.*, 1999).

Excited water molecules may be produced directly in an initial act [reaction (7)] or by neutralization of an ion [reaction (9)]. Very little is known about the channels of the dissociation of an excited water molecule. Fortunately, the contribution of the water excited states to the primary radical and molecular products in the water radiolysis is of relatively minor importance in comparison with that of the ionization processes, so that the lack of information about their decomposition has only limited consequences. Hence, the competing de-excitation mechanisms of H_2O^* are generally assumed to be essentially the same as those reported for an isolated water molecule. It should be noted here that the same decay processes have been reported to occur for the electronically and vibrationally excited H_2O molecules in the gas phase, specifically (see, for example: SWIATLA-WOJCIK and BUXTON, 1995; COBUT *et al.*, 1998; MEESUNGNOEN and JAY-GERIN, 2005*a*):

$$H_2O^* \rightarrow H^\bullet + {}^\bullet OH \qquad (14a)$$

$$H_2O^* \rightarrow H_2 + O(^1D) \qquad (14b)$$

$$H_2O^* \rightarrow 2\,H^{\bullet} + O(^3P) \qquad (14c)$$

$$H_2O^* \rightarrow H_2O + \text{release of thermal energy} \qquad (14d)$$

where $O(^1D)$ and $O(^3P)$ are the singlet and triplet state of the oxygen atoms, respectively (see Figure. 1.2). It is believed that reaction (14*a*) is the main source of the "initial" yield of hydrogen atoms at ~10^{-12} s, (i.e., at the end of the physicochemical stage, prior to spur or track expansion). Note that the $O(^1D)$ atoms produced in reaction (14*b*) react very efficiently with water to form H_2O_2 or possibly also $2^{\bullet}OH$ (TAUBE, 1957; BIEDENKAPP *et al.*, 1970). By contrast, ground-state oxygen atoms $O(^3P)$ in aqueous solution are rather inert to water but react with most additives, such as the scavenger or other solute added to the solution (AMICHAI and TEININ, 1969). As for the different branching ratios (or decay probabilities) associated with reactions (14*a-d*), they are chosen in order to consistently match the observed picosecond *G*-values of the various spur species (MUROYA *et al.*, 2002; MEESUNGNOEN and JAY-GERIN, 2005*a*).

*(*iii) The "nonhomogeneous chemical stage" consists of the period after ~10^{-12} s, at the end of the physicochemical stage, during which the radiolytic species generated previously in a very high concentration track (e^-_{aq}, $^{\bullet}OH$, $H^{\bullet}$, H_3O^+, H_2, H_2O_2, OH^-, $^{\bullet}O^{\bullet}$). They diffuse in the medium then encounter other species to undergo chemical reactions. These species react together to form molecular or secondary radical products, or with dissolved solutes (if any) present at the time of irradiation, until all spur/track reactions are complete. Many reactions are known to occur in pure liquid water; however Table 1 gives the most important reactions that are likely to occur while the spurs expand. The time for completion of spur expansion is generally taken to be ~10^{-7}-10^{-6} s. By this time, the spatially nonhomogeneous distribution of reactive species has relaxed. The remaining species called "primary product" consist of short-lived reactive radicals ($^{\bullet}OH$, e^-_{aq}, H) and long lived molecular products (H_2, H_2O_2) become available to react with added solutes in the water. Radiation chemical reactions in this stage are not special. Reaction kinetics is the same as other systems. The uniqueness of the radiolysis is that several kinds of radicals are simultaneously generated by those radicals and molecular products as mentioned above

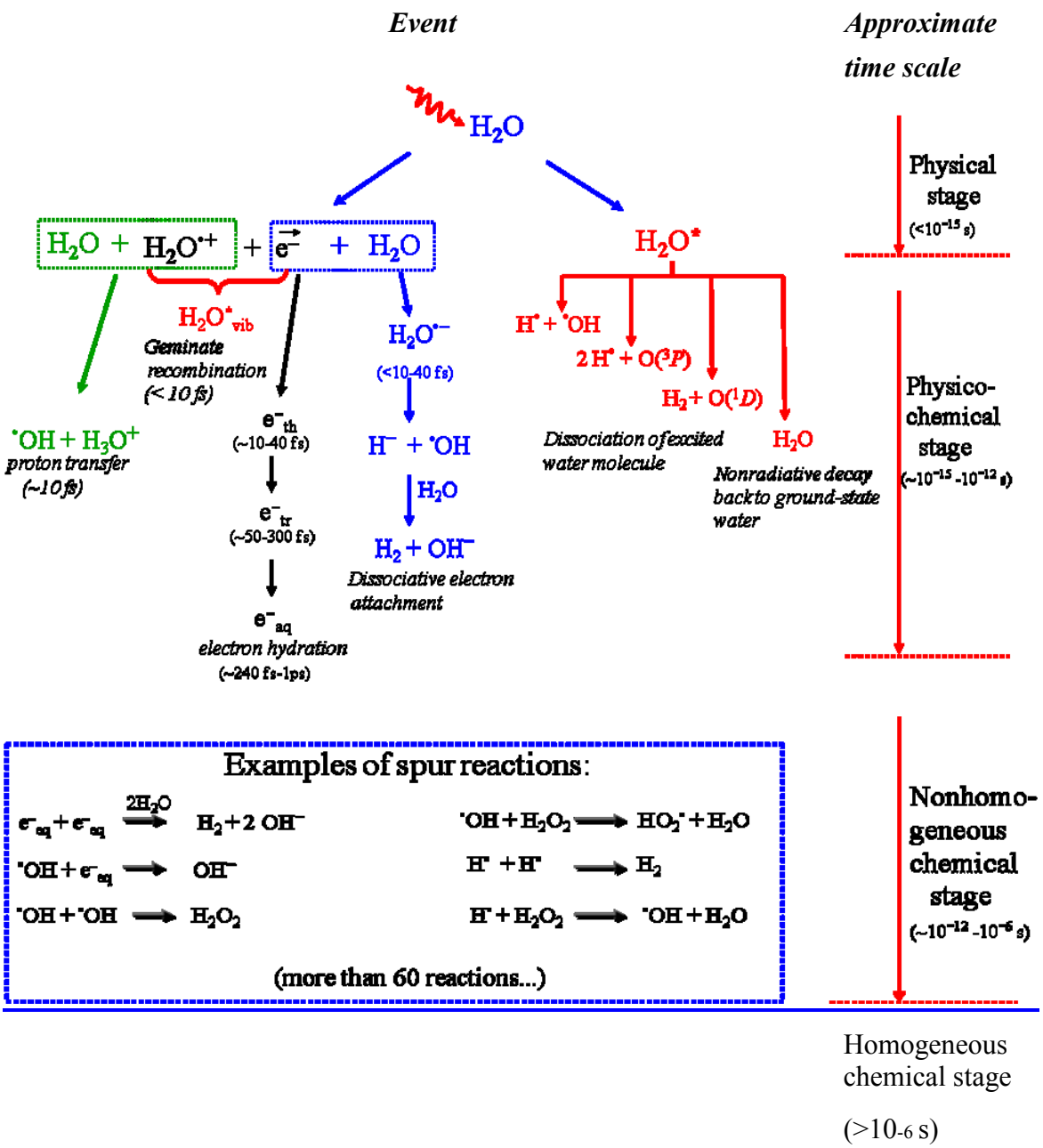

Figure 1.2 Time scale of events that occur in the low-LET radiolysis of neutral, deaerated water (MEESUNGNOEN, 2007; MEESUNGNOEN and JAY-GERIN, 2010). As a guide to the eyes, we chose to use different colors in the figure in order to contrast the individual process occurred during the radiolysis of water.

Table 1 Main spur/track reactions and rate constants (k) for the radiolysis of pure liquid water at 25 ºC (from MEESUNGNOEN, 2007). Some values of k have been updated by using the most recently available data of ELLIOT and BARTELS (2009).

Reaction	k (M^{-1} s^{-1})	Reaction	k (M^{-1} s^{-1})
$H^{\bullet} + H^{\bullet} \rightarrow H_2$	5.2×10^{9}	$e^{-}_{aq} + e^{-}_{aq} \rightarrow H_2 + 2\ OH^{-}$	7.3×10^{9}
$H^{\bullet} + {}^{\bullet}OH \rightarrow H_2O$	1.6×10^{10}	$e^{-}_{aq} + H^{+} \rightarrow H^{\bullet}$	2.1×10^{10}
$H^{\bullet} + H_2O_2 \rightarrow H_2O + {}^{\bullet}OH$	3.6×10^{7}	$e^{-}_{aq} + O_2^{\bullet-} \rightarrow H_2O_2 + 2\ OH^{-}$	1.3×10^{10}
$H^{\bullet} + e^{-}_{aq} \rightarrow H_2 + OH^{-}$	2.8×10^{10}	$e^{-}_{aq} + HO_2^{-} \rightarrow O^{\bullet-} + OH^{-}$	3.51×10^{9}
$H^{\bullet} + OH^{-} \rightarrow H_2O + e^{-}_{aq}$	2.4×10^{7}	$e^{-}_{aq} + O^{\bullet-} \rightarrow 2\ OH^{-}$	2.31×10^{10}
$H^{\bullet} + O_2 \rightarrow HO_2^{\bullet}$	1.3×10^{10}	$e^{-}_{aq} + H_2O \rightarrow H^{\bullet} + OH^{-}$	15.8
$H^{\bullet} + HO_2^{\bullet} \rightarrow H_2O_2$	1.1×10^{10}	$e^{-}_{aq} + O_2 \rightarrow O_2^{\bullet-}$	2.3×10^{10}
$H^{\bullet} + O_2^{\bullet-} \rightarrow HO_2^{-}$	1.1×10^{10}	$e^{-}_{aq} + HO_2^{\bullet} \rightarrow HO_2^{-}$	1.3×10^{10}
$H^{\bullet} + HO_2^{-} \rightarrow {}^{\bullet}OH + OH^{-}$	1.5×10^{9}	$e^{-}_{aq} + O(^3P) \rightarrow O^{\bullet-}$	2.0×10^{10}
$H^{\bullet} + O(^3P) \rightarrow {}^{\bullet}OH$	2.0×10^{10}	$e^{-}_{aq} + O_3 \rightarrow O_3^{\bullet-}$	3.6×10^{10}
$H^{\bullet} + O^{\bullet-} \rightarrow OH^{-}$	2.0×10^{10}	$H^{+} + O^{\bullet-} \rightarrow {}^{\bullet}OH$	5.0×10^{10}
$H^{\bullet} + O_3 \rightarrow O_2 + {}^{\bullet}OH$	3.7×10^{10}	$H^{+} + O_2^{\bullet-} \rightarrow HO_2^{\bullet}$	5.0×10^{10}
$H^{\bullet} + O_3^{\bullet-} \rightarrow OH^{-} + O_2$	1.0×10^{10}	$H^{+} + OH^{-} \rightarrow H_2O$	1.2×10^{11}
${}^{\bullet}OH + {}^{\bullet}OH \rightarrow H_2O_2$	6.3×10^{9}	$H^{+} + O_3^{\bullet-} \rightarrow {}^{\bullet}OH + O_2$	9.0×10^{10}
${}^{\bullet}OH + H_2O_2 \rightarrow HO_2^{\bullet} + H_2O$	2.9×10^{7}	$H^{+} + HO_2^{-} \rightarrow H_2O_2$	5.0×10^{10}
${}^{\bullet}OH + H_2 \rightarrow H^{\bullet} + H_2O$	4.0×10^{7}	$OH^{-} + O(^3P) \rightarrow HO_2^{-}$	4.2×10^{8}
${}^{\bullet}OH + e^{-}_{aq} \rightarrow OH^{-}$	3.6×10^{10}	$OH^{-} + HO_2^{\bullet} \rightarrow O_2^{\bullet-} + H_2O$	1.3×10^{10}
${}^{\bullet}OH + OH^{-} \rightarrow O^{\bullet-} + H_2O$	1.3×10^{10}	$O_2 + O^{\bullet-} \rightarrow O_3^{\bullet-}$	3.7×10^{9}
${}^{\bullet}OH + HO_2^{\bullet} \rightarrow O_2 + H_2O$	9.0×10^{9}	$O_2 + O(^3P) \rightarrow O_3$	4.0×10^{9}
${}^{\bullet}OH + O_2^{\bullet-} \rightarrow O_2 + OH^{-}$	1.1×10^{10}	$HO_2^{\bullet} + O_2^{\bullet-} \rightarrow HO_2^{-} + O_2$	9.7×10^{7}
${}^{\bullet}OH + HO_2^{-} \rightarrow HO_2^{\bullet} + OH^{-}$	8.3×10^{9}	$HO_2^{\bullet} + HO_2^{\bullet} \rightarrow H_2O_2 + O_2$	1.94×10^{8}
${}^{\bullet}OH + O(^3P) \rightarrow HO_2^{\bullet}$	2.02×10^{10}	$HO_2^{\bullet} + O(^3P) \rightarrow O_2 + {}^{\bullet}OH$	2.02×10^{10}
${}^{\bullet}OH + O^{\bullet-} \rightarrow HO_2^{-}$	1.0×10^{9}	$HO_2^{\bullet} + H_2O \rightarrow H^{+} + O_2^{\bullet-}$	1.4×10^{4}
${}^{\bullet}OH + O_3^{\bullet-} \rightarrow O_2^{\bullet-} + HO_2^{\bullet}$	8.5×10^{9}	$O_2^{\bullet-} + O^{\bullet-} \rightarrow O_2 + 2\ OH^{-}$	6.0×10^{8}
${}^{\bullet}OH + O_3 \rightarrow O_2 + HO_2^{\bullet}$	1.11×10^{8}	$O_2^{\bullet-} + H_2O \rightarrow HO_2^{\bullet} + OH^{-}$	0.155
$H_2O_2 + e^{-}_{aq} \rightarrow OH^{-} + {}^{\bullet}OH$	1.1×10^{10}	$O_2^{\bullet-} + O_3 \rightarrow O_3^{\bullet-} + O_2$	1.5×10^{9}
$H_2O_2 + OH^{-} \rightarrow HO_2^{-} + H_2O$	1.33×10^{10}	$HO_2^{-} + H_2O \rightarrow H_2O_2 + OH^{-}$	1.27×10^{6}
$H_2O_2 + O(^3P) \rightarrow HO_2^{\bullet} + {}^{\bullet}OH$	1.6×10^{9}	$HO_2^{-} + O^{\bullet-} \rightarrow O_2^{\bullet-} + OH^{-}$	8.02×10^{8}
$H_2O_2 + O^{\bullet-} \rightarrow HO_2^{\bullet} + OH^{-}$	5.55×10^{8}	$HO_2^{-} + O(^3P) \rightarrow O_2^{\bullet-} + {}^{\bullet}OH$	5.3×10^{9}
$H_2 + O(^3P) \rightarrow H^{\bullet} + {}^{\bullet}OH$	4.77×10^{3}	$O^{\bullet-} + O^{\bullet-} \rightarrow H_2O_2 + 2\ OH^{-}$	1.0×10^{8}
$H_2 + O^{\bullet-} \rightarrow H^{\bullet} + OH^{-}$	1.3×10^{8}	$O^{\bullet-} + O_3^{\bullet-} \rightarrow 2\ O_2^{\bullet-}$	7.0×10^{8}
$O(^3P) + O(^3P) \rightarrow O_2$	2.2×10^{10}	$O^{\bullet-} + H_2O \rightarrow {}^{\bullet}OH + OH^{-}$	1.3×10^{6}
$O(^3P) + H_2O \rightarrow 2\ {}^{\bullet}OH$	1.9×10^{3}	$O_3^{\bullet-} + H_2O \rightarrow O^{\bullet-} + O_2$	46.5

1.4 Interaction of fast neutron with water

1.4.1 Types of interactions

The neutron (*n*) is a radioactive particle that carries no electric charge and mass slightly greater (by ~1.293 MeV) than that of a proton (*p*). Together with the proton, the neutron is a constituent particle of all atomic nuclei (except, obviously, ^{1}H). Proton and neutron bind each other in nuclei strongly in a very short range (at distances of about 1 fm), called the *nuclear force* or nucleon–nucleon interaction. While neutrons can be stable when bound inside nuclei, free neutrons are unstable and undergo β-decay with a mean lifetime about 15 min, disintegrating into a proton, an electron (with a maximum kinetic energy of 782 keV), and an antineutrino with a characteristic half-life of 10.61 ± 0.16 min (CHRISTENSEN *et al.*, 1972).

The neutron is a key to the production of nuclear power. Neutrons can be generated from a variety of nuclear reactions over a very wide range of energies. High-energy neutrons can be moderated through collisions with atoms of various materials. The interaction of the neutron depends very much on its kinetic energy. In this respect, it is common to classify the possible neutron kinetic energies into four ranges to facilitate discussion about the different possible interactions of neutrons with matter. Some commonly used energy ranges and the names applied are: slow neutrons ($0 \leq E_n < 1$ keV),[2] intermediate neutrons (1 keV $\leq E_n <$ 500 keV), fast neutrons (500 keV $\leq E_n <$ 10 MeV), and high-energy neutrons ($E_n \geq$ 10 MeV) (ANDERSON, 1984). These categories are useful since dominant interactions can usually be identified in the regions given.

---

[2]The "slow" neutron category listed here includes several other well-known groups, such as "thermal" and "cold" neutrons. Thermal neutrons are in thermal equilibrium with the medium in which they are diffusing; they possess a Maxwell-Boltzmann velocity distribution determined by the absolute temperature of the medium. At 20 ºC, thermal neutrons have a most probable energy of 0.025 eV. Cold neutrons have energies considerably less than 0.025 eV, often as low as 0.001 eV.

Since neutrons are uncharged particles, they are categorized as indirectly ionizing. They can easily enter into a nucleus and cause reaction. They interact almost exclusively with nucleus of absorbing material and their interaction with atomic electrons is exceedingly small. The main interaction between neutrons and nuclei are *elastic* and *inelastic scattering*, *nuclear reactions*, and *capture processes*. The energy of neutron, of course, is a major factor in determining the type of reaction. When a neutron is *scattered* by an atomic nucleus, its energy and direction change but the nucleus is left with the same number of protons and neutrons it had before the interaction. The nucleus will have some recoil velocity and it may be left in an excited state, which will lead to the eventual release of radiation. In "elastic" scattering, indicated by (*n*,*n*),[3] the energy of the incident neutron is shared between the recoiling neutron and nucleus, and this type of reaction is probable for neutron with energies larger than that of thermal motion, for example in the range of 0.5 keV-10 MeV. "Inelastic" scattering, referred to (*n*,*n'*), is similar to elastic scattering except that the nucleus undergoes an internal rearrangement into an excited state from which it eventually releases radiation (most reactions are accompanied by the emission of a nuclear deexcitation γ-ray); in this case, part of the original kinetic energy of the incoming neutron is used to place the nucleus into an excited state. Obviously, if the energy of incoming neutron is less than the energy of all the excited states, then inelastic scattering is impossible. Interestingly, the hydrogen nucleus does not have internal excitation states, so only elastic scattering events can occur in that case. When a neutron is *absorbed* or *captured* by a nucleus, radiation can be emitted or fission can be induced. The compound

---

[3]Note that a simple notation for nuclear reactions is used to give a concise indication of an interaction of interest and to distinguish between scattering and absorption reactions. If a neutron *n* impinges on a target nucleus T, a resultant nucleus R is formed and an outgoing particle *g* is released; this interaction is shown as T(*n*,*g*)R. To denote a type of interaction without regard for the initial and final nuclei involved, only the portion written in parentheses is shown. The symbols *n*, *p*, *d*, α, e^-, and γ, are used in this notation to represent neutron, proton, deuteron, α-particle, electron, and gamma ray, respectively.

nucleus may rearrange its internal structure and release one or more γ-rays. Charged particles may also be emitted; the main ionizing species are protons, deuterons, α-particles, or heavier positive ions. The nucleus may also promptly reemit excess neutrons (note that the reemission of one neutron is indistinguishable from a scattering event). Finally, there may be a fission event in which, after the neutron is captured, the nucleus fragments into several parts with creation of fission products (nuclei of intermediate atomic weight).

1.4.2 Slowing down of fast neutrons

1.4.2.1 Hydrogen-containing substances as the most effective media for neutron moderation

For "fast" neutrons (i.e., those with kinetic energies below about 10 MeV) which will concern us in this work, most slowing down is accomplished through a process of many successive "billiard-ball" elastic collisions with atomic nuclei, following the simple laws of conservation of energy and momentum of classical particle physics.[4] Elastic scattering is the most likely interaction between (lower energy) fast neutron and low Z absorbers. In elastic scattering, the total kinetic energy of the neutron and nucleus is unchanged by the interaction. During the interaction, a fraction of the neutron's kinetic energy is transferred to the nucleus. For an incoming neutron of kinetic energy E_n, encountering a mass of target nucleus A, the recoil nucleus kinetic energy E_r (assumed to be initially at rest) is given by the following relation (for example, see ANDERSON, 1984; AUXIER *et al.*, 1968; RINARD, 1991; FRIEDLANDER *et al.*; KRANE, 1998):

$$E_r = E_n \frac{4A}{(1+A)^2} \cos^2\theta_r , \qquad (15)$$

where θ_r is the recoil-nucleus angle with respect to the original direction of travel of the neutron (in the laboratory system of coordinates). Noted that all scattering angles are

---

[4] In this energy range, fast neutrons can be considered as non-relativistic particles, since their mass is much larger than their kinetic energy; the description of neutron elastic collision can thus be performed using non-relativistic mechanics.

allowed, however, for most target nuclei, forward and backward scattering are favoured. According to Eq. (15), E_r ranges from zero up to a *maximum*:

$$(E_r)_{max} = E_n \frac{4A}{(1+A)^2}, \tag{16}$$

If all energy transfers between zero and $(E_r)_{max}$ are equally probable (i.e., if the elastic scattering angular distribution is spherically symmetric in the centre-of-mass coordinate system, which is certainly a good assumption at the energies considered here), the *average* energy of recoil nucleus after a collision is

$$\overline{E_r} = E_n \frac{2A}{(1+A)^2}, \tag{17}$$

which leads to (by energy conservation)

$$\overline{E'_n} = E_n \left[1 - \frac{2A}{(1+A)^2}\right] \tag{18}$$

for the average energy of the outgoing neutron (quantities with bars over them denote mean values). Clearly, Eqs. (17) and (18) show that the smaller the mass of nucleus encountered by the neutron, the greater the fraction of the neutron's kinetic energy that can be transferred in the elastic collision or the larger the energy loss. To reduce or moderate the speed of neutrons with the fewest number of elastic collisions, it requires low atomic number target nuclei. Therefore, biological tissues and other materials containing a large proportion of hydrogen or deuterium (such as light or heavy water) are favoured of slow down the neutrons. Hydrogen atoms (A = 1) as one of the constituent of water molecule receive most of the energy (the largest value) of colliding neutrons, on the average about half of neutron energy. Then hydrogen atom will lose its electron through the ionization event and begins to move as a proton. In other words, the interaction of neutron with an H atom gives rise to a proton, just like interaction of photon with an atom of medium gives rise to an electron. Therefore, proton radiolysis can simulate the fast neutron radiolysis as a model.

1.4.2.2 Average logarithmic energy decrement per collision

By considering a series of moderating collisions $1 \rightarrow k$ for a single neutron, the initial neutron kinetic energy is $(E_n)_0$ and the final value is $(E_n)_k$. Intermediate kinetic energies are $(E_n)_1$, $(E_n)_2$,..., $(E_n)_i$,..., and so forth. After k individual elastic scattering collisions, the average value of $\ln(E_n)_k$ is[5] (FRIEDLANDER *et al.*, 1981)

$$\overline{\ln\left(E_n\right)_k} = \overline{\ln\left(E_n\right)_0} - k\xi\,, \qquad (19)$$

where

$$\xi = \overline{\ln\left[\frac{(E_n)_{i-1}}{(E_n)_i}\right]} \qquad (20)$$

is defined as the "average change in the natural logarithm of the neutron energy after a single collision". It can be shown that decrement ξ is independent of the initial energy and expressed as (for a derivation, see refs. AUXIER *et al.*, 1968; FRIEDLANDER *et al.*, 1981; PERALTA, 2002)

$$\xi = 1 + \frac{(A-1)^2}{2A}\ln\left(\frac{A-1}{A+1}\right). \qquad (21)$$

It follows that the average value of $\ln(E_n)$ decreases after each collision by an amount ξ.

For collisions with hydrogen (A = 1) which gives rise to a proton, ξ becomes unity.[6] For oxygen (A = 16), ξ = 0.120. Interestingly, when A is large (A>> 1), for heavy elements: $\xi \approx 2/A$. Equations (19) and (21) are abundantly used in the present study.

---

[5]Average kinetic energy values are desired since one usually deals with a beam of many neutrons.

[6]Note that Eq. (21) is not defined when A = 1, but the limit as A approaches unity is valid in this case.

1.4.3 Energy dependence of scattering cross sections

Cross section σ (in units of barn, where 1 barn = 10^{-24} cm^2) is the probability of any particular event occurring between a neutron and a nucleus. As seen above, a neutron can have many types of interactions (scattering or absorption) with a nucleus, each of them having its own probability and cross section. The probability of occurrence for each type of event is independent of the probabilities of the others, so the sum of all the possible individual cross sections defines what we call the "total cross section".

All of the cross sections are critically dependent on the neutron energy and on the type of the target nucleus (for reviews, see refs. ANDERSON, 1984; RINARD, 1991; KRANE, 1998**;** SHULTIS and FAW, 2008). As a general rule the cross section is a lot larger at low energies than at high energies. At low energies, usually less than 1 MeV, the elastic cross section is nearly constant, whereas the inelastic scattering cross section and absorption (capture) cross sections exhibit a $1/\sqrt{E_n}$ behavior (this inverse proportionality is also called the $1/v$ law, where v is the neutron velocity; e.g., see CEMBER and JOHNSON, 2009). So at low energies the total cross section can be nearly constant or decreasing with increasing energy, depending on which type of event dominates. At higher energies the cross section may have large peaks superimposed on the $1/v$ tendency. These peaks are called resonances and occur at neutron kinetic energies where reactions with nuclei are enhanced. For example, a resonance will occur if the target nucleus and the captured neutron form a "compound" nucleus, and the excitation energy brought by the incident neutron corresponds to a quantum state of the resulting compound system. Scattering and absorption cross sections exhibit resonance peaks at neutron kinetic energies corresponding to those quantum nuclear states. In general, resonances occur at lower energies for heavy nuclei than for light nuclei. In heavy nuclei, large and narrow resonances appear in the slow neutron region, eV range. For intermediate energies, keV range, the resonances can be too close together to elucidate. As we move to energies in the MeV range, the resonances are sparser and have very broad shapes. For light nuclear targets, resonances appear only in the MeV region and are broad and relatively small. Of all the nuclides, only hydrogen and its isotope deuterium exhibit *no* resonances at all. Exceptions

to the general trends also exist in some nuclei with "magic" numbers of protons or neutrons[7] where the behaviour may be similar to that of light nuclei despite the actual atomic weight. In practice, since there is no simple way to calculate cross sections, it is necessary to rely on tables of cross sections for the nuclei of interest [e.g., see: Nucl. Data Sheets 107, 2931 (2006), a special issue ("Evaluated nuclear data file ENDF/B-VII.0") on evaluations of neutron cross sections from the U.S. Cross Section Evaluation Working Group of the National Nuclear Data Center of Brookhaven National Laboratory (http://www.nndc.bnl.gov/csewg/); see also the T-2 Nuclear Information Service of the Los Alamos National Laboratory (http://t2.lanl.gov/data/data.html), which provides access to a variety of nuclear data, including the ENDF/B-VII.0 library of evaluated neutron data with links to PDF plots of the cross sections and angular distributions for most nuclides over the neutron energy range up to 200 MeV].

1.4.4 Elastic scattering interactions of fast neutrons in water

Fast neutrons whose energy above thermal motion or at incident energies less than about 10 MeV give up their energy in elastic collisions with charged nuclei of the absorbing medium. In the case of the fast-neutron radiolysis of water, the ionizing particles involved are thus proton and oxygen ion recoils. It is in fact important to note that, in this energy range, the contributions resulting from the $^{16}O(n,\alpha)^{13}C$ reaction (threshold at ~3.8 MeV), producing α-particles and recoiling carbon ions, and especially from the inelastic scattering with oxygen (first level at ~6.05 MeV), producing gamma radiation, can be neglected to a very good approximation.[8] From the radiolysis point of view and as long as

---

[7] Those nuclei have a completely filled shell of either protons or neutrons; they are said to be "magic" because they are relatively more stable than nuclei with either a larger or a smaller number of nucleons.

[8] This is because the cross sections for these nuclear reactions are about an order of magnitude less than the cross sections for hydrogen and oxygen elastic scattering for most of the energies that interest us here. Notice that they rise steeply, however, as neutron energy increases, but become significant only at neutron energies around or greater than 10

the energy is less than ~10 MeV, we therefore need only consider *elastic* neutron-proton (*n-p* collisions) and to a smaller extent (see below) neutron-oxygen scattering interactions. The corresponding interaction with oxygen is practically negligible.

Figure 1.3 shows a comparison of the elastic cross sections for *n-p* scattering and for neutrons incident on oxygen nuclei in the energy range from 5 keV to 10 MeV. As can be seen, the cross-section curve for neutrons incident on ^{1}H is featureless (no resonances are present) and decreases continuously with neutron energy. For neutrons incident on ^{16}O, the cross section is quite flat in the region below ~0.3 MeV but shows resonance peaks at higher energies.

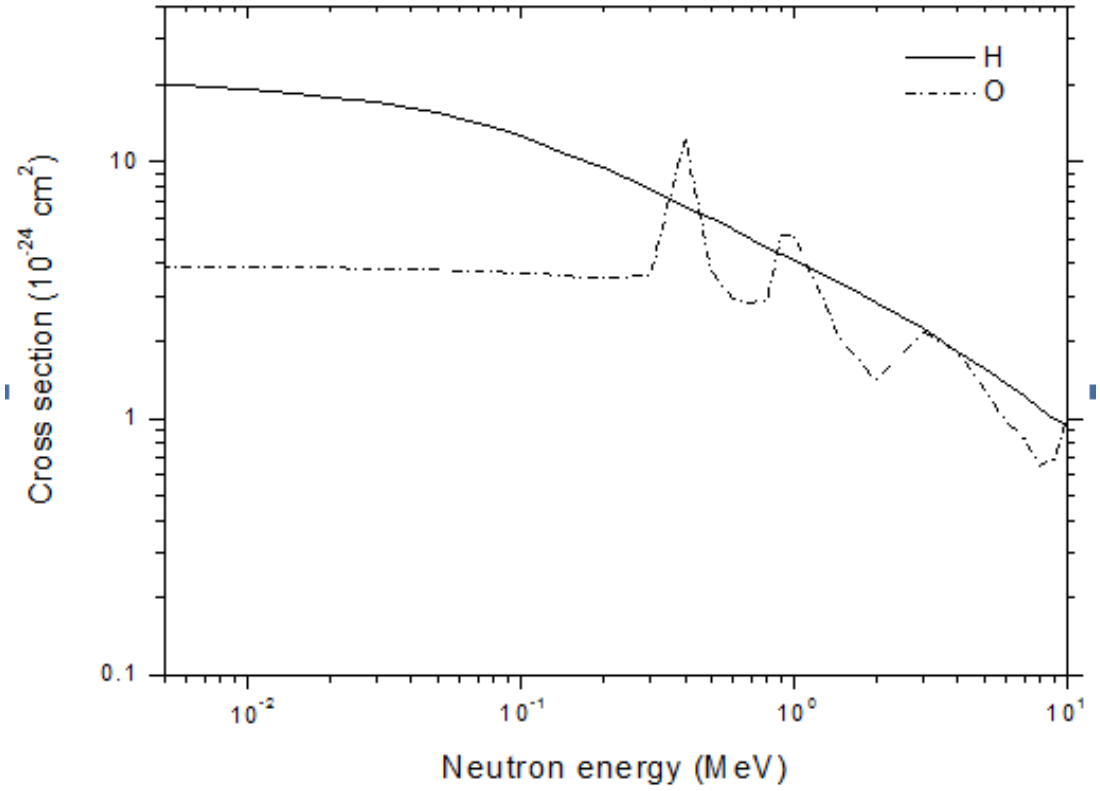

Figure 1.3 Comparison of elastic scattering cross sections (in barn) for fast neutrons incident on hydrogen (solid line) and oxygen (dash-dot line) targets as a function of neutron energy (from WATT, 1996).

MeV [data from the Brookhaven ENDF/B-VII.0 library (2006); see also AUXIER *et al.*, 1968].

Figure 1.3 describes the cross section elastic scattering interactions of a neutron with a *single* nucleus, hydrogen or oxygen. Moreover, below about 0.3 MeV, the scattering for proton recoils is very high and largely dominates the oxygen elastic scattering; however, in the energy range ~0.3-10 MeV, because of the occurrence of the various resonances in oxygen, the cross section for oxygen elastic scattering tends to become more or less the same as that for *n-p* collisions. These cross sections, referring to an individual element called "microscopic" cross sections (RINARD, 1991). If the studied sample contains several elements instead of a simple element, the cross section is simply the sum of the cross sections of the individual target nuclei. For example, for the case of the water molecule (H_2O), which contains two hydrogen atoms and one oxygen atom, the cross section describing the interaction of a neutron with the molecule is

$$\sigma_{H_2O} = 2\sigma_H + \sigma_O \,, \tag{22}$$

where σ_H and σ_O are the microscopic cross sections for hydrogen and oxygen, respectively. More generally, for bulk materials containing a mixture of elements *i* with density N_i and individual cross section σ_i, we can define the so-called "macroscopic" cross section (denoted here by the symbol μ and with dimensions of cm^{-1}), given by (RINARD, 1991)

$$\mu = \sum_i N_i \sigma_i \,. \tag{23}$$

This equation actually is the same with Eq. (1) which is addressed to the total cross section, summed over all considered individual processes of secondary electron. However Eq. (23) is addressed more to the total cross section for neutrons in water as sum of microscopic cross sections for hydrogen and oxygen.

As an illustration of Eq. (23), the macroscopic cross section for neutrons in water is

$$\mu_{water} = \frac{N_{Av}\rho}{M}\left(n_H \sigma_H + n_O \sigma_O\right), \tag{24}$$

where ρ is the density of water, M = 18 is water molecular weight, N_{Av}= 6.022 x 10^{23} atoms/mole is Avogadro's number, and n_H = 2 and n_O = 1 are the numbers of atoms of hydrogen and oxygen in one molecule, respectively. Interestingly, the fact that there are twice as many hydrogen atoms as oxygen atoms per given volume of water also contributes to making oxygen ion recoils of minor importance in the fast-neutron radiolysis of water. In fact, Edwards *et al.* (2007) estimated that, in the energy range below 10 MeV, 88% of the neutron energy is absorbed by protons and 12% by oxygen recoils.

1.4.5 Neutron mean free path and ranges of recoil protons and oxygen ions in water: information on track structure

A very descriptive feature of the transmission of neutrons through bulk matter is the mean-free-path length (λ), which is the average distance a neutron travels between two successive interactions. The mean-free-path length λ is the reciprocal of the macroscopic cross section μ given in Eq. (23):

$$\lambda = \frac{1}{\mu} \qquad (25)$$

λ is a key parameter in the study of neutron transport and interactions in matter and has many qualitative applications in assay instruments and shielding. For example, it is found that, under the conditions of the transmission of a pencil beam of monoenergetic neutrons incident normally (along the direction z) on a thick sample of infinite lateral extent, the relative number of neutrons that travel a distance z in the sample (the origin being at the point where the neutrons enter the sample) without experiencing a collision falls off exponentially as exp(-z/λ) (RINARD, 1991; CEMBER and JOHNSON, 2009). Mathematically, this is a representation of the Poisson distribution and corresponds to the probability of no event when, on the average, z/λ events should occur (EVANS, 1955). Importantly, λ also determines the free flight distances of individual neutrons in Monte-Carlo procedures that are used to simulate how neutrons are transported through matter.In those computer calculations, individual free flight distances for a large number of simulated neutrons must be selected randomly so as to give the observed exp(-z/λ) distribution

(TURNER *et al.*, 1985). Note that Eq. (25) is similar with Eq. (1), the difference is that the macroscopic cross section for neutron in water (μ) is the sum of microscopic cross sections for hydrogen and oxygen.

The mean free path length depends on both the type of material and the energy of the neutron. For the case of 100-keV incident neutrons in water, λ can easily be calculated from Eqs. (24) and (25) to be ~1.04 cm, using the microscopic cross section values $\sigma_H \approx$ 12.5 and $\sigma_O \approx$ 3.65 barns (WATT, 1996). The mean free path of neutrons in water as a function of neutron energy is shown in Figure 1.4. After each collision, the energy of neutron is decreased and the cross section changes, thereby affecting the mean free path accordingly. For the range of the energies that interest us here, λ decreases as the neutron's energy decreases.

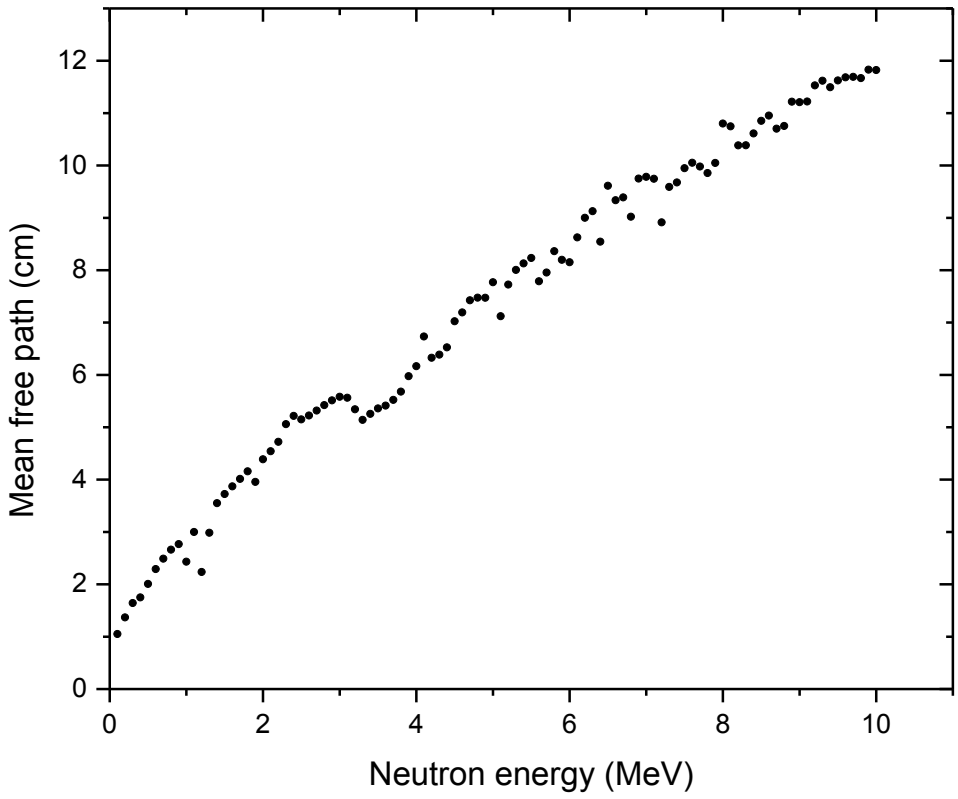

Figure 1.4 Neutron mean free path in water as a function of neutron energy (from Schröder, 2009).

Table 2 gives some values for the mean free path and secondary-particle (recoil proton and oxygen ion) maximum range for several neutron energies in water. As can be seen, the elastically scattered proton and oxygen ion recoils generated by the passage of the incident neutron are widely separated from one another along the path of the neutron.[9] Moreover, these recoil nuclei have maximum ranges (i.e., track lengths) much less than the average separation between two successive neutron interactions (λ), so that they can be considered as behaving *independently* of each other: their ionizing energy is deposited locally in dense tracks in the water in the immediate vicinity of the collision sites (the points of generation of the recoil particles) with virtually no allowance for overlap of the reaction zones of neighbouring tracks.[10]

Table 2 Neutron mean free path (taken from Fig. 1.4) and maximum ranges for elastically scattered protons and oxygen ions in water (WATT, 1996).

Neutron energy (MeV)	Neutron mean free path (λ) (cm)	Secondary-proton maximum range (μm)	Secondary-oxygen-ion maximum range (μm)
0.1	1.04	1.6	0.1
0.5	2.01	8.9	0.5
1.0	2.43	24.6	0.9
3.0	5.58	149	1.9
5.0	7.77	362	2.7
10.0	11.8	1230	4.1

[9]Like photons, neutrons are uncharged and hence can travel appreciable distances without interacting.

[10]This approximation would not necessarily be correct at very high neutron intensities or dose rates. It can cause overlap of track; therefore the result of interaction of two successive neutrons with water cannot be treated separately.

As a consequence, under normal irradiation conditions, fast neutrons deposit their energy in water primarily through the generation of "isolated" tracks of recoil nuclei and the observed water radiolysis chemistry should tend to be much like that induced by *independent, high-LET protons and oxygen ions*. This track structure information for the elastically scattered proton and oxygen ion recoils strongly supports the procedure used in the present study to calculate the radiolysis *G*-values for fast neutrons by simply summing the yields for each of these recoil ions after allowance has been made for the appropriate weighting according to energy.

1.5 The effect of temperature on water radiolysis

The effect of temperature on water radiolysis is practically applicable in nuclear reactor, since it is operated at high temperature ~275-310 ^{o}C. The cooling water is subjected to an intense mixed radiation field such as low-LET γ–radiation and also fast neutrons, as a result of fission process in nuclear reactor, which interact with water molecules to produce recoil high-LET protons. As mentioned previously, the action of mixed neutron/γ-radiation fields on water under such extreme conditions, which is at high temperature and at high pressure, results in the unwanted radiolytic formation of oxidizing species, such as $^{\bullet}OH$, H_2O_2, O_2, and $O_2^{\bullet-}$ (or $HO_2^{\bullet}$, depending on the pH). These oxidizing species are highly reactive with most metal alloys and can significantly increase the corrosion and degradation of reactor components. It is necessary to select optimum conditions in the reactor in order to suppress oxidizing which can furthermore cause deleterious corrosion, hydriding, and cracking processes both in the core and in the associated piping components (BURNS and MOORE, 1976; COHEN, 1980; HICKEL, 1991; ELLIOT, 1994; ELLIOT *et al.*, 1996*a*; McCRACKEN *et al.*, 1998; BUXTON, 2001; STUART *et al.*, 2002; KATSUMURA, 2004; CHRISTENSEN, 2006; EDWARDS *et al.*, 2007). It can be achieved most efficiently when the radiation chemistry of water under reactor operation conditions is understood. Rate constant of all these reactions are known at Pressurized Water Reactor (PWR), the most common use of nuclear power reactor worldwide, operating temperature range and the behaviour can be modelled with reasonable

confidence. However, direct measurement of the chemistry in and around reactor cores is extremely difficult, due to the conditions of high temperature, pressure, and mixed neutron/gamma radiation fields. Certainly there are no compatible with normal chemical instrumentation. For these reasons, theoretical calculations and chemical models have been used, with some simplifying assumptions. It has been acknowledged that a computer simulation of the radiation-induced water decomposition is a powerful method to simulate and predict the detailed radiation chemistry of the water in the core of nuclear reactor and the consequences for materials.

To predict the effect of radiation at elevated temperature in particular or in reactor condition in general, it is necessary to know the temperature dependence on chemical yields of oxidizing ($^{\bullet}OH$, H_2O_2) and reducing (e^-_{aq}, $H^{\bullet}$, H_2) radiolytic products for both the γ- and fast neutron radiolysis as well as the temperature dependence of rate constants for the reactions taking place in spurs and tracks that result in these primary yields. The *g*-values for the primary yields formed by using low-LET (gamma or fast electrons) radiation at ambient temperature up to ~300 ºC are widely well-known. These chemical yield have been determined by several groups of experimentalists (KENT and SIMS, 1992*a*,*b*; ELLIOT *et al.*, 1993, 1994, 1996*a*,*b*; 1994; SUNARYO *et al.*, 1995*a*,*b*; ISHIGURE *et al.*, 1995; KATSUMURA *et al.*, 1998; ŠTEFANIĆ and LAVERNE, 2002). Several data showed that the yields of free radicals increase with temperature, which can readily be explained from the fact that many important reactions are not diffusion controlled and therefore have rate constants that increase *less* steeply with temperature than the diffusion coefficients of the individual species (for example, see: ELLIOT *et al.*, 1996*b*; HERVÉ DU PENHOAT *et al.*, 2000).[11] In other words, as the temperature is raised, diffusion of free radical species out of spurs/tracks increases more rapidly than combination or recombination, and one should have less molecular recombination products (namely, water, H_2, and H_2O_2) (ELLIOT *et al.*, 1993; JANIK *et al.*, 2007). Deterministic diffusion-kinetic modeling of spur processes (KABAKCHI and BUGAENKO, 1992; LAVERNE and PIMBLOTT, 1993; SWIATLA-

[11]Just recall here that, most generally, the yield of a species that escapes the spur/track depends on the competition between reactions in the spur/track and escape by diffusion out of the spur/track.

WOJCIK and BUXTON, 1995, 1998, 2000) and stochastic Monte-Carlo simulations (HERVÉ DU PENHOAT *et al.*, 2000, 2001) have also reproduced those experimental data satisfactorily. However, there is one difficulty in explaining the experimentally increasing of H_2 yield as a temperature increases, even though H_2 is a molecular product where it is expected to decrease as radical-radical combination is not favoured. Unlikely other molecular products such as H_2O_2 yield decreases with increasing temperature. In fact, although the above calculations have explained an increase of $g(H_2)$ up to about 200 ºC as resulting from the bimolecular reaction of e^-_{aq} (SWIATLA-WOJCIK and BUXTON, 1995; HERVÉ DU PENHOAT *et al.*, 2000), above 200 ºC the computed $g(H_2)$ tends to decrease with increasing temperature. The fact that $g(H_2)$ continues to increase with temperature raises interesting questions. Production of H_2 at very early time in the physicochemical stage of the radiolysis of water such as, dissociative electron attachment and the decomposition of excited water, might contribute to this phenomenon. In addition SWIATLA-WOJCIK and BUXTON (2005), BARTELS, (2009) showed a need to postulate an additional channel for H_2 formation in chemical stage.

In this work, we used a most recent report compiled by ELLIOT and BARTELS (2009) which reviews the radiolysis data now available and, where possible, corrected the reported *g*-values and rate constants to provide a recommendation for the best values to use in the high-temperature modelling of light water radiolysis up to 350 °C. In this work, the authors have re-measured or re-evaluated the *g*-values for the primary radiolysis species for low-LET radiation as well as many of the reaction rate constants. Generally, they have been able to extend the measurements to higher temperatures than the original investigations, thereby reducing or eliminating the need to "extrapolate" the data to the temperatures of interest.

1.6 Research Objective

The goal of this research is to better understand the radiation chemistry and the mechanisms involved in the radiolysis of water by 2 MeV fast neutrons as a function of temperature in the range of 25 – 350 ^oC. In this work we neglected the radiation effects due to oxygen ion recoils and assuming that the most significant contribution to the radiolysis came from these first four recoil protons with energy 1.264, 0.465, 0.171, and 0.063 MeV,

respectively. Then the sum of the g-values for these protons after allowance was made for the appropriate weightings according to their energy.

The g-values were calculated at 10^{-7}, 10^{-6} and 10^{-5} s after the ionization event at all temperatures, in accordance with the time range associated with the scavenging capacities generally used for fast neutron radiolysis experiments. The results of the simulations compared with the available experimental data and also compared with data obtained for low-LET radiation (^{60}Co γ-rays or fast electrons).

2. MONTE CARLO SIMULATIONS

The complex sequence of events that are generated in liquid water and dilute aqueous solutions after the absorption of ionizing radiation can be modelled using Monte-Carlo simulation techniques. Such a procedure is well adapted to account for the *stochastic* nature of the phenomena, provided the realistic probabilities and the cross sections for all possible events. The simulation then allows one to reconstruct the complicated action of the radiation. It also offers a powerful tool for estimating the validity of different assumptions, for making a critical examination of proposed reaction mechanisms, and for estimating some unknown parameters. The accuracy of these calculations is best determined by comparing their predictions with experimental data on well-characterized chemical systems that have been examined with a wide variety of incident radiation particles and energies.

TURNER and his coworkers (1981, 1983, 1988*b*) at the Oak Ridge National Laboratory (Oak Ridge, Tennessee, U.S.A.) jointly with MAGEE and CHATTERJEE at Lawrence Berkeley Laboratory (Berkeley, California, U.S.A.) were the first to use Monte-Carlo calculations to derive computer-plot representations of the chemical evolution of a few keV electron tracks in liquid water at times between ~10^{-12} and 10^{-7} s. Zaider and Brenner (1984) also described such an approach, and their calculated time-dependent yields of e^-_{aq} and $^{\bullet}OH$ radicals were somewhat similar to values measured or derived in pulse-radiolysis studies of pure water. Following this pioneering works, stochastic simulation codes employing Monte Carlo procedures were used with success by a number of researchers to study the relationship between the track structure and the following chemical processes that occur in the radiolysis of both pure water and water containing solutes (for a comprehensive list and reviews, see, for example: BALLARINI *et al.*, 2000; UEHARA and NIKJOO, 2006). Two main approaches have been widely used: (1) the "step-by-step" (or random flights Monte Carlo simulation) method, in which the trajectories of the diffusing species of the system are modeled by time-discretized random flights and in which reaction occurs when reactants undergo pair wise encounters, and (2) the "independent reaction times" (IRT) method (CLIFFORD *et al.*, 1986; PIMBLOTT *et al.*, 1991; PIMBLOTT and GREEN, 1995), which allows the calculation of reaction times without having to follow the

trajectories of the diffusing species. Among the stochastic approaches, the most reliable is certainly the full random flights simulation, which is generally considered as a measure of reality. However, this method can be exceedingly consuming in computer time when large systems (such as complete radiation tracks or track segments) are studied. The IRT method, a computer efficient stochastic simulation technique, has been devised to achieve much faster realisation than are possible with the full Monte-Carlo model. In essence, it relies on the approximation that the distances between pairs of reactants evolve independently of each other, and therefore the reaction times of the various potentially reactive pairs are independent of the presence of other reactants in the system.

In a program begun in the early 1990's, the Sherbrooke group has also developed and progressively refined with very high levels of detail several Fortran-based Monte Carlo codes that simulate the track structure of ionizing particles in water, the production of the various ionized and excited species, and the subsequent reactions of these species in time with one another or with available solutes (COBUT *et al.*, 1994, 1998; FRONGILLO *et al.*, 1996, 1998; HERVÉ DU PENHOAT *et al.*, 2000; MEESUNGNOEN *et al.*, 2001, 2003 MEESUNGNOEN and JAY-GERIN, 2005*a*,*b*; MUROYA *et al.*, 2002, 2006; PLANTE *et al.*, 2005; AUTSAVAPROMPORN *et al.*, 2007). A most recent version of the Sherbrooke codes, called IONLYS-IRT (MEESUNGNOEN and JAY-GERIN, 2005*a*,*b*), has been used in the present work. Briefly, the IONLYS step-by-step simulation program models all the event of the physical and physicochemical stages in the track development. The third and final nonhomogeneous chemical stage is covered by the program IRT, which employs the IRT method (CLIFFORD *et al.*, 1986; GREEN *et al.*, 1990; PIMBLOTT *et al.*, 1991) to model the chemical development that occur during this stage and to simulate the formation of measurable yields of chemical products. The detailed description and implementation of the IONLYS-IRT has already been given (MEESUNGNOEN and JAY-GERIN, 2005*a*,*b*, and references therein), and will not be reproduced here, only a brief overview of the most essential features of the simulation methodology and reaction scheme, pertinent to the current calculations, is given below.

2.1 The IONLYS code

The IONLYS simulation code is used to cover the early "physical" and "physicochemical" stages of radiation action up to ~10^{-12} s. It is actually composed of two codes, one (named TRACPRO) for transporting the investigated incident charged particle (proton or any other heavy ion projectile) and another one (named TRACELE) for transporting all of the energetic electrons (collectively named "secondary electrons") that result from the passage of ionizing particle in liquid water. The code models, event by event, *all* the basic physical interactions (energy deposition) and the subsequent establishment of thermal equilibrium in the system (conversion of the physical products created locally after completion of the physical stage into the various "initial" chemical species of the radiolysis).

In particular, IONLYS provides the detailed distribution of coordinates of *all* physical events, including ionization, electronic and vibrational excitation of single water molecules, and excitation of plasmon-type collective modes, that occur locally during the slowing-down of the irradiating charged particle and of all the secondary electrons that it has generated. The particle will interact with water based on the probability per unit distance of each particle's energy or cross section. The code begins by selecting a particular distance to the first interaction site for the incident particle. The calculation continues with the random choice of the type of interaction (ionization, excitation of electronic, vibrational and rotational levels of single water molecules, excitation of plasmon-type collective modes, and elastic scattering) that occurs. This cross section entered as input data in the code, based on direct measurement or on theoretical estimations. These collisions cross sections are needed to follow the history of charged particle. If an inelastic collision is ionization, the particle's energy is reduced by the energy loss selected. The secondary electron produced is given a kinetic energy equal to this energy loss minus the binding energy (or ionization energy) of the target electron. The energy-dependent cross sections for the elastic and inelastic processes occurred, angular distributions, are entered as input data as well. Delta rays are produced at sites of high energy loss. Each time a secondary electron is produced, the code proceeds by transporting it until its energy falls below the threshold for electronic excitations, equal to ~7.3 eV for liquid water (MICHAUD *et al.*, 1991) (these electrons are denoted as "subexcitation" electrons). If a collision is elastic, an

angle of scatter is selected and the flight distance for the next collision site is chosen. The probabilities or cross sections for all of the individual molecular processes and their alternatives are entered as input data in Monte-Carlo code, based on direct measurements (where available, cross section data in the case of liquid water are scarce) or on the theoretical estimations (COBUT *et al.*, 1998; MEESUNGNOEN and JAY-GERIN, 2005*a*). These collision cross sections are needed to follow the history of an energetic charged particle and its products, covering all ranges of energy transferred in individual collisions. Most importantly, they provide the mean free path used to determine the distance to the next interaction, the type of interaction at each event, energy loss, and the angle of emission of the scattered particle (for example, see: DINGFELDER and FRIEDLAND, 2001; NIKJOO *et al.*, 2006; DINGFELDER *et al.*, 2008). The computer simulation thus provides complete information on the spatial distribution of ionized and excited water, $H_2O^{\bullet+}$ and H_2O^*, and subexcitation electrons, e^-_{sub} (energy < 7.3 eV), produced along the incident charged particle trajectory during the physical stage of the radiation action. This stage is concluded in ~10^{-15} s. Full details of the *cross-section database* used in the IONLYS code can be found in the references cited (COBUT, 1993; COBUT *et al.*, 1998; MEESUNGNOEN and JAY-GERIN, 2005*a*). It is worth mentioning that this code, which uses protons or heavy ions as the primary particles, is particularly well adapted to the study of the fast-neutron radiolysis of water, since the ionizing particles involved in this case are proton and oxygen ion recoils. Interestingly, the choice of proton impact in the Sherbrooke code was originally adopted owing to the fact that protons represent, by far, the most comprehensive database of cross sections for bare ion collisions (not only on water but also on a number of different target atoms or molecules; e.g., see RUDD, 1990; RUDD *et al.*, 1992; IAEA-TECDOC-799, 1995; DINGFELDER, *et al.*, 2000), and also because they constitute a valuable tool for studying LET effects on radiolytic yields (COBUT, *et al.*, 1998). Another great advantage of the code is that, while it was devised for protons, it can also be used for heavier ion projectiles by assuming that the interaction cross sections scale as Z^2, where Z is the projectile charge number. In this scaling procedure, based on the lowest-order (or first Born) approximation of perturbation theories, the cross sections for bare ion impact are approximately Z^2 times the cross sections for proton impact *at the same velocity*. This simple Z^2 scaling rule, which holds at sufficiently high impact energies (say

above ~1 MeV/nucleon) where the interactions are not too strong, is particularly useful for providing cross sections for ionization and excitation by ion projectiles, especially as there are only limited experimental data available involving ions heavier than proton or helium in collision with water molecules (MEESUNGNOEN and JAY-GERIN, 2005; MEESUNGNOEN, 2007; MEESUNGNOEN and JAY-GERIN, 2010; INOKUTI, 1971). In practice, the stochastic selection of the scattering events is done with various sampling techniques (direct inversion, etc.; e.g., see KNUTH, 1998; DEGROOT and SCHERVISH, 2002) in accordance to the appropriate scattering cross sections for each process induced by the considered charged particle. All these techniques use pseudo-random numbers uniformly distributed on the interval between 0 and 1.

The simulations performed with IONLYS consist in the generation of short high-energy proton (ion) *track segments* in water. The primary particle is simulated until it has penetrated the chosen length of the track segment into the medium. Note that, due to its large mass, the proton (or the impacting heavy ion) is almost not deflected by collisions with the target electrons. In the present simulations, these deflections are simply neglected. The use of small path segments is particularly useful as the instantaneous LET of the incident particle is nearly constant over such segments and can be varied simply by changing its energy. All of the produced energetic (dry) secondary electrons are explicitly transported spatially from their initial energies until they reach the subexcitation energy region below ~7.3 eV, the threshold assumed for electronic excitation in liquid.[12] The location, type of collision, specific quantum transition, and energy transferred are determined by the IONLYS code, event by event. All physical details about the various

---

[12]Recall here that most energy-loss events by the fast primary charged particle involve small transfers of energy. In fact, Monte-Carlo simulations have shown that the most probable energy loss for liquid water is 15-20 eV, while the track-averaged mean energy loss is around 50-60 eV, depending on the authors (LAVERNE and PIMBLOTT, 1995; COBUT *et al.*, 1998; AUTSAVAPROMPORN, 2006). COBUT *et al.* (1998) also calculated that, if we sum all the electrons ejected directly by the primary particle and by the successive generations of secondary electrons, 88% of them have kinetic energies less than 20 eV.

elastic and energy-loss processes involved and the corresponding scattering cross sections employed by IONLYS for the simulation can be found in COBUT (1993), COBUT *et al.* (1998), and MEESUNGNOEN and JAY-GERIN (2005*a*). The time that it takes a secondary electron to reach a subexcitation energy is $<10^{-15}$ s.

The thermalization of subexcitation electrons is treated by IONLYS using the distribution of thermalization distances obtained from Monte-Carlo track-structure calculations (GOULET and JAY-GERIN, 1989; GOULET *et al.*, 1990, 1996; MEESUNGNOEN *et al.*, 2002*b*) based on experimental scattering cross sections of slow (~1-100 eV) electrons in amorphous ice films at 14 K (MICHAUD *et al.*, 2003) with corrections to account for the liquid phase. Given the initial position of the subexcitation electron, its position is simply displaced in a randomly selected, isotropic direction by the corresponding, energy-dependent mean penetration distance. At this new position, the electron is regarded as thermalized and subsequently trapped and hydrated. However, an approximation likely to be valid in a highly polar medium such as liquid water in which very-low energy (e.g., "subvibrational") electrons have a strong tendency – due to the presence of a large density of possible electron trapping sites – to get instantly trapped prior to thermalization (MOZUMDER, 1999). As mentioned before, the time scale of thermalization, trapping, and hydration of a subexcitation electron in liquid water at 25 ºC is less than $\sim 10^{-12}$ s. Finally, it is worth recalling here that a certain proportion of subexcitation electrons actually never get thermalized, but instead undergo prompt recombination[13] with their positive parent ion $H_2O^{\bullet +}$ or dissociative attachment (DEA) onto

---

[13] About 25.5% of the subexcitation electrons are found to initially recombine with $H_2O^{\bullet +}$ (MEESUNGNOEN and JAY-GERIN, 2005*a*), with an average recombination time as short as a few femtoseconds (GOULET *et al.*, 1990). This average recombination time shows that the recombination process mainly occurs on the water cation and *not* on H_3O^+, that is, before the proton transfer reaction $H_2O^{\bullet +} + H_2O \rightarrow H_3O^+ + {}^{\bullet}OH$ takes place (~10 fs) (which would change the nature of the cation and therefore affect the values of the recombination cross section). In other words, the subexcitation electron recombines quickly (in the first steps of its random walk) on $H_2O^{\bullet +}$. If it does not recombine quickly, it will never

a surrounding H_2O molecule (see Figure 1.2). All details about the various parameters intervening in the IONLYS code to describe this competition between thermalization, geminate recombination, and dissociative attachment, as well as the values of the branching ratios used in the code for the different dissociative decay channels of the electronically and vibrationally excited H_2O molecules, can be found in (SANGUANMITH *et al.*, 2011*a*).

2.2 The IRT code

The complex spatial distribution of reactants at the end of the physicochemical stage (~10^{-12} s; we assume that this time also marks the beginning of diffusion), which is provided as an output of the IONLYS program, is then used directly as the starting point for the subsequent nonhomogeneous chemical stage. This third and final stage, during which the individual reactive species diffuse randomly at rates determined by their diffusion coefficients and react with one another (or with any added solutes present at the time of irradiation) until all spur or track processes are complete, is covered by the IRT program (CLIFFORD *et al.*, 1986; GREEN *et al.*, 1990; PIMBLOTT *et al.*, 1991). IRT is a computer efficient stochastic simulation technique that is used to simulate reaction times without following the trajectories of the diffusing species. This method is based on the approximation that the distances between pairs of reactants evolve independently of each other, and therefore the reaction times of the various potentially reactive pairs are independent of the presence of other reactants in the system. In essence, the simulation begins by considering the initial, or "zero-time", spatial distribution of the reactants (given by the IONLYS program). The separations between all the pairs of reactants are first calculated. Overlapping pairs (i.e., pairs formed in a reactive configuration) are assumed to combine immediately. For each remaining pair, a reaction time is stochastically sampled according to the reaction time probability distribution function (GREEN *et al.*, 1990;

---

recombine, and will thus become thermalized (unless, of course, it makes a dissociative attachment on a water molecule) (~56 fs), trapped (~50-300 fs), and hydrated (~240 fs-1 ps) (MEESUNGNOEN and JAY-GERIN, 2005*a*; JAY-GERIN *et al.*, 2008 and references therein).

GOULET and JAY-GERIN, 1992; FRONGILLO *et al.*, 1998) that is appropriate for the type of reaction considered. This function depends upon the initial distance separating the species, their diffusion coefficients, their Coulomb interaction (for reactions between ionic species), their encounter distance,[14] and the probability of reaction during one of their encounters. The competition between the various reactions is taken into account by realizing them in the ascending order of sampled reaction times. When a reaction occurs, the reactants become unavailable for the competing reactions that are sampled to occur at longer times but one must then consider the possible reactions of the newly formed products with the species that have survived up to that point. The minimum of the new ensemble of reaction times is the next reaction time. The simulation proceeds in this manner until a pre-defined cut-off time is reached or all the potentially reactive pairs have reacted. Since the IRT method is solely based on a comparison of reaction times, it does not follow the trajectories of the diffusing species. Therefore, a special procedure must be devised to sample the positions of the reaction products and of the species with which newly formed species can in turn react (CLIFFORD *et al.*, 1986). The inclusion of a scavenger in the system does not affect the general simulation technique. In fact, the IRT program allows one to incorporate in a simple way pseudo first-order reactions of the radiolytic products with various scavengers that are homogeneously distributed in the solution, such as H^+, OH^-, and H_2O itself, or more generally any solute for which the relevant reaction rates are known. Similarly, the truly first-order fragmentations of the species are easily simulated. Finally, the IRT method is very well suited for the description of reactions that are only partially diffusion-controlled (most reactions that occur in irradiated water are not diffusion-controlled even at room temperature), an adequate description of the activation processes that are involved in those reactions is a prerequisite for the modeling of the effects of high temperature on water radiolysis), in which the species do not react instantaneously on encounter but experience, on the average, many encounters and separations before they actually react with each other. The ability of the IRT method to give accurate time-dependent chemical yields under different irradiation

[14]The "encounter distance" ($a_{A,B}$) for each pair of interacting species A and B can be derived from the Smoluchowski equation.

conditions has been well validated by comparison with full random flights (or "step-by-step") Monte-Carlo simulation, which does follow the particle trajectories in detail (PIMBLOTT *et al.*, 1991 and references cited therein; GOULET *et al.*, 1998; PLANTE, 2009).

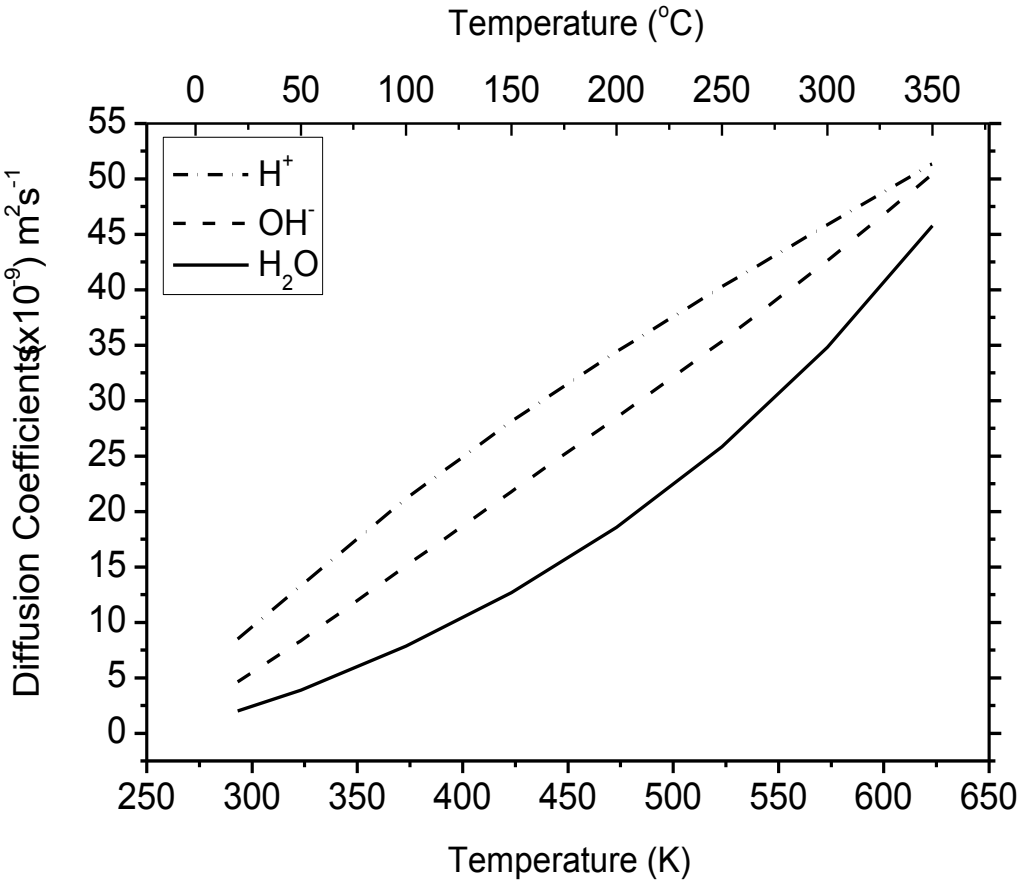

Figure 2.1 Diffusion coefficients (D) for the various track species involved in our simulations (ELLIOT and BARTELS, 2009).

An approximate dependence of the diffusion coefficient on temperature in liquids can often be found using Stokes–Einstein equation (STUART, 2009), which predicts that

$$\frac{D_{T1}}{D_{T2}} = \frac{T_1}{T_2}\frac{\mu_{T2}}{\mu_{T1}} \qquad (26)$$

where

T_1 and T_2 denote temperatures 1 and 2, respectively

D is the diffusion coefficient (cm^2/s)

T is the absolute temperature (K),

μ is the dynamic viscosity of the solvent (Pa·s)

Compared to the original version of our IRT program some diffusion coefficients (D) of reactive species and temperature dependence of reaction rate constants have been updated. Figure 2.1 shows the diffusion coefficients of various species as a function of temperature which has been updated in our Monte-Carlo simulations. The list of the main spur/track chemical reactions and values of reaction rate constants considered in our pure liquid water radiolysis simulations as a function of temperature is taken from the report compiled by ELLIOT and BARTELS (2009).

As mentioned previously, fast neutrons impinging on liquid water at incident energies less than ~10 MeV generate primarily energetic protons and to a smaller extent oxygen ion recoils. For example, the first four recoil protons generated by a 2-MeV neutron have energies of 1.264, 0.465, 0.171, and 0.063 MeV, which had, at 25 °C, linear energy transfers (LETs) of 22, 43, 69, and 76 keV/μm, respectively. To reproduce the effects of fast-neutron radiolysis on the yields of the various radiation-induced species in neutral liquid water, we simulate short (~15-100 μm) track segments of each of those generated recoil protons. Over such simulated track segments, the energy and LET of the protons are well defined and remain nearly constant. Such model calculations thus give track segment yields at a well-defined LET. To be well compared between the simulation predictions with experimental radiation chemical yields, it is high demanded the summation of a series of segments for different incident energy, called integral yields. The integral yields increase with increasing energy of particle because the decreased density of radiation in the track. In this work, the number of proton histories (usually ~10-150, depending on the proton energy) is chosen so as to ensure only small statistical fluctuations in the computed averages of chemical yields, while keeping acceptable computer time limits.

2.3 Simulation of the effect of temperature

In this work, we use an extended version of our Monte Carlo computer code which was developed previously to include the effects of high temperature (from 25 up to 350 ºC) on water radiolysis at high LET (HERVE DU PENHOAT *et al.*, 2001; MEESUNGNOEN *et* al., 2001; MEESUNGNOEN *et al.*, 2002; SANGUANMITH *et al.*, 2011*a,b*). Briefly, the scattering cross sections used in the simulations are independent of the medium's temperature because the energy of the ionizing particles is much larger than the thermal energies and because the motion of the target (water molecules) can be neglected. The influence of temperature on the physical stage of radiation action is thus mainly due to the fact that temperature brings the water molecules further apart without changing their ability to interact with the ionizing particles. For example, the density (ρ) of pressurized water varies with temperature (from ρ = 1 g/cm^3 at room temperature to ρ = 0.575 g/cm^3 at 350 ^{o}C), and this influences the particles scattering mean free paths (MFP) which are related to the scattering cross sections through the simple relation MFP = 1/(σ*N*), where σ is the total cross section and *N* is the number of scatterers per unit volume. The 42.5% decrease in *N* that takes place when the temperature is increased from 25-350 ^{o}C thus causes the energy depositions to become significantly further apart. As a result of the invariance of the scattering cross sections, this dilatation is proportional to the inverse of the density.

In the "physicochemical" stage, the influence of the temperature is not well understood. It looks like many parameters intervening in this stage (such as the dissociative decay channels for H_2O^*, the migration of the ions H_2O^+ and of the subexcitation electrons) are feasible sensitive with temperature. SWIATLA-WOJCIK and BUXTON (1995) have suggested that the temperature could possibly change the relative contributions of the dissociative decay channels for H_2O^* through a diminution of hydrogen bonding in liquid water. First of all, the variations of density would act as they did in the physical stage, increasing (on average) each step of the random walk. But any number of other phenomena could come into play. For example, when a "hot" (subvibrational) electron is slowing down before eventually getting trapped, it goes through a stage during which its energy is nearly thermal, so that it cannot only lose energy but also gain some from the surrounding

medium. If the duration of this quasi-equilibrium stage depends on temperature, it could affect the electron thermalization distances.

The influence on the scattering cross section of the low-energy electrons is another temperature effect in the physicochemical stage. In fact, electrons in the subexcitation energy range are known to be sensitive to the structural order of the surrounding medium, owing to their noneglible delocalized character. In various media, their scattering cross-sections have been shown to increase rapidly when the degree of order diminishes (HERVÉ DU PENHOAT *et al.*, 2000 and references cited therein). This also seems to be the case for water, since the electron cross sections found in amorphous ice at low incident energy (MICHAUD and SANCHE, 1987) appear to be somewhat smaller (by a factor of ~2) than those that apply to liquid water (COBUT *et al.*, 1998; GOULET *et al.*,1996) and much smaller (by at least an order of magnitude) than those reported for the gas phase (MICHAUD and SANCHE, 1987). One could expect the scattering cross sections of subexcitation electrons to increase with temperature in the range 25-350 ^{o}C, since the breaking of the hydrogen bonds gives rise to a decrease of the structural order. It is difficult to estimate to what extent this could affect thermalization distances, but one cannot exclude the possibility that this effect could overcome the 42.5% decrease in the density as temperature increases from 25-350 ^{o}C and in turn reduce those distance significantly. A similar conclusion was obtained previously by HOCHANADEL and GHORMLEY (1962), who suggested that, at higher temperature, "subexcitation electrons are thermalized more rapidly". And it seems that, our simulations are better to reproduce the experimental yields if the electron thermalization distances decrease with increasing temperature.

In the "nonhomogeneous chemical" stage, the radiolytic species, that formed at the end of the "physicochemical" stage, diffuse and react with one another with a kinetic ruled by their initial nonhomogeneous spatial distribution. At room temperature, this nonhomogeneous stage is primarily completed at the end of spur expansion time. It should be noted that the time at the end of spur is dependent on temperature.

Some chemical reactions can occur before start of any diffusion of species because they are formed already "in contact" at the end of the physicochemical stage (COBUT *et al.*, 1998; FRONGILLO *et al.*, 1998). To simplify, we consider that those "contact reactions" occur at ~10^{-12} s (i.e., the starting point of the nonhomogeneous kinetics). The incidence of

other reactions depends on the ability of reactants to meet and react; noted that most reactions are not diffusion-controlled. The physical parameters that will determine the time-dependent reaction probability of a pair of reactants such as (i) their initial separation, (ii) their diffusion coefficient, (iii) their electrostatic interaction (i.e., their charge and the dielectric constant of the medium), (iv) their reaction radius, and (v) their probability of reaction per encounter. The temperature of the medium has an influence on many of those parameters. The effect of temperature on the initial position of the species comes from the temperature dependence of the scattering mean free paths mentioned in the first two stages. Its influence on the diffusion coefficient depends on the actual species considered, but this parameter always increases with temperature. In the simulation, the temperature dependences of the diffusion coefficients of H_3O^+, OH^-, e^-_{aq}, and H_2O are represented by polynomial fits to the experimental data (ELLIOT and BARTELS, 2009). For the other species, whose diffusion coefficients are unknown at elevated temperatures, the following scaling procedure has been adopted:

$$D_I(t)=D_I(25^\circ C)+\frac{D_{H_2O}}{D_{H_2O}(25^\circ C)} \qquad (27)$$

where t denotes the temperature in degrees Celsius and I denotes the specie.

Rate constants are known as sensitive functions of temperature and for this reason are important parameters in predictive modeling of high-temperature water chemistry. Temperature dependence of the "observed" reaction rate constant (k_{obs}) is known, then it is possible to extract information on the temperature dependences of the "activation" and "diffusion" processes that are involved in the reaction. For those reactions whose rates are nearly diffusion-controlled at room temperature, k_{obs} is best described by the Noyes equation:

$$\frac{1}{k_{obs}} = \frac{1}{k_{diff}} + \frac{1}{k_{act}} , \qquad (28)$$

where k_{diff} is the rate constant for a truly diffusion-controlled reaction and k_{act} is the rate constant that would be measured if diffusion had no influence on the reaction rate (NOYES, 1961). A number of reactions pertinent to the radiation chemistry of water have

been found to be best described by Eq. (27) (see, for example: ELLIOT, 1994). The Arrhenius equation is used to evaluate k_{act} empirically:

$$k_{act} = A\exp(E_{act}/RT) \,, \tag{29}$$

where E_{act} is the activation energy of the process, A is referred to as the pre-exponential factor, R is the gas constant and T is the absolute temperature. k_{diff} is given by the Smoluchowski equation (see, for example: ELLIOT *et al.*, 1990; ELLIOT, 1994; SWIATLA-WOJCIK and BUXTON, 1995; HERVÉ DU PENHOAT *et al.*, 2000):

$$k_{diff} = 4\pi\beta\, N_{Av}\, (D_A + D_B)\, a_{A,B} \tag{30}$$

where N_{Av} is Avogadro's number, $(D_A + D_B)$ is the sum of diffusion coefficients for both reacting species, β is a spin statistical factor for radical-radical reactions, and $a_{A,B}$ is the encounter (or reaction) distance. When the reactants are ions, Eq. (28) is multiplied by the Debye factor (DEBYE, 1942):

$$f_D = \frac{\delta}{e^{\delta} - 1} \tag{31}$$

where δ is given by

$$\delta = \frac{Z_A\, Z_B\, e^2}{4\pi\,\varepsilon_o\;\varepsilon(T)\, a_{A,B}\; k_B T} \,, \tag{32}$$

where Z_A and Z_B are the charges on the ions, e is the electron charge, ε_o is the permittivity of free space, $\varepsilon(T)$ is the dielectric constant of the medium at temperature T, and k_B is Boltzmann's constant.

To reproduce the effect of temperature on the fast neutron radiolysis of water from ambient up to 350 °C, we used an extended version of our IONLYS-IRT code which was developed previously (HERVÉ DU PENHOAT *et al.*, 2000; TIPPAYAMONTRI *et al.*, 2009; SANGUANMITH *et al.*, 2011*a*). In this version, we used the self-consistent radiolysis database, including rate constants, diffusion coefficients, reaction mechanisms, and *g*-values, compiled by ELLIOT and BARTELS (2009). This new database provides a recommendation for the best values to use in high-temperature modeling of water radiolysis

up to 350 °C. All Monte-Carlo simulations reported here were performed along the liquid-vapor coexistence curve, the density of the pressurized water decreasing from 1 g/cm^3 (1 bar or 0.1 MPa) at 25 °C to 0.575 g/cm^3 (16.5 MPa) at 350 °C (LINSTROM and MALLARD, 2005). For this range of temperature, calculations show that *g*-values vary only little with the applied pressure.

3. ARTICLE 1

ON THE TEMPERATURE DEPENDENCE OF THE RATE CONSTANT OF THE BIMOLECULAR REACTION OF TWO HYDRATED ELECTRONS

Authors: **S.L. Butarbutar**, Y. Muroya, L. Mirsaleh Kohan, S. Sanguanmith, J. Meesungnoen, J.-P. Jay-Gerin

Status: published in *Atom Indonesia Vol. 39 No. 2 (2013) 51-56*

Foreword: This study focus on the investigation of the unexpected a downward discontinuity at ~150 °C of $G(H_2)$ exhibited in our calculation of the radiolysis of water by *fast* (2 MeV) *neutrons* (which produce high-LET recoil protons and oxygen ions) that are similar to that observed at our previous work for low LET. Closer examination revealed that this discontinuity was due, here again, to the abrupt drop in the (e^-_{aq} + e^-_{aq}) reaction rate constant above 150 °C used in the simulations. In this work we validate our simulation results with the only experimental work of Elliot *et al.* (1996b) reporting the temperature dependence (up to 180 °C) of $g(H_2)$ for the radiolysis of water at high LET. This experimental work apparently showed no abrupt drop on H_2 yields. By this work, we believe that the applicability of the sudden drop in the (e^-_{aq} + e^-_{aq}) reaction rate constant observed at ~150 °C in alkaline water to *neutral* or *slightly acidic* remain uncertain and should be examined further. I performed all the calculations, plotting the figures. Finally, I had a significant contribution to the main idea of this work and to all the preparation process for the first version of this article.

Résumé: Cette étude porte sur la discontinuité inattendue à la baisse à ~150 °C de $g(H_2)$ montrée dans notre calcul de la radiolyse de l'eau par des neutrons rapides (2 MeV) (produisant des protons de recul et des ions d'oxygène de haute TEL) étant similaire à celle observée dans notre travail précédent à bas TEL. Un examen plus approfondi a révélé que cette discontinuité est due, là encore, à la chute brutale de la constante de vitesse de réaction supérieure à 150 °C utilisée dans les simulations de (e^-_{aq} + e^-_{aq}). Dans ce travail, nous validons nos résultats de simulation avec le seul travail expérimental rapportant la dépendance de la température (jusqu'à 180°C) de $g(H_2)$ pour la radiolyse de l'eau à haut TEL publié par Elliot *et al.* (1996b). Ce travail expérimental a montré qu'il n'y a apparemment pas de chute brutale des rendements de H_2. Par ce travail, nous pensons que l'applicabilité de la chute soudaine de la constante de vitesse de réaction (e^-_{aq} + e^-_{aq}) observée à ~150 °C dans l'eau alcaline à neutre ou légèrement acide demeure incertaine et devrait être examinée plus en profondeur. J'ai effectué tous les calculs, tracer la figure. Enfin, j'ai eu une contribution significative à l'idée principale de ce travail et à tout le processus de préparation de la première version de cet article.

On the Temperature Dependence of the Rate Constant of the Bimolecular Reaction of Two Hydrated Electrons

S.L. Butarbutar[1,2], Y. Muroya[3], L. Mirsaleh Kohan[1], S. Sanguanmith[1], J. Meesungnoen[1], J.-P. Jay-Gerin[1]*

[1]Département de médecine nucléaire et de radiobiologie, Faculté de médecine et des sciences de la santé, Université de Sherbrooke, 3001, 12[e] Avenue Nord, Sherbrooke (Québec) J1H 5N4, Canada.

[2]Center for Reactor Technology and Nuclear Energy Agency (BATAN), Kawasan Puspiptek, Serpong, Tangerang 15314, Indonesia.

[3]Institute of Scientific and Industrial Research (ISIR), Osaka University, Mihogaoka 8-1, Ibaraki, Osaka 567-0047, Japan.

*Corresponding author (e-mail: jean-paul.jay-gerin@USherbrooke.ca)

Atom Indonesia Vol. 39 No. 2 (2013) 51-56

ABSTRACT

It has been a longstanding issue in the radiation chemistry of water that, even though H_2 is a molecular product, its "escape" yield $g(H_2)$ increases with increasing temperature. A main source of H_2 is the bimolecular reaction of two hydrated electrons (e^-_{aq}). The temperature dependence of the rate constant of this reaction (k_1), measured under *alkaline* conditions, reveals that the rate constant drops abruptly above ~150 °C. Recently, it has been suggested that this temperature dependence should be regarded as being independent of pH and used in high-temperature modeling of *near-neutral* water radiolysis. However, when this drop in the e^-_{aq} self-reaction rate constant is included in low (isolated spurs) and high (cylindrical tracks) linear energy transfer (LET) modeling calculations, $g(H_2)$ shows a marked downward discontinuity at ~150 °C which is *not* observed experimentally. The consequences of the presence of this discontinuity in $g(H_2)$ for both low and high LET radiation are briefly discussed in this communication. It is concluded that the applicability of the sudden drop in k_1 observed at ~150 °C in alkaline water to near-neutral water is questionable and that further measurements of the rate constant in pure water are highly desirable.

Key words: Water radiolysis, high temperature, self-reaction of the hydrated electron, rate constant, yield of H_2, linear energy transfer (LET), Monte Carlo track chemistry calculations.

In nuclear power plants (NPPs), water is used as both a coolant and neutron moderator. Over the operating temperature range of 275-325 °C, water is irradiated heavily in the reactor core by some mixture of fast electrons and recoil ions of hydrogen and oxygen, which have characteristically different linear energy transfer (LET) values (in the range from ~0.3 to 40-60 keV/μm, respectively). This irradiation results in the chemical decomposition (radiolysis) of water and leads to the formation of the short-lived reactive radicals e^-_{aq} (hydrated electron), $H^\bullet$, $^\bullet OH$, and $HO_2^\bullet$ (or $O_2^{\bullet-}$, depending on pH) and the longer-lived molecular products H_2 and H_2O_2 (and eventually O_2). These species can promote corrosion, cracking, and hydrogen pickup both in the core and in the associated piping components of the reactor [1-5].

Theoretical calculations and chemical models of the radiation chemistry of water in the reactor core require the radiolytic yields (defined as the number of species formed or destroyed per 100 eV of energy absorbed [6,7]) of the primary species for both fast neutrons and γ-radiation. The rate constants for *all* of the reactions involving these species are also required. The yields and chemical kinetic data for high-temperature light water radiolysis, up to 350 °C, have recently been compiled and reviewed by Elliot and Bartels [8].

For water at neutral or near-neutral pH under low-LET radiation (such as ^{60}Co γ-rays and fast electrons), the *primary* (or "escape") yields (commonly denoted *g*-values) of the free radicals e^-_{aq}, $H^\bullet$, and $^\bullet OH$ continuously increase when the temperature is increased, while the primary yield of H_2O_2 decreases [8,9]. Although H_2 is a molecular product, $g(H_2)$ increases monotonically with temperature, particularly above 200 °C [8-13]. H_2, whose formation is favored by fast neutron (high-LET recoil-ion) radiolysis [4], is an important component associated with the corrosion environment of the coolant system in NPPs. Knowledge of the production of H_2 from irradiated water and the amount of "excess" H_2 to be added to the primary coolant to mitigate water decomposition and O_2 production is crucial to develop better reactor chemistry control and to optimize plant performance [14-16].

In the γ-radiolysis of water, there are several different mechanisms for the production of molecular hydrogen. Recent studies have shown that a major fraction of the total H_2 formed [$g(H_2)$ = 0.45 molecule/100 eV at 25 °C (for conversion into SI units, 1

molecule per 100 eV ≈ 0.10364 μmol J^{-1})] is due to reactions involving the precursors of the hydrated electron at short (< 1 ps) times after the initial passage of the radiation [17,18]. These reactions include the dissociation of excited water molecules formed by recombination of the nonhydrated electron with its parent cation $H_2O^{\bullet+}$ (geminate recombination) and the dissociative attachment of subexcitation-energy electrons (those that have kinetic energies lower than the first-electronic excitation threshold of the medium, i.e., ~7.3 eV in liquid water) to a water molecule (DEA) [19]. Most of the rest of the formation of H_2 is due to the following combination reactions between e^-_{aq} and $H^\bullet$ atoms during spur/track expansion (typically, on time scales from ~1 ps to 1 μs) [6-8,10]:

$$e^-_{aq} + e^-_{aq} + 2\ H_2O \rightarrow H_2 + 2\ OH^- \qquad \text{(R1)}$$

$$e^-_{aq} + H^\bullet + H_2O \rightarrow H_2 + OH^- \qquad \text{(R2)}$$

$$H^\bullet + H^\bullet \rightarrow H_2 \qquad \text{(R3)}$$

and (above ~200 °C) [9,15,20-22]

$$H^\bullet + H_2O \rightarrow H_2 + {}^\bullet OH \qquad \text{(R4)}$$

The new self-consistent radiolysis database of Elliot and Bartels [8] provides recommendations for the best values to use to model water radiolysis at temperatures up to 350 °C. Of particular significance, the rate constant for the self-reaction of e^-_{aq} (R1) (k_1), measured in *alkaline* water [23-27], exhibits a "catastrophic" drop between 150 and 200 °C and, above 250 °C, is too small to be measured reliably [8,27]. The mechanism behind this non-Arrhenius behavior above 150 °C is not well understood, but it is generally thought to involve the formation of some transient intermediate, such as a hydrated electron dimer (or "dielectron", $e_2^{2-}{}_{aq}$) sharing the same solvent cavity, a hydride ion (H^-), or yet an "incompletely relaxed" localized electron (e^-_{ir}) [23,27-29]. The applicability of this drop in k_1 above 150 °C to *neutral* solution, however, has long been a subject of discussion because it could be a function of the pH of the solution [24]. For example, in a report published in 2002, Stuart *et al.* [26] wrote, "It still needs to be established whether there is a turnover of the rate constant in neutral solution". In fact, up to now, most computer modelers of the radiolysis of water at high temperatures have employed, in neutral solution, an Arrhenius

extrapolation previously proposed by Elliot [24] and Stuart *et al.* [26]. This approach assumes that such an abrupt change in k_1 does *not* occur and that reaction (R1) is diffusion controlled at temperatures greater than 150 °C. This assumption was justified by the good agreement obtained between models and experiment [30-33].

However, in recent reports (and personal communication), Bartels and coworkers [8,27] emphasized that the measured temperature dependence of the (R1) reaction rate constant in alkaline solution should, in fact, be regarded as *independent* of pH and thus used in high-temperature modeling of near-neutral water radiolysis. As predicted earlier, including the drop in k_1 above 150 °C in deterministic diffusion-kinetic modeling calculations [30,31,34] and in Monte Carlo simulations [9,32,33] resulted in a sharp downward discontinuity in $g(H_2)$, which is *not* observed experimentally. Figure 1 illustrates the simulation results of $g(H_2)$ as a function of temperature as obtained recently by our group at the Université de Sherbrooke [9]. Indeed, above ~150 °C the calculations predict a decrease in $g(H_2)$ instead of the observed increase.

To obtain acceptable fits of our calculated values of $g(H_2)$ to the experimental data above 150 °C, we had to adjust the temperature dependence of certain parameters involved in the early ($<10^{-12}$ s) "physicochemical stage" [35] of radiolysis, *i.e.*, the thermalization distance of subexcitation-energy electrons (r_{th}), the DEA [19,36,37], and the branching ratios of the different excited water molecule decay channels [9]. Interestingly, $g(H_2)$ was found to be the yield most sensitive to r_{th}. In fact, *to compensate* for the decrease of k_1, a sharp decrease of r_{th} above ~100-150 °C had to be included in the simulations. This decrease in r_{th} was supposed to be the signature of an increase in the scattering cross sections of subexcitation electrons probably reflecting a rapid deterioration in the degree of structural order of water (due to increased breaking of hydrogen bonds) at these temperatures (these subexcitation electrons are known to be very sensitive to the structural order of the surrounding medium, owing to their non-negligible delocalized character) [9,32]. Despite the lack of clear experimental evidence for such a change in the topology of intermolecular hydrogen bonding in water above 150 °C, very good agreement was found under these conditions between simulated and experimental $g(H_2)$, and the sharp downward discontinuity predicted at 150 °C (Fig. 1) no longer appeared (see dotted line in Fig. 2) [9].

Recently, however, in the course of a Monte Carlo simulation study of the radiolysis of water by *fast* (2 MeV) *neutrons* (which produce high-LET recoil protons and oxygen ions) [38], our calculations showed, somewhat unexpectedly, that $g(H_2)$ exhibited a downward discontinuity at ~150 °C similar to that observed at low LET (Fig. 1). Closer examination revealed that this discontinuity was due, here again, to the abrupt drop in the $(e^-_{aq} + e^-_{aq})$ reaction rate constant above 150 °C used in the simulations. Unfortunately, the large amount of scatter in the experimental neutron radiolysis H_2 yield data and also their limited availability could not allow us to determine whether or not the predicted discontinuity at 150 °C was confirmed experimentally.

The recurrence of this discontinuity of $g(H_2)$ at ~150 °C in the case of the radiolysis of water by fast neutrons prompted us to further investigate the influence of *high-LET radiation*. To our knowledge, the only experimental work reporting the temperature dependence (up to 180 °C) of $g(H_2)$ for the radiolysis of water at high LET is that of Elliot *et al.* [39] (23-MeV $^2H^+$ and 157-MeV $^7Li^{3+}$ ions, with dose-average LETs of ~11.9 and 62.3 keV/μm, respectively [40]). Judging from the results of these authors (see Table 2 of [39]), there is apparently *no* evidence of a discontinuity in $g(H_2)$ at ~150 °C (note that measurements were made at three temperatures only: 25, 95, and 180 °C for both studied ions) (Fig. 2). However, as for the 2-MeV neutron radiolysis of water and as can clearly be seen from Fig. 2, our simulations of Elliot *et al.*'s experiments (using our IONLYS Monte Carlo simulation code under these particular experimental conditions [41,42]) do reveal the presence of a pronounced discontinuity in $g(H_2)$ at ~150 °C whose magnitude increases as the LET increases.

At low LET, we could compensate for the decrease in $g(H_2)$ predicted by the calculations (instead of the observed increase) by modifying the temperature dependence of r_{th} (and invoking a change in the structure of water at ~150 °C), whereas at high LET this compensation is, at first sight, no longer straightforward. Briefly, this happens because the number of self-reactions of e^-_{aq} that occur in tracks greatly increases with increasing LET. This means that the influence of the abrupt drop in k_1, which is at the origin of the $g(H_2)$ discontinuity, becomes increasingly important as the LET increases. Eventually, it will outweigh the compensation that was made at low LET, where the number of reactions (R1) in spurs is comparatively much less, thereby allowing the discontinuity of $g(H_2)$ at 150 °C

to reappear. A confirmation of these results is offered by the deterministic calculations of Swiatla-Wojcik and Buxton [31] who also modeled Elliot *et al.*'s experiments [39] but without including the drop in k_1 at 150 °C; reasonable agreement between the model and experiment was obtained and *no* discontinuity in $g(H_2)$ at 150 °C was observed (see Fig. 1 of [31]).

Under such high-LET conditions, it seems rather difficult, if not impossible, to further modify the temperature dependence of r_{th} (as we did at low LET) in order to counterbalance the effect of the drop in k_1 and obtain acceptable fits of our calculated yields to experimental data. It is, indeed, hardly conceivable that r_{th} would be a function of the LET of the radiation, unless one considers the effects of local temperature increases associated with "thermal spikes" that have sometimes been proposed to occur in the tracks of heavy ions [43-45]).

Based on the above findings and in accordance with previous studies [24,26,30-33], we believe that the applicability of the sudden drop in the ($e^-_{aq} + e^-_{aq}$) reaction rate constant observed at ~150 °C in alkaline water to *neutral* or *slightly acidic* (as the pH of water at 150-200 °C is about 5.7-6 [2]) solution, as proposed by Bartels and coworkers [8,27], remain uncertain and should be examined further.

Considering the importance of the self-reaction of e^-_{aq} as a main source of molecular hydrogen in high-temperature water radiolysis, further measurements of its rate constant in pure water are obviously highly desirable. These measurements, which would be extremely beneficial to the modeling community [46], would generate valuable insight for better understanding and predicting reactor coolant water chemistry in NPPs.

ACKNOWLEDGMENTS

We thank Dr. A. John Elliot, Dr. Craig R. Stuart, Professor Yosuke Katsumura, Professor Mingzhang Lin, and Professor David M. Bartels for a number of helpful discussions and correspondence. Financial assistance from Atomic Energy of Canada Limited, the Natural Sciences and Engineering Research Council of Canada, and Natural Resources Canada is gratefully acknowledged.

REFERENCES

[1]. W.G. Burns and P.B. Moore, Radiat. Effects **30** (1976) 233.

[2]. P. Cohen, Water Coolant Technology of Power Reactors, American Nuclear Society, La Grange Park, Illinois (1980).

[3]. G.R. Sunaryo, Y. Katsumura, D. Hiroishi and K. Ishigure, Radiat. Phys. Chem. **45** (1995) 131.

[4]. D.R. McCracken, K.T. Tsang and P.J. Laughton, *Aspects of the Physics and Chemistry of Water Radiolysis by Fast Neutrons and Fast Electrons in Nuclear Reactors*, Report AECL-11895, Atomic Energy of Canada Limited, Chalk River, Ontario, Canada (1998).

[5]. H. Christensen, *Fundamental Aspects of Water Coolant Radiolysis*, SKI Report 2006:16, Swedish Nuclear Power Inspectorate, Stockholm, Sweden (2006).

[6]. J.W.T. Spinks and R.J. Woods, An Introduction to Radiation Chemistry, 3rd ed., Wiley, New York (1990).

[7]. C. Ferradini and J.-P. Jay-Gerin, Can. J. Chem. **77** (1999) 1542.

[8]. A.J. Elliot and D.M. Bartels, *The Reaction Set, Rate Constants and g-Values for the Simulation of the Radiolysis of Light Water over the Range 20 to 350 °C Based on Information Available in 2008*, Report AECL No. 153-127160-450-001, Atomic Energy of Canada Limited, Chalk River, Ontario, Canada (2009).

[9]. S. Sanguanmith, Y. Muroya, J. Meesungnoen, M. Lin, Y. Katsumura, L. Mirsaleh Kohan, D.A. Guzonas, C.R. Stuart and J.-P. Jay-Gerin, Chem. Phys. Lett. **508** (2011) 224, and references therein.

[10]. A.J. Elliot, M.P. Chenier and D.C. Ouellette, J. Chem. Soc. Faraday Trans. **89** (1993) 1193.

[11]. D. Janik, I. Janik and D.M. Bartels, J. Phys. Chem. A **111** (2007) 7777.

[12]. G.R. Sunaryo, Y. Katsumura, D. Hiroishi and K. Ishigure, Radiat. Phys. Chem. **45** (1995) 131.

[13]. M.C. Kent and H.E. Sims, *The Yield of γ-Radiolysis Products from Water at Temperatures up to 300 °C*, Proceedings of the 6th International Conference on Water

Chemistry of Nuclear Reactor Systems, British Nuclear Energy Society, London, UK (1992) 153.

[14]. C.C. Lin, Radiochemistry in Nuclear Power Reactors, Nuclear Science Series NAS-NS-3119, National Academy Press, Washington, D.C. (1996).

[15]. C.D. Alcorn, J.-Cl. Brodovitch, K. Ghandi, A. Kennedy, P.W. Percival and M. Smith, *Kinetics of the Reaction between $H^{\bullet}$ and Superheated Water Probed with Muonium*, Proceedings of the 5th International Symposium on Supercritical-Water-Cooled Reactors, Vancouver, British Columbia, Canada (2011).

[16]. D.M. Bartels, J. Henshaw and H.E. Sims, Radiat. Phys. Chem. **82** (2013) 16.

[17]. B. Pastina, J.A. LaVerne and S.M. Pimblott, J. Phys. Chem. A **103** (1999) 5841.

[18]. J.A. LaVerne and S.M. Pimblott, J. Phys. Chem. A **104** (2000) 9820.

[19]. V. Cobut, J.-P. Jay-Gerin, Y. Frongillo and J.P. Patau, Radiat. Phys. Chem. **47** (1996) 247.

[20]. G.R. Sunaryo, Y. Katsumura and K. Ishigure, Radiat. Phys. Chem. **45** (1995) 703.

[21]. D. Swiatla-Wojcik and G.V. Buxton, Radiat. Phys. Chem. **74** (2005) 210.

[22]. D.M. Bartels, Radiat. Phys. Chem. **78** (2009) 191.

[23]. H. Christensen and K. Sehested, J. Phys. Chem. **90** (1986) 186.

[24]. A.J. Elliot, *Rate Constants and g-Values for the Simulation of the Radiolysis of Light Water over the Range 0-300 °C*, Report AECL-11073, Atomic Energy of Canada Limited, Chalk River, Ontario, Canada (1994).

[25]. A.J. Elliot, D.C. Ouellette and C.R. Stuart, *The Temperature Dependence of the Rate Constants and Yields for the Simulation of the Radiolysis of Heavy Water*, Report AECL-11658, Atomic Energy of Canada Limited, Chalk River, Ontario, Canada (1996).

[26]. C.R. Stuart, D.C. Ouellette and A.J. Elliot, *Pulse Radiolysis Studies of Liquid Heavy Water at Temperatures up to 250 °C*, Report AECL-12107, Atomic Energy of Canada Limited, Chalk River, Ontario, Canada (2002).

[27]. T.W. Marin, K. Takahashi, C.D. Jonah, S.D. Chemerisov and D.M. Bartels, J. Phys. Chem. A **111** (2007) 11540.

[28]. C. Ferradini and J.-P. Jay-Gerin, Radiat. Phys. Chem. **41** (1993) 487.

[29]. K.H. Schmidt and D.M. Bartels, Chem. Phys. **190** (1995) 145.

[30]. D. Swiatla-Wojcik and G.V. Buxton, J. Phys. Chem. **99** (1995) 11464.

[31]. D. Swiatla-Wojcik and G.V. Buxton, J. Chem. Soc., Faraday Trans. **94** (1998) 2135.

[32]. M.-A. Hervé du Penhoat, T. Goulet, Y. Frongillo, M.-J. Fraser, Ph. Bernat and J.-P. Jay-Gerin, J. Phys. Chem. A **104** (2000) 11757.

[33]. T. Tippayamontri, S. Sanguanmith, J. Meesungnoen, G.R. Sunaryo and J.-P. Jay-Gerin, Recent Res. Devel. Physical Chem. **10** (2009) 143.

[34]. J.A. LaVerne and S.M. Pimblott, J. Phys. Chem. **97** (1993) 3291.

[35]. R.L. Platzman, The Vortex **23** (1962) 372.

[36]. T. Goulet and J.-P. Jay-Gerin, Radiat. Res. **118** (1989) 46.

[37]. A. Mozumder, Fundamentals of Radiation Chemistry, Academic Press, San Diego, California, 1999.

[38]. S.L. Butarbutar, S. Sanguanmith, J. Meesungnoen, G.R. Sunaryo and J.-P. Jay-Gerin, *Calculation of the Yields for the Primary Species Produced in Liquid Water by Fast Neutron Radiolysis at Temperatures between 25 and 350 °C*, Proceedings of the 6th International Symposium on Supercritical Water-Cooled Reactors, Shenzhen, Guangdong, China (2013).

[39]. A.J. Elliot, M.P. Chenier, D.C. Ouellette and V.T. Koslowsky, J. Phys. Chem. **100** (1996) 9014.

[40]. D.E. Watt, Quantities for Dosimetry of Ionizing Radiations in Liquid Water, Taylor & Francis, London, UK (1996).

[41]. J. Meesungnoen and J.-P. Jay-Gerin, J. Phys. Chem. A **109** (2005) 6406.

[42]. J. Meesungnoen and J.-P. Jay-Gerin, *Radiation Chemistry of Liquid Water with Heavy Ions: Monte Carlo Simulation Studies*, Charged Particle and Photon Interactions with Matter: Recent Advances, Applications, and Interfaces, Y. Hatano, Y. Katsumura and A. Mozumder (Eds.), Taylor & Francis, Boca Raton, Florida (2011), 355.

[43]. A. Norman, Radiat. Res. Suppl. **7** (1967) 33.

[44]. R.E. Apfel, Y.Y. Sun and R. Nath, Radiat. Res. **131** (1992) 124.

[45]. J.A. LaVerne, Radiat. Res. 153 (2000) 487.

[46]. P. Causey and C.R. Stuart, Test Plan for Pulse Radiolysis Studies of Water at High Temperature and Pressure, Report AECL No. 217-127160-TP-001, Atomic Energy of Canada Limited, Chalk River, Ontario, Canada (2011).

FIG. 1

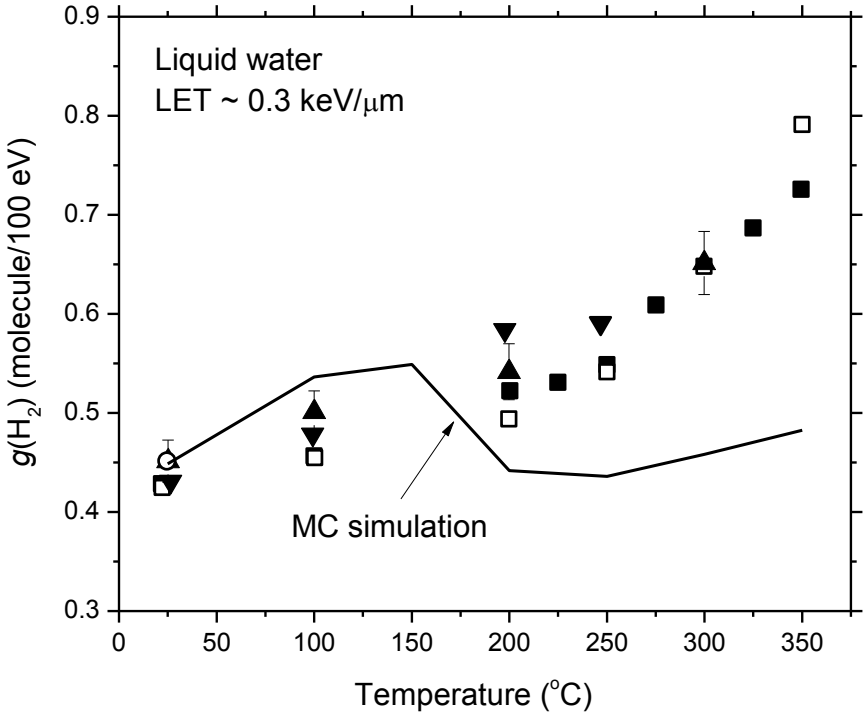

Fig. 1.Temperature dependence of the *primary* yield of H_2 in the low-LET radiolysis of water. The solid line shows the values of $g(H_2)$ obtained from our Monte Carlo simulations when the drop in the rate constant for the self-reaction of e^-_{aq} above 150 °C is included in the calculations [9]. The predicted $g(H_2)$ shows a marked inflection around 150-200 °C, which is *not* observed experimentally. Symbols are experimental data [6,8,10,11,20].

FIG. 2

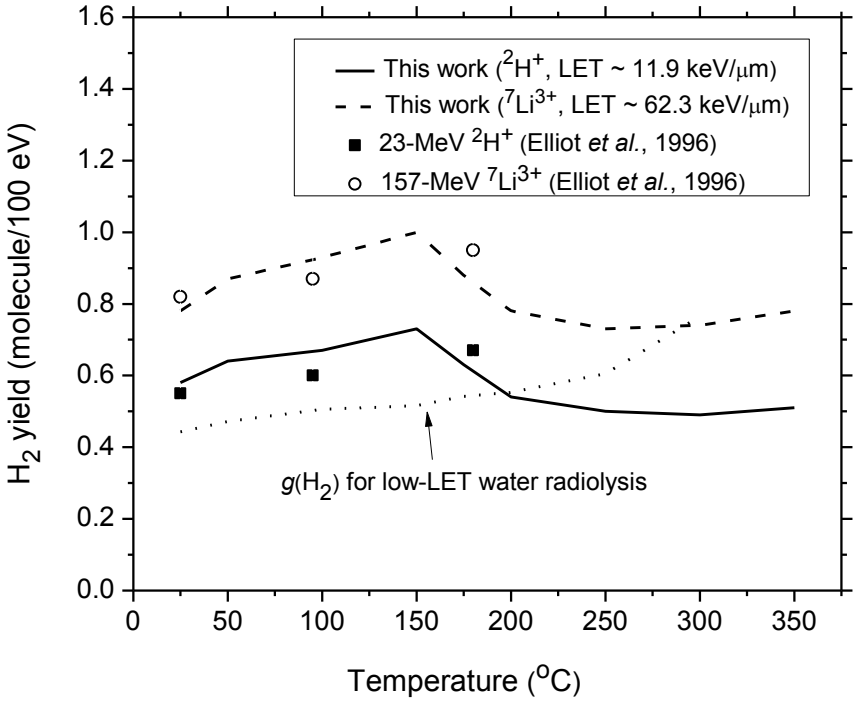

Fig. 2. Variation of the H_2 yield (in molecule/100 eV) of the radiolysis of liquid water by 23-MeV $^2H^+$ and 157-MeV $^7Li^{3+}$ ions as a function of temperature over the range 25-350 °C. Symbols (○,■) represent the scavenging experimental data of Elliot *et al.* [39] at 25,95, and 180 °C, as indicated in the inset. Simulated results (assuming the scavenging power varied linearly from 2×10^7 s^{-1} at 25 °C to 6.5×10^7 s^{-1} at 95 °C and remaining constant thereafter) are shown as solid (23-MeV deuterons) and dashed (157-MeV $^7Li^{3+}$) lines. The dotted line shows our simulated primary H_2 yield values for the low-LET (~0.3 keV/μm) radiolysis of water after incorporating a discontinuity around 150 °C in r_{th}, DEA, and the branching ratios of the different excited water molecule decay channels [9] [the sharp downward discontinuity predicted for $g(H_2)$ at 150 °C (Fig. 1) no longer appears].

4. ARTICLE 2

Calculation of the Yields for the Primary Species Formed from the Radiolysis of Liquid Water by Fast Neutrons at Temperatures between 25 and 350 °C

Authors: Sofia Loren Butarbutar, Sunuchakan Sanguanmith, Jintana Meesungnoen, Geni Rina Sunaryo, Jean-Paul Jay-Gerin

Status: published in *Radiation Research 181, 659-665(2014)*

Foreword: This study focuses on the chemistry of pure water after being irradiated by 2 MeV fast neutrons. The purpose of this study was mainly to investigate the effects of temperature on radical and molecular species yields. In this work, we considered that neutrons generated only recoil protons, or in other words, the most significant contribution to the radiolysis came from recoil protons. Yields were calculated at 10^{-7}, 10^{-6} and 10^{-5} s after the ionization event at all temperatures. By taking the yields at those times, we found that scavenging time of variation species measured could be done at that time range. Our simulation results were consistent with the experiment. I performed all the calculations, plotted the figures. Finally, I had a significant contribution to the main idea of this work and to all the preparation process for the first version of this article.

Résumé : Cette étude se concentre sur la chimie de l'eau après avoir été irradiée par des neutrons rapides de 2MeV. Le but de cette étude était principalement d'étudier les effets de la température sur le rendement en espèces radicales et moléculaires. Dans ce travail, nous avons considéré que les neutrons produisant seulement des protons de recul, ou en d'autres termes, la contribution la plus significative de la radiolyse est due aux protons de recul. Les rendements ont été calculés à 10^{-7}, 10^{-6} et 10^{-5} s après ionisation à toutes températures. En prenant les rendements à ces instants, nous avons constaté que le temps d'absorption de variation des espèces mesurées pourrait se faire dans cet intervalle de temps. Nos résultats de la simulation étaient en accord avec les données expérimentales. J'ai effectué tous les calculs, tracer la figure. Enfin, j'ai eu une contribution significative à l'idée principale de ce travail et à tout le processus de préparation de la première version de cet article.

Calculation of the Yields for the Primary Species Formed from the Radiolysis of Liquid Water by Fast Neutrons at Temperatures between 25 and 350 °C

Sofia Loren Butarbutar,[a,b] Sunuchakan Sanguanmith,[a] Jintana Meesungnoen,[a] Geni Rina Sunaryo[b] and Jean-Paul Jay-Gerin[a,15]

[a] *Département de Médecine Nucléaire et de Radiobiologie, Faculté de Médecine et des Sciences de la Santé, Université de Sherbrooke, Sherbrooke (Québec) J1H 5N4, Canada;* [b] *Center for Reactor Technology and Nuclear Safety, National Nuclear Energy Agency, Puspiptek Area, Serpong, Tangerang 15314, Indonesia*

Number of pages: **25**
(including text, references, listing of footnotes, figure captions, and figures)

Total number of words: **6338**

Number of figures: **1**

Number of references: **42**

Number of footnotes: **17**

Running title: **Fast neutron radiolysis of water at elevated temperatures**

Radiation Research ("Short Communications" section)

February 2014

---

[15] Address for correspondence: Département de Médecine Nucléaire et de Radiobiologie, Faculté de Médecine et des Sciences de la Santé, Université de Sherbrooke, 3001, 12ème Avenue Nord, Sherbrooke (Québec) J1H 5N4, Canada. Tel. +1-819-346-1110, ext. 14682 or 14773; fax: +1-819-564-5442; e-mail : jean-paul.jay-gerin@USherbrooke.ca

Butarbutar, S. L., Sanguanmith, S., Meesungnoen, J., Sunaryo, G. R. and Jay-Gerin, J.-P. Calculation of the Yields for the Primary Species Formed from the Radiolysis of Liquid Water by Fast Neutrons at Temperatures between 25 and 350 °C.*Radiat.Res.*

ABSTRACT

Monte Carlo simulations were used to calculate the yields for the primary species (e^-_{aq}, $H^\bullet$, H_2, $^\bullet OH$, and H_2O_2) formed from the radiolysis of neutral liquid water by mono-energetic 2-MeV neutrons at temperatures between 25 and 350 °C. The 2-MeV neutron was taken as representative of a fast neutron flux in a reactor. For light water, the moderation of these neutrons generated elastically scattered recoil protons of ~1.264, 0.465, 0.171, and 0.063 MeV, which had, at 25 °C, linear energy transfers (LETs) of ~22, 43, 69, and 76 keV/μm, respectively. Neglecting the radiation effects due to oxygen ion recoils and assuming that the most significant contribution to the radiolysis came from these first four recoil protons, the fast neutron yields could be estimated as the sum of the yields for these protons after allowance was made for the appropriate weightings according to their energy. Yields were calculated at 10^{-7}, 10^{-6} and 10^{-5} s after the ionization event at all temperatures, in accordance with the time range associated with the scavenging capacities generally used for fast neutron radiolysis experiments. The results of the simulations agreed reasonably well with the experimental data, taking into account the relatively large uncertainties in the experimental measurements, the relatively small number of reported radiolysis yields, and the simplifications included in the model. Compared with data obtained for low-LET radiation (^{60}Co γ-rays or fast electrons), our computed yields for fast neutron radiation showed essentially similar temperature dependences over the range of temperature studied, but with lower values for yields of free radicals and higher values for molecular yields. This general trend is a reflection of the high-LET character of fast neutrons. Although the results of the simulations were consistent with the experiment, more experimental data are

required to better describe the dependence of radiolytic yields on temperature and to test more thoroughly our modeling calculations.

Keywords: radiolysis, linear energy transfer (LET), fast neutrons, recoil protons, high temperature, radiolytic yields, kinetics, scavenging capacity, Monte Carlo track chemistry simulations.

INTRODUCTION

Most current commercial nuclear power plants in operation use either normal light (H_2O) water or heavy (D_2O) water (like CANDU[16]) as a coolant and, at the same time, as a neutron moderator (*1*). The primary heat-transport system of a water-cooled nuclear power reactor usually operates under conditions of high pressure (~7-15MPa) and high temperature (~275-325 °C) with a 25 °C pH of 6.5-10.5 (*2*). Since the coolant water is circulated in the reactor core, it is irradiated by intense fluxes of ionizing radiations, a mixture of fast electrons and recoil ions of hydrogen and oxygen, which have characteristically different "linear energy transfer" (LET) values (in the range from ~0.3 to 40-60 keV/μm, typically) (*3*). This irradiation results in the chemical decomposition (radiolysis) of water and leads to the formation of short-lived radicals (e^-_{aq}, $H^\bullet$, $^\bullet OH$, and $HO_2^\bullet/O_2^{\bullet-}$) and long-lived molecular products (H_2 and H_2O_2) which can promote corrosion, cracking, and hydrogen pickup both in the core and in the associated piping components of the reactor (*2-5*). Corrosion problems can increase operation and maintenance costs, besides increasing radioactive contamination and radiation risk to personnel. While the mechanism of corrosion depends on a variety of factors, optimal water chemistry control plays an important role in minimizing the corrosion of materials and its adverse effects on the plants (*6*).

A reliable understanding of the aqueous radiolysis processes in the reactor environment is crucial to controlling water reactor chemistry (*7*). Key parameters to evaluate the chemical effects of ionizing radiation are the radiation-chemical yields or *G*-values[17] of the species for γ-rays (low LET, mainly due to high-energy Compton electrons)

---

[16]CANDU, CANada Deuterium Uranium, is a registered trademark of Atomic Energy of Canada Limited (AECL).

[17]The number of species produced (or consumed) per unit of energy absorbed is termed the *G*-value and is used to express radiation-chemical yield. Throughout this paper, *G*-values

and fast neutrons (high LET, corresponding to both recoil protons and oxygen nuclei formed when the neutrons are moderated) in a reactor, and the rate constants for all of the reactions involving these species. Although a large body of data relevant to the radiolysis of water by ^{60}Co γ-rays or fast electrons is readily available in the literature, there is only limited information available for fast neutron radiolysis. In particular, fast neutron *G*-values at reactor operating temperatures are not well established (*3*, *10-12*).

Direct observations or measurements of the chemistry in and around the high-flux core region of a nuclear reactor are difficult due to the extreme conditions of high temperature, pressure, and mixed radiation fields. For this reason, chemical models and computer simulations of the radiolysis of water under these conditions are an important route of investigation. In this work, Monte Carlo simulations were used to calculate *G*-values for the primary species (e^-_{aq}, $H^\bullet$, H_2, $^\bullet OH$, and H_2O_2) formed from the radiolysis of neutral liquid water by incident mono-energetic 2-MeV neutrons at temperatures between 25 and 350 °C. We chose 2-MeV neutrons because the in-reactor fission-neutron flux spectrum[18] is known to peak at about this energy (*2*, *3*, *10*, *13*). For light water, it can be shown that the most significant contribution to the radiolysis comes from the first four neutron collisions that generate mostly recoil protons with different energies (*11*, *13-15*). These elastically scattered recoil protons deposit their energy through the production of

---

are quoted in conventional units of "molecule per 100 eV", as *g*(X) for the so-called *primary* (or "escape") yields of the species in parentheses (which are normally measured after reactions within tracks are complete or, in other words, at the time for which the tracks are considered to be completely dissipated) and *G*(product) for experimentally measured or final yields. For conversion into SI units (mol/J): 1 molecule/100 eV ≈ 0.10364 μmol/J (*4*, *8*, *9*).

[18]In general, the spectrum is expected to only vary slightly from reactor-to-reactor using uranium as a fuel (*10*).

ionizations and electronic excitations of the surrounding water. Neglecting the radiation effects due to oxygen ion recoils, the fast neutron yields were estimated as the sum of the yields for the four recoil protons (obtained from our Monte Carlo simulations) after appropriate weightings were applied according to the energy deposited by each of these protons. The results were tested against available experimental data and compared with the corresponding *g*-values for γ-radiolysis.[19]

FAST NEUTRON INTERACTION WITH WATER

The interaction of the neutron depends very much on its kinetic energy, whereas radiation effects induced by γ-rays are hardly dependent on their energy (*1*). For "fast" neutrons (*i.e.*, those with kinetic energies ranging from ~0.5 to 10 MeV) that concern us in this work, most of the slowing down occurs through a process of many successive "billiard-ball" elastic collisions with atomic nuclei, following the laws of conservation of energy and momentum of classical particle physics (*16*).[20] In elastic scattering, the total kinetic energy of the neutron and nucleus is unchanged by the interaction. During the interaction, a fraction of the neutron's kinetic energy is transferred to the nucleus. In the case of the fast neutron radiolysis of water and aqueous solutions, the neutrons are "moderated" mainly by both hydrogen (proton) and oxygen nuclei. Thereby, a spectrum of recoil-ion energies is produced from which the LET along the track of each released recoil charged particle can be assigned and the chemical yields for the various species formed can be obtained.

---

[19] A preliminary report of this work was presented at the 6th International Symposium on Supercritical Water-Cooled Reactors, Shenzhen, Guangdong, China, March 3-7, 2013.

[20] In this energy range, fast neutrons can be considered as non-relativistic particles, since their mass is much larger than their kinetic energy; the description of neutron elastic collision can thus be performed using non-relativistic mechanics.

The proton and oxygen ion recoils generated by the passage of the incident neutron are widely separated from one another along the path of the neutron (*11*). Moreover, these recoil nuclei – whose energy is distributed from zero to the energy of the incident neutrons – have maximum "ranges" (*i.e.*, track lengths) much less than the average separation between two successive neutron interactions.[21] Thus, they can be considered as behaving *independently* of each other: their ionizing energy is deposited locally in dense tracks in the water in the immediate vicinity of the collision sites (the points of generation of the recoil particles) with virtually no allowance for overlap of the reaction zones of neighboring tracks. As a consequence, under normal irradiation conditions, fast neutrons deposit their energy in water primarily through the generation of "isolated" tracks of recoil nuclei and the observed water radiolysis chemistry should tend to resemble that induced by *independent, high-LET protons and oxygen ions*.[22]

In the neutron energy range of interest here, oxygen ion recoils are of minor importance in the fast-neutron radiolysis of water due to their low average energies.[23] Neglecting the small yields anticipated due to oxygen ion recoils (*11*, *12*), the fast neutron

---

[21]The mean free path of a 2-MeV neutron in water is about 4 cm, while the recoil proton and oxygen ion maximum ranges for this energy are ~75.5 and 1.5 μm, respectively (*11*).

[22]This track structure information for the elastically scattered ion recoils strongly supports the procedure used here to calculate the radiolysis *G*-values for fast neutrons by simply summing the yields for each of these recoil ions after allowance has been made for the appropriate weighting according to energy. Obviously, this approximation would not necessarily be correct at very high neutron intensities or dose rates.

[23]The greatest energy deposition in the solution comes from recoil protons. Edwards *et al.* (*12*) showed that, in the energy range below 10 MeV, 88% of the neutron energy is absorbed by recoil protons and the remaining 12% by oxygen nuclei.

G-values were estimated on the basis of the *G*-values calculated for the first four recoil protons.[24] The energy of a recoil proton can be calculated using the equation (*11*, *13*,*17*)

$$\ln\left(\frac{E_0}{E_n}\right) = n\left[1 + \frac{(A-1)^2}{2A}\ln\left(\frac{A-1}{A+1)}\right)\right], \qquad (1)$$

where A is the mass number of the struck nucleus (A = 1 for collisions with protons),[25] E_0 is the initial neutron kinetic energy, and E_n is the average energy of the neutron after n individual elastic scattering collisions.[26] The quantity $E_{p_1} = (E_0 - E_1)$ is the energy imparted to the first recoil proton, and so on. For a 2-MeV neutron, the first four collisions generated recoil protons of ~1.264, 0.465, 0.171, and 0.063 MeV having LET values (*11*, *18*) of ~22, 43, 69, and 76 keV/μm at 25 °C, and ~13, 25, 40, and 44 keV/μm at 350 °C, respectively.The final neutron yields were then calculated by summing the *G*-values for each recoil proton(obtained from our Monte Carlo simulations) weighted by its fraction of the total neutron energy absorbed (*11*,*13*):

$$G(\mathrm{X}) = \frac{\sum_{i=1}^{4}\left(G(\mathrm{X})_{p_i} E_{p_i}\right)}{E_T}, \qquad (2)$$

where $G(\mathrm{X})_{p_i}$ is the free radical or molecular yield associated with the recoil proton p_i (i = 1 to 4) and

$$E_T = \sum_{i=1}^{4} E_{p_i} \qquad (3)$$

---

[24]Further recoils are generated from the neutron as it is further moderated, but their average energies are low and do not contribute significantly to the radiolysis (*14*).

[25]Note that Eq. (1) is not defined when A = 1, but the limit as A approaches unity is valid. In this case, Eq. (1) reduces to $E_n = E_0\, e^{-n}$.

[26]Average kinetic energy values are desired since one usually deals with a beam of many neutrons.

is the sum of all recoil proton energies.

MONTE CARLO SIMULATIONS

Monte Carlo simulations of the complex succession of events that are generated in the radiolysis of pure, deaerated liquid water by impacting protons of various initial energies were performed using our IONLYS-IRT code. A detailed description of the code at both ambient and elevated temperatures has been reported previously (*11*,*18*,*19*). Briefly, the IONLYS "step-by-step" simulation program models all the events of the early *physical* and *physicochemical* stages of radiation action up to ~10^{-12} s in the track development. The species created on this subpicosecond time scale rapidly reorganize and produce the "initial" free radicals and molecular products e^-_{aq}, H^+, OH^-, $H^\bullet$, H_2, $^\bullet OH$, H_2O_2, $O_2^{\bullet-}$ (or $HO_2^\bullet$, depending on pH), $^\bullet O^\bullet$, etc., of the radiolysis. The complex, highly nonhomogeneous spatial distribution of reactants at the end of the physicochemical stage, which is provided as an output of the IONLYS program, is then used directly as the starting point for the subsequent *nonhomogeneous chemical* stage (from ~10^{-12} s to ~10^{-7}-10^{-6} s at 25 °C). This third stage, during which the different radiolytic species diffuse randomly at rates determined by their diffusion coefficients and react with one another until all track processes are complete, is covered by our IRT program. This program employs the *independent reaction times* (IRT) method (*20*, *21*), a computer-efficient stochastic simulation technique that is used to simulate reaction times without having to follow the trajectories of the diffusing species. Its ability to give accurate time-dependent chemical yields under different irradiation conditions has been well validated by comparison with full random flights (or "step-by-step") Monte Carlo simulations, which do follow the reactant trajectories in detail (*22*, *23*). This IRT program can also be used to efficiently describe the reactions that occur in the bulk solution during the *homogeneous chemical* stage, *i.e.*, in the time domain beyond a few microseconds.

In the current version of IONLYS-IRT, we use the self-consistent radiolysis database, including rate constants, diffusion coefficients, reaction mechanisms, and *G*-values, recently compiled by Elliot and Bartels (*10*). This new database provides recommendations for the best values to use in high-temperature modeling of light water radiolysis over the range of 20-350 °C.

All Monte Carlo simulations reported here were performed along the liquid-vapor coexistence curve, the density of the pressurized water decreasing from 1 g/cm^3 at 25 °C to 0.575 g/cm^3 (16.5 MPa) at 350 °C (*24*). For this temperature range, calculations show that *G*-values of transient species, to a large extent, depend relatively little on the applied pressure (or density).

Finally, to reproduce the effects due to 2-MeV neutrons, we simulated short (~15-150 μm) track segments of each of the first four generated recoil protons. Over these simulated track segments, the energy and LET of the protons were well defined and remained nearly constant. Such model calculations thus gave track segment yields at a well-defined LET. The number of proton histories (usually ~10-150, depending on the proton energy) was chosen so as to ensure only small statistical fluctuations in the computed averages of chemical yields, while keeping acceptable computer time limits. The total neutron yields of the various radiolytic products were then calculated by summing the corresponding weighted *G*-values for each recoil proton according to Eq. (2).

RESULTS AND DISCUSSION

The resulting temperature dependences of our computed yields of e^-_{aq}, $^\bullet OH$, $H^\bullet$, H_2O_2, and H_2 in deaerated liquid water irradiated by 2-MeV incident neutrons from ambient up to 350 °C are shown in Fig. 1 along with available experimental data and other modeled or estimated fast neutron *G*-value results. For the sake of comparison, our *G*-values were calculated at three different times, namely 10^{-7}, 10^{-6}, and 10^{-5} s after the

ionization event at all temperatures (solid, dashed, and dotted blue lines in Fig. 1, respectively), here chosen in accordance with the time scales associated with the "scavenging powers"[27] of solutes (in the range of ~10^5-10^7 s^{-1}) generally used in fast neutron scavenger experiments to measure the yields. There is reasonably good overall agreement between the simulated and experimental *G*-values (*2*, *10*, *14*, *25-32*) given the relatively large uncertainties in the experimental measurements[28,29] at high temperatures, the relative paucity of *G*-values for fast neutron radiolysis, and the simplifications included in the model. This agreement between the experiment and model supports a posteriori the validity of the assumptions employed in the calculations.

Compared with the data obtained for low-LET radiation (γ-rays from ^{60}Co or fast electrons), our computed yields for fast neutron radiation show essentially similar temperature dependences over the range of temperature studied, but with *lower* values for yields of free radicals and *higher* values for molecular yields. This general trend is a resultof the *high-LET character of fast neutrons*. Indeed, upon increasing the LET of the radiation, there was an increased intervention of radical-radical reactions as the local concentration of radicals along the radiation track was high and many radical interactions

---

[27]The product of a solute's (or scavenger's) concentration and its rate constant for reaction with one of the primary radical species is called its *scavenging power*, with units of s^{-1}. The reciprocal of the scavenging power gives a measure of the time scale over which the scavenging is occurring (*3*).

[28]It is difficult to obtain accurate dosimetry for a mixed neutron/gamma radiation field (present in any reactor) and to separate neutron chemistry yields from the background gamma radiolysis yields (*3*, *10*, *12*, *14*, *32*, *35*).

[29]There is also a large degree of uncertainty associated with the temperature dependence of the peroxide yields, which is difficult to obtain experimentally due to the thermal decomposition of H_2O_2 above 100 °C (*3*, *36*, *37*).

occurred before the products could escape into the bulk solution. This allowed fewer radicals to escape combination and recombination reactions during the expansion of the tracks and in turn led to the formation of more molecular products (*19*).[30]

A striking feature of our simulated results obtained at 10^{-6} s and especially at 10^{-5} s, was the large increase with temperature, particularly above ~200-300 °C, of $G(^{\bullet}OH)$ and $G(H_2)$ and the corresponding decrease of $G(H^{\bullet})$. The mechanism directly responsible for these behaviors is the oxidation of water by the $H^{\bullet}$ atom:

$$H^{\bullet} + H_2O \rightarrow {}^{\bullet}OH + H_2 \quad , \qquad (4)$$

which was recently proposed to quantitatively explain the large, anomalous increase of the primary yield of H_2 observed experimentally in the low-LET radiolysis of water above 200 °C (*10*, *18*, *39-41*). However, a controversy currently exists in the literature regarding the rate constant of reaction (4), including estimates of 10^4 (*34*) (value used in the present calculations), 3.18×10^4 (*39*), 2.2×10^3 (*10*, *40*), and 1.75×10^4 (*41*) M^{-1} s^{-1} at 300 °C, depending on the authors. As a result of this uncertainty, no clear conclusion has yet been obtained as to the real contribution of this potentially important reaction in the radiolysis of water at elevated temperatures.

Judging from Fig. 1b and e, these fast neutron radiolysis yields for $^{\bullet}OH$ and H_2 can hardly provide information about the value of the rate constant for reaction (4), given the lack of experimental data above ~300 °C. However, as can be seen in Fig. 1c, a switch from

---

[30] As already discussed (*38*), the *initial* yields (formed in ~10^{-12} s) of the radiolytic species are assumed in our simulations to be independent of the temperature. Hence, the variation of the yields of the various species with temperature only results from the various chemical reactions that contribute to their formation or decay, while the tracks expand by diffusion. Note that, in contrast, temperature effects can significantly affect the initial *spatial* distribution of those species within the track and, in turn, their subsequent reaction kinetics.

increasing to rapidly decreasing values is observed at 10^{-6} and 10^{-5} s around ~200-300 °C in our calculated $G(H^{\bullet})$ values (in contrast to the corresponding yields at 10^{-7} s, which increase monotonically with temperature). As the agreement between the experiment and model seems to be much improved, this suggests that the measured yields at these temperatures could have been obtained from scavenger experiments with scavenging powers in the range of ~10^5-10^6 s^{-1} and that reaction (4) may indeed need to be invoked to explain the temperature dependence of $G(H^{\bullet})$. More experimental data are needed above ~300 °C to better describe the dependence of $G(H^{\bullet})$ on temperature.

Finally, we should briefly emphasize the discontinuity that is observed around 150 °C in the calculated yields of e^-_{aq}, $H^{\bullet}$, and H_2. As can be seen from Fig. 1a, c and e, $G(e^-_{aq})$ and $G(H^{\bullet})$ increase above this temperature while $G(H_2)$ decreases. This is especially noticeable at 10^{-7} s and is due to the fact that the rate constant for the self-reaction of the hydrated electron:

$$e^-_{aq} + e^-_{aq} (+ 2H_2O) \rightarrow H_2 + 2OH^- \qquad (5)$$

drops abruptly above ~150 °C (*10*, *18*).[31] As a consequence, more and more hydrated electrons are available as the temperature increases to either react in other intra-track reactions, such that

$$e^-_{aq} + H^+ \rightarrow H^{\bullet} \qquad (6)$$

and

$$e^-_{aq} + {}^{\bullet}OH \rightarrow OH^- , \qquad (7)$$

---

[31]This drop in the rate constant for the self-reaction of e^-_{aq} around 150 °C has always been measured under *alkaline* conditions (*10*). The applicability of this drop to *neutral*or *slightly acidic* solution (as the pH of water at 150-200 °C is about 5.7-6) (*2*) has been discussed recently (*42*).

or to escape into the bulk solution. Concomitantly, the increased occurrence of reaction (7) above 150 °C also leads to a (slight but nevertheless noticeable in Fig. 1b and d) downward discontinuity in the yields of $^{\bullet}OH$ and H_2O_2 (as hydrogen peroxide is formed predominantly by the reaction of the $^{\bullet}OH$ radical with itself). Unfortunately, the large amount of scatter in the experimental data and also their limited availability could not allow us to determine whether or not the predicted discontinuity at 150 °C was confirmed experimentally.

CONCLUSION

In this work, Monte Carlo simulations were used to calculate the *G*-values for the primary species of the radiolysis of neutral liquid water by mono-energetic 2-MeV neutrons at temperatures between 25 and 350 °C. The fast neutron *G*-values were obtained by assuming that the most significant contribution to the radiolysis comes from the first four elastically scattered recoil protons generated by the passage of the incident neutron and by neglecting the radiation effects due to oxygen ion recoils. Overall, the results of the simulations agreed reasonably well with existing experimental data. Compared with the data obtained for low-LET radiation, our computed yields for fast neutrons showed essentially similar temperature dependences over the range of temperature studied, but with lower values for yields of free radicals and higher values for molecular yields; this result reflects the high-LET character of fast neutrons. More experimental data are required to better describe the dependence of radiolytic yields on temperature, to test more thoroughly our modeling calculations, and to specify the potential role of the reaction of hydrogen atoms with water at high temperatures.

ACKNOWLEDGMENTS

The authors gratefully acknowledge the support of the Natural Sciences and Engineering Research Council of Canada (NSERC), Natural Resources Canada (NRCan), and Atomic Energy of Canada Limited (AECL) through Canada's National Program on

Generation IV Energy Technologies. Particular thanks are also due to Dr. D. A. Guzonas and Dr. C. R. Stuart (AECL, Chalk River Laboratories) for their continued support and encouragement.

REFERENCES

1. Katsumura Y, Sunaryo G, Hiroishi D, Ishigure K. Fast neutron radiolysis of water at elevated temperatures relevant to water chemistry. Prog Nucl Energy 1998; 32:113-121.
2. Cohen P. Water coolant technology of power reactors. La Grange Park (IL): American Nuclear Society; 1980.
3. McCracken DR, Tsang KT, Laughton PJ. Aspects of the physics and chemistry of water radiolysis by fast neutrons and fast electrons in nuclear reactors. Report AECL No.: 11895. Chalk River (Ontario): Atomic Energy of Canada Ltd.; 1998.
4. Woods RJ, Pikaev AK. Applied radiation chemistry: Radiation processing. New York (NY): Wiley; 1994.
5. Research needs and opportunities in radiation chemistry workshop, Chesterton (IN), 19-22 April 1998, Report No.: DOE/SC-0003.Germantown (MD): U.S. Department of Energy, Office of Basic Energy Sciences; 1999.Available from http://www.science.doe.gov/ production/bes/chm/Publications/RadRprt.pdf
6. Data processing technologies and diagnostics for water chemistry and corrosion control in nuclear power plants (DAWAC). Report No.: IAEA-TECDOC-1505.Vienna (Austria): International Atomic Energy Agency; 2006.
7. Stuart CR. Radiation chemistry in the nuclear power reactor environment: From laboratory study to practical application. In: Moriarty M, Mothersill C, Seymour C, Edington M, Ward JF, Fry RJM, editors. Radiation research. Vol. 2. Lawrence (KS): Allen Press; 2000. p. 63-66.
8. Burton M. Radiation chemistry. JPhys Colloid Chem 1947; 51:611-625.
9. Ferradini C, Jay-Gerin J-P. La radiolyse de l'eau et des solutions aqueuses: historique et actualité. Can J Chem 1999; 77:1542-1575.
10. Elliot AJ, Bartels DM. The reaction set, rate constants and *g*-values for the simulation of the radiolysis of light water over the range 20° to 350 °C based on information

available in 2008. Report AECL No.: 153-127160-450-001. Chalk River (Ontario): Atomic Energy of Canada Ltd.; 2009.

11. Tippayamontri T, Sanguanmith S, Meesungnoen J, Sunaryo GR, Jay-Gerin J-P. Fast neutron radiolysis of the ferrous sulfate (Fricke) dosimeter: Monte Carlo simulations. Recent Res Devel Physical Chem 2009;10:143-211.

12. Edwards EJ, Wilson PPH, Anderson MH, Mezyk SP, Pimblott SM, Bartels DM. An apparatus for the study of high temperature water radiolysis in a nuclear reactor: Calibration of dose in a mixed neutron/gamma radiation field. Rev Sci Instrum 2007;78:124101.

13. Gordon S, Schmidt KH, Honekamp JR. An analysis of the hydrogen bubble concerns in the Three-Mile Island Unit-2 reactor vessel. Radiat Phys Chem 1983;21:247-258.

14. Elliot AJ, Chenier MP, Ouellette DC, Koslowsky VT. Temperature dependence of *g* values for aqueous solutions irradiated with 23 MeV $^{2}H^{+}$ and 157 MeV $^{7}Li^{3+}$ ion beams. J Phys Chem 1996; 100:9014-9020.

15. Swiatla-Wojcik D, Buxton GV. Modelling of linear energy transfer effects on track core processes in the radiolysis of water up to 300 °C. J Chem Soc Faraday Trans 1998; 94:2135-2141.

16. Anderson DW. Absorption of ionizing radiation. Baltimore (MD):University Park Press; 1984.

17. Friedlander G, Kennedy JW, Macias ES, Miller JM. Nuclear and radiochemistry. 3rd ed. New York (NY): Wiley; 1981.

18. Sanguanmith S, Muroya Y, Meesungnoen J, Lin M, Katsumura Y, Mirsaleh Kohan L, Guzonas DA, Stuart CR, Jay-Gerin J-P. Low-linear energy transfer radiolysis of liquid water at elevated temperatures up to 350 °C: Monte Carlo simulations. Chem Phys Lett 2011; 508:224-230.

19. Meesungnoen J, Jay-Gerin J-P. Radiation chemistry of liquid water with heavy ions: Monte Carlo simulation studies. In: Hatano Y, Katsumura Y, Mozumder A, editors.

Charged particle and photon interactions with matter: recent advances, applications, and interfaces. Boca Raton (FL): Taylor & Francis; 2011. p. 355-400.

20. Pimblott SM, Pilling MJ, Green NJB. Stochastic models of spur kinetics in water. Radiat Phys Chem1991; 37:377-388.

21. Frongillo Y, Goulet T, Fraser M-J, Cobut V, Patau JP, Jay-Gerin J-P. Monte Carlo simulation of fast electron and proton tracks in liquid water. II. Nonhomogeneous chemistry. Radiat Phys Chem 1998; 51:245-254.

22. Goulet T, Fraser M-J, Frongillo Y, Jay-Gerin J-P. On the validity of the independent reaction times approximation for the description of the nonhomogeneous kinetics of liquid water radiolysis. Radiat Phys Chem 1998; 51:85-91.

23. Plante I. Développement de codes de simulation Monte-Carlo de la radiolyse de l'eau et de solutions aqueuses par des électrons, ions lourds, photons et neutrons. Applications à divers sujets d'intérêt expérimental.PhD Thesis. Université de Sherbrooke; 2009.

24. NIST chemistry webbook, Linstrom PJ, Mallard WG, editors. NIST standard reference database No.: 69.Gaithersburg (MD): National Institute of Standards and Technology; 2005. Available fromhttp://webbook.nist.gov.

25. Sunaryo GR, Katsumura Y, Shirai I, Hiroishi D, Ishigure K. Radiolysis of water at elevated temperatures. I. Irradiation with gamma-rays and fast neutrons at room temperature. Radiat Phys Chem 1994; 44:273-280.

26. Sunaryo GR, Katsumura Y, Hiroishi D, Ishigure K. Radiolysis of water at elevated temperatures. II. Irradiation with γ-rays and fast neutrons up to 250 °C. Radiat Phys Chem 1995; 45:131-139.

27. Sunaryo GR, Katsumura Y, Ishigure K. Radiolysis of water at elevated temperatures. III. Simulation of radiolytic products at 25 and 250 °C under the irradiation with γ-rays and fast neutrons. Radiat Phys Chem1995; 45:703-714.

28. Ishigure K, Katsumura Y, Sunaryo GR, Hiroishi D. Radiolysis of high temperature water.Radiat Phys Chem 1995; 46:557-560.

29. Burns WG, Moore PB. Water radiolysis and its effect upon in-reactor zircaloy corrosion. Radiat Eff 1976; 30:233-242.

30. Christensen H, Molander A, Lassing A, Tomani H. Experimental studies of radiolysis in an in-core loop in the Studsvik R2 reactor. Proceedings of the 7th international conference on water chemistry of nuclear reactor systems, October 13-17, 1996, Bournemouth, UK. London (UK): British Nuclear Energy Society; 1996. p. 138-140.

31. Christensen H. Fundamental aspects of water coolant radiolysis. SKI report 2006:16. Nyköping (Sweden): Swedish Nuclear Power Inspectorate; 2006.

32. Edwards EJ. Determination of pure neutron radiolysis yields for use in chemical modeling of supercritical water. PhD Thesis. University of Wisconsin-Madison; 2007.

33. Sanguanmith S, Meesungnoen J, Muroya Y, Lin M, Katsumura Y, Jay-Gerin J-P. On the spur lifetime and its temperature dependence in the low linear energy transfer radiolysis of water. Phys Chem Chem Phys 2012; 14:16731-16736.

34. Alcorn CD, Brodovitch J-C, Ghandi K, Kennedy A, Percival PW, Smith M. Kinetics of the reaction between $H^{\bullet}$ and superheated water probed with muonium. Chem Phys (submitted for publication).

35. Katsumura Y. Dosimetry of mixed field of neutrons and γ-rays. In: Tabata Y, Ito Y, Tagawa S, editors. CRC handbook of radiation chemistry. Boca Raton (FL): CRC Press; 1991. p. 85-95.

36. Kent MC, Sims HE. The yield of γ-radiolysis products from water at temperatures up to 300 °C. Proceedings of the 6th international conference on water chemistry of nuclear reactor systems, October 12-15, 1992, Bournemouth, UK. London (UK): British Nuclear Energy Society; 1992. p. 153-160.

37. Takagi J, Ishigure K. Thermal decomposition of hydrogen peroxide and its effect on reactor water monitoring of boiling water reactors. Nucl Sci Eng 1985; 89:177-186.

38. Hervé du Penhoat M-A, Goulet T, Frongillo Y, Fraser M-J, Bernat Ph, Jay-Gerin J-P. Radiolysis of liquid water at temperatures up to 300 °C: A Monte Carlo simulation study. J Phys Chem A 2000; 104:11757-11770.

39. Swiatla-Wojcik D, Buxton GV. On the possible role of the reaction $H^{\bullet} + H_2O \rightarrow H_2 + {}^{\bullet}OH$ in the radiolysis of water at high temperatures. Radiat Phys Chem 2005; 74:210-219.

40. Bartels DM. Comment on the possible role of the reaction $H^{\bullet} + H_2O \rightarrow H_2 + {}^{\bullet}OH$ in the radiolysis of water at high temperatures. Radiat Phys Chem 2009; 78:191-194.

41. Swiatla-Wojcik D, Buxton GV. Reply to comment on the possible role of the reaction $H + H_2O \rightarrow H_2 + OH$ in the radiolysis of water at high temperatures. Radiat Phys Chem 2010; 79:52-56.

42. Butarbutar SL, Muroya Y, Mirsaleh Kohan L, Sanguanmith S, Meesungnoen J, Jay-Gerin J-P. On the temperature dependence of the rate constant of the bimolecular reaction of two hydrated electrons. Atom Indonesia J 2013; 39:51-56.

LISTING OF FOOTNOTES

1. Address for correspondence: Département de Médecine Nucléaire et de Radiobiologie, Faculté de Médecine et des Sciences de la Santé, Université de Sherbrooke, 3001, 12ème Avenue Nord,Sherbrooke (Québec) J1H 5N4, Canada. Tel. +1-819-346-1110, ext. 14682 or 14773; fax: +1-819-564-5442; e-mail :jean-paul.jay-gerin@USherbrooke.ca.
2. CANDU, CANada Deuterium Uranium, is a registered trademark of Atomic Energy of Canada Limited (AECL).
3. The number of species produced (or consumed) per unit of energy absorbed is termed the *G*-value and is used to express radiation-chemical yield. Throughout this paper, *G*-values are quoted in conventional units of "molecule per 100 eV", as *g*(X) for the so-called *primary* (or "escape") yields of the species in parentheses (which are normally measured after reactions within tracks are complete or, in other words, at the time for which the tracks are considered to be completely dissipated) and *G*(product) for experimentally measured or final yields. For conversion into SI units (mol/J): 1 molecule/100 eV ≈ 0.10364 μmol/J (*8*, *9*).
4. In general, the spectrum is expected to only vary slightly from reactor-to-reactor using uranium as a fuel (*10*).
5. A preliminary report of this work was presented at the 6th International Symposium on Supercritical Water-Cooled Reactors, Shenzhen, Guangdong, China, March 3-7, 2013.
6. In this energy range, fast neutrons can be considered as non-relativistic particles, since their mass is much larger than their kinetic energy; the description of neutron elastic collision can thus be performed using non-relativistic mechanics.
7. The mean free path of a 2-MeV incident neutron in water is about 4 cm, while the recoil proton and oxygen ion maximum ranges at this energy are ~75.5 and 1.5 μm, respectively(*11*).

8. This track structure information for the elastically scattered ion recoils strongly supports the procedure used here to calculate the radiolysis *G*-values for fast neutrons by simply summing the yields for each of these recoil ions after allowance has been made for the appropriate weighting according to energy. Obviously, this approximation would not necessarily be correct at very high neutron intensities or dose rates.
9. The greatest energy deposition in the solution comes from recoil protons. Edwards *et al.* (*12*) showed that, in the energy range below 10 MeV, 88% of the neutron energy is absorbed by recoil protons and the remaining 12% by oxygen nuclei.
10. Further recoils are generated from the neutron as it is further moderated, but their average energies are low and do not contribute significantly to the radiolysis(*14*).
11. Note that Eq. (1) is not defined when $A = 1$, but the limit as A approaches unity is valid. In this case, Eq. (1) reduces to $E_n = E_0\, e^{-n}$.
12. Average kinetic energy values are desired since one usually deals with a beam of many neutrons.
13. The product of a solute's (or scavenger's) concentration and its rate constant for reaction with one of the primary radical species is called its *scavenging power*, with units of s^{-1}. The reciprocal of the scavenging power gives a measure of the time scale over which the scavenging is occurring (*3*).
14. It is difficult to obtain accurate dosimetry for a mixed neutron/gamma radiation field (present in any reactor) and to separate neutron chemistry yields from the background gamma radiolysis yields (*3*, *10*, *12*, *14*, *32*, *35*).
15. There is also a large degree of uncertainty associated with the temperature dependence of the peroxide yields, which is difficult to obtain experimentally due to the thermal decomposition of H_2O_2 above 100 °C (*3*, *36*, *37*).
16. As already discussed (*38*), the *initial* yields (formed in ~10^{-12} s) of the radiolytic species are assumed in our simulations to be independent of the temperature. Hence, the variation of the yields of the various species with temperature only results from

the various chemical reactions that contribute to their formation or decay, while the tracks expand by diffusion. Note that, in contrast, temperature effects can significantly affect the initial *spatial* distribution of those species within the track and, in turn, their subsequent reaction kinetics.

17. This drop in the rate constant for the self-reaction of e^-_{aq} around 150 °C has always been measured under *alkaline* conditions (*10*). The applicability of this drop to *neutral* or *slightly acidic* solution (as the pH of water at 150-200 °C is about 5.7-6) (*2*) has been discussed recently (*42*).

FIGURE CAPTIONS

Figure 1: Variation of the *G*-values (in molecule/100 eV) for the radiolysis of liquid water by 2-MeV neutrons as a function of temperature in the range of 25-350 °C: (a) $G(e^-_{aq})$, (b) $G(^{\bullet}OH)$, (c) $G(H^{\bullet})$, (d) $G(H_2O_2)$, and (e) $G(H_2)$. Our simulated results, obtained at 10^{-7}, 10^{-6}, and 10^{-5} s based on the radiation effects in 1.264, 0.465, 0.171, and 0.063 MeV recoil proton tracks, are shown as solid, dashed and dotted red lines, respectively. Experimental data are from: *(2)* (○) (estimated yields for reactor fast neutrons, effective average LET: 40 keV/μm), *(14)* (●) (2-MeV neutron *G*-values estimated from the ~23 MeV $^2H^+$ and 157 MeV $^7Li^{3+}$ ion radiolysis of water using a weighting procedure), *(1, 25-28)* (■) (from combined measurements and computer modeling; irradiations carried out using the YAYOI fast-neutron source reactor at the University of Tokyo, with an average energy for fast neutrons of ~0.8 MeV), *(29)* (◊), *(30)* (□), *(31)* (▲) (mean *G*-values from different research groups calculated by disregarding the highest and lowest value for each species; according to the author, these values are probably correct within about 25%), and *(32)* (Δ). The purple dash-dot lines show the fast neutron *G*-values estimated in *(10)* for natural uranium (for which most of the in-reactor fast neutron flux spectrum falls into the 0.5 to 6 MeV energy range with a peak of about 2 MeV). The olive dash-dot-dot lines show the *G*-values for 2-MeV neutron radiolysis calculated by Swiatla-Wojcik and Buxton *(15)* at 10^{-6} s after the ionization event.The primary (or "escape") yields for the low-LET (~0.3 keV/μm) radiolysis of water *(18)* obtained using our previously calculated spur lifetimes between 25 and 350 °C *(33)* are also shown (blue dotted lines) for the sake of comparison. The reaction of the $H^{\bullet}$atom with water was assumed to follow an Arrhenius temperature dependence over the 25-350 °C range studied, with a rate constant of ~$4.6 \times 10^{-5} M^{-1}$ s^{-1} at 25 °C *(10)*

and $10^4 M^{-1}$ s^{-1} at 300 °C, in agreement with recent muon spin spectroscopy experiments using muonium as an analogue of a hydrogen atom (*34*).

FIG. 1

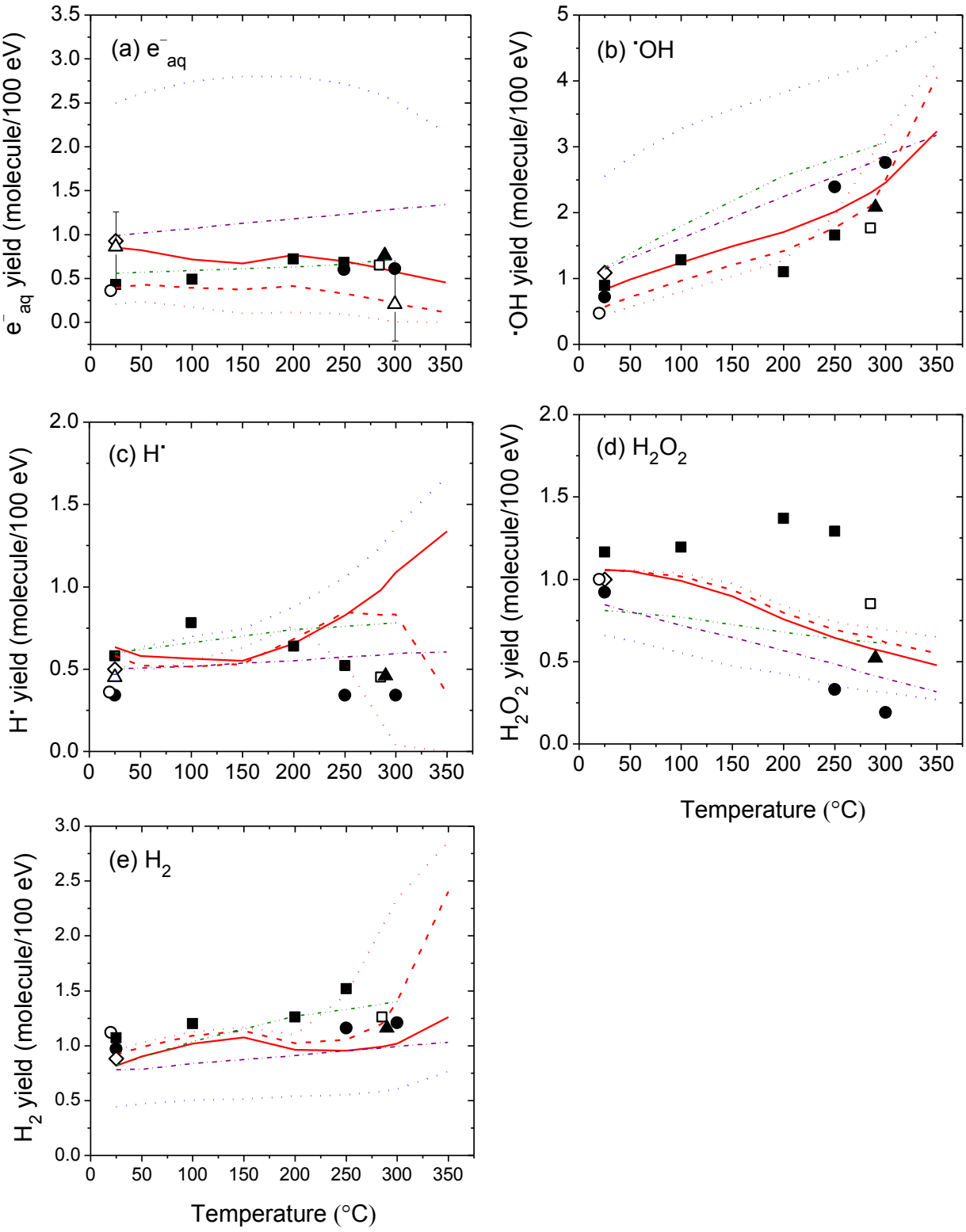
(a) e^-_{aq}
e^-_{aq} yield (molecule/100 eV)
(b) ·OH
·OH yield (molecule/100 eV)
(c) H·
H· yield (molecule/100 eV)
(d) H_2O_2
H_2O_2 yield (molecule/100 eV)
(e) H_2
H_2 yield (molecule/100 eV)
Temperature (°C)
Temperature (°C)

5. DISCUSSION

5.1. Fast neutron radiolysis of water at high temperature

There are two types of interaction between ionizing radiations with reactor component material. They are (i) direct interaction between ionizing radiation and reactor material, such as neutrons might knock out some atoms in material causing changing of atoms position, furthermore material properties may be changed from macroscopic aspect; (ii) indirect interaction, where the radiations interact with coolant water, actually with the electron of water, that results in water radiolysis forming radiolysis products, eventually these species will interact with reactor component causing corrosion or in other words called chemistry issue. The main radiation fields generated in the reactor core are fast neutrons and gamma rays. Radiolysis of water by fast neutrons at high temperature is a subject of interest in nuclear technology as water used as a coolant. It is due to the product of water radiolysis such as H_2O_2 and H_2 can cause corrosion and hydriding of in-core components. For this reason, it is necessary to select conditions such that the radiolytic decomposition of the water is suppressed. To predict the effects of radiolysis in the reactor cooling circuit at high temperature, one needs to know:

1. The chemical yields (*G*-values) of the radiolytic products that remain after reaction in radiation tracks are complete.
2. The rate constants for the reaction taking place in spurs and tracks that result in these primary yields.

Although a large body of data relevant to the radiolysis of water by γ-rays and fast electrons is readily available in the literature, there is only limited information available for fast neutron radiolysis. In particular, fast neutron *g*-values at reactor operating temperatures are not well established. In addition, the temperature dependence of some reaction rate constants at high temperature is unknown.

For those reasons mentioned above, simulation under reactor operation condition with some simplifying assumptions is an important investigation route. In the present work, the effect of temperature on the *G*-values of the various radiolytic products (e^-_{aq}, $^{\bullet}OH$, $H^{\bullet}$, H_2O_2, and H_2) with re-assessed experimental data up to 350 ^oC were carried on using Monte Carlo simulations.

5.2 Consideration in choosing the first four proton recoil for calculating the yields

In this work, as mentioned previously elsewhere, we only consider the contribution of first four recoil proton in term of yield calculations. This is not a magic number, but we decided to choose the first four proton recoil contributions through some tests. SWIATLA and BUXTON (1998) in a similar work, using deterministic diffusion-kinetic modelling, simply consider the first three collisions of a neutron in calculating radiolytic yields. However to ensure only small statistical difference in the computed averages of chemical yields, we chose to include the fourth neutron collisions in our calculation.

We have tested that there is insignificant difference between taking the first three and first four protons recoil contribution into account. To justify our hypothesis, we showe in Table 3 the variation of final yields as a function of temperature in the range of 25 – 350 ^{o}C by using first three and first four recoil protons.

Table 3: Variation of final yields as a function of temperature in the range of 25 – 350 ^{o}C by using first three and compare with first four recoil protons, obtained at 10^{-7}, 10^{-6} and 10^{-5} s. The difference is about 0-0.2 molecule/100 eV.

T	G(•OH) (molecule/100eV)			G(•OH) (molecule/100eV)			G(e^-_{aq}) (molecule/100eV)			G(e^-_{aq}) (molecule/100eV)		
(^{o}C)	(contributed by first four proton)			(contributed by first three proton)			(contributed by first four proton)			(contributed by first three proton)		
	10^{-7} s	10^{-6} s	10^{-5} s	10^{-7} s	10^{-6} s	10^{-5} s	10^{-7} s	10^{-6} s	10^{-5} s	10^{-7} s	10^{-6} s	10^{-5} s
25	0.83	0.57	0.44	0.84	0.58	0.45	0.85	0.4	0.21	0.87	0.41	0.22
50	0.99	0.72	0.58	1	0.73	0.59	0.82	0.43	0.23	0.83	0.44	0.24
100	1.24	0.97	0.8	1.26	0.98	0.82	0.72	0.39	0.17	0.73	0.4	0.18
150	1.49	1.21	1.03	1.5	1.22	1.04	0.67	0.37	0.10	0.68	0.38	0.11
200	1.7	1.42	1.27	1.71	1.43	1.28	0.77	0.41	0.11	0.78	0.42	0.12
250	2.01	1.77	1.95	2.02	1.78	1.96	0.7	0.33	0.1	0.71	0.34	0.11
300	2.46	2.5	3.21	2.47	2.51	3.22	0.57	0.21	0	0.58	0.22	0.1
350	3.23	4.06	4.29	3.24	4.07	4.3	0.45	0.12	0	0.45	0.13	0

The less the energy of proton recoil released from neutron collisions with water, the less their contribution to the final yield, due to the appropriate weightings applied according to their energy to calculate the yields. Therefore, it is worth mentioning here that the sixth, the seventh and so forth proton recoil will not give any difference in our computed yields.

5.3 Time evolution of various yields over the range of temperature from 25 to 350 ^{o}C

For the sake of illustration, Figure 5.1 shows the time evolutions of various yields calculated from our Monte Carlo simulations of the radiolysis of pure liquid water by 2 MeV neutrons at two fixed temperatures, 25 and 350 ^{o}C. From this figure we can see the formation and the decay in detail of certain yields at time ~ 10^{-12} – 10^{-5} s after the deposition of radiation energy in water. This figure is linked with the next figure in section 5.4, but more detailed if we are interesting in temperature dependence of cumulative yield ΔG(molecule/100 eV). It shows that all the rate of decay and the formation of various yields take faster at higher temperature.

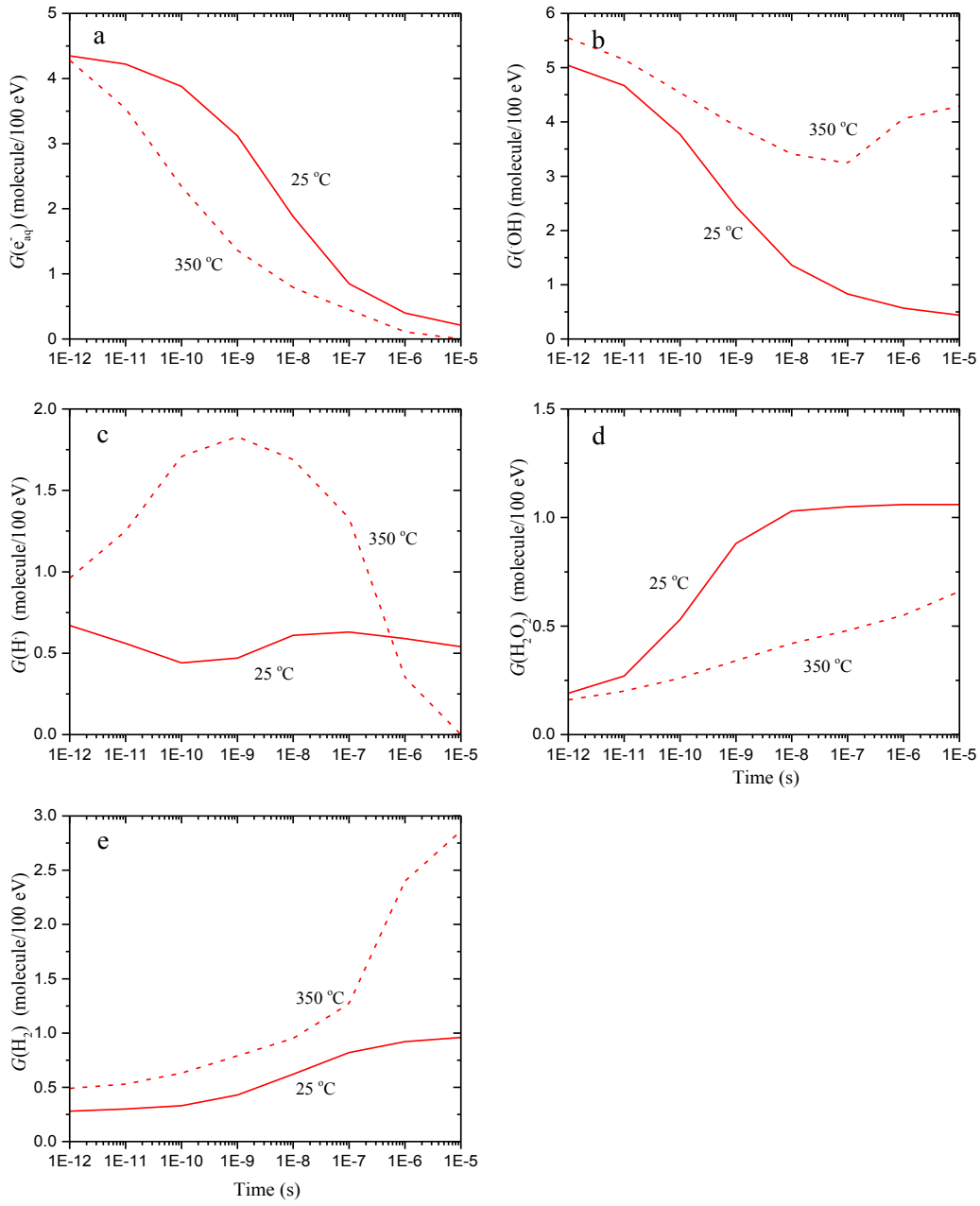

Figure 5.1 Variation of calculated g-values (in molecule/100 eV) for the radiolysis of liquid water by 2 MeV neutrons as a functions of time for temperature 25 and 300 °C are shown as dashed and solid lines, respectively: (a) $G(e^-_{aq})$, (b) $G(^{\bullet}OH)$, (c) $G(H^{\bullet})$, (d) $G(H_2O_2)$, and (e) $G(H_2)$

5.4 Contributions of the various reactions to the radiolytic yields

The variations of the yields of the various species with temperature mainly result from those reactions involved in their formation or decay that occur during the time interval of nonhomogeneous spur chemistry. To gain further insight into the effects of temperature in the radiolysis of water, it is of interest to examine the unfolding of the various reactions that contribute to the formation or decay of each species in the radiation track. This can readily be done with our Monte-Carlo simulations. The importance of these reactions can be quantified by the yield variation that they cause, expressed as a cumulative ΔG-value. Figures 5.2 show the effect of increasing temperature on the main spur reactions that are involved in the formation and decay of e^-_{aq}, $^\bullet OH$, $H^\bullet$, H_2O_2, and H_2 as they expand by diffusion in the time interval ~10^{-12}-10^{-5} s.

5.4.1 Production and decay of hydrated electrons

The hydrated electron, $e^-_{aq,}$ is probably the most studied of the transient chemical species produced in the radiolysis of water. In addition, hydrated electron is the major reducing species formed in the radiolysis of water. From Figure 5.2, it can be seen a slightly decrease (< 150 and > 200 ^oC) on e^-_{aq} yield as a function of temperature and uniformly for the three time frames. In neutral liquid water, decay of e^-_{aq} up to 10^{-5} s, as shown in Figure 5.2a is mainly due to the spur reactions of e^-_{aq} with H^+ ions and $^\bullet OH$ radicals (R1) and (R2) (in order of decreasing importance):

$$e^-_{aq} + H^+ \rightarrow H^\bullet \qquad \text{(R1)}$$

$$e^-_{aq} + {}^\bullet OH \rightarrow OH^- \qquad \text{(R2)}$$

then followed by other three reactions as below (in order of decreasing importance):

$$e^-_{aq} + H^\bullet\ (+H_2O) \rightarrow H_2 + {}^\bullet OH \qquad \text{(R3)}$$

$$e^-_{aq} + H_2O_2 \rightarrow {}^\bullet OH + OH^- \qquad \text{(R4)}$$

$$e^-_{aq} + e^-_{aq}\ (+2H_2O) \rightarrow H_2 + 2OH^- \qquad \text{(R5)}$$

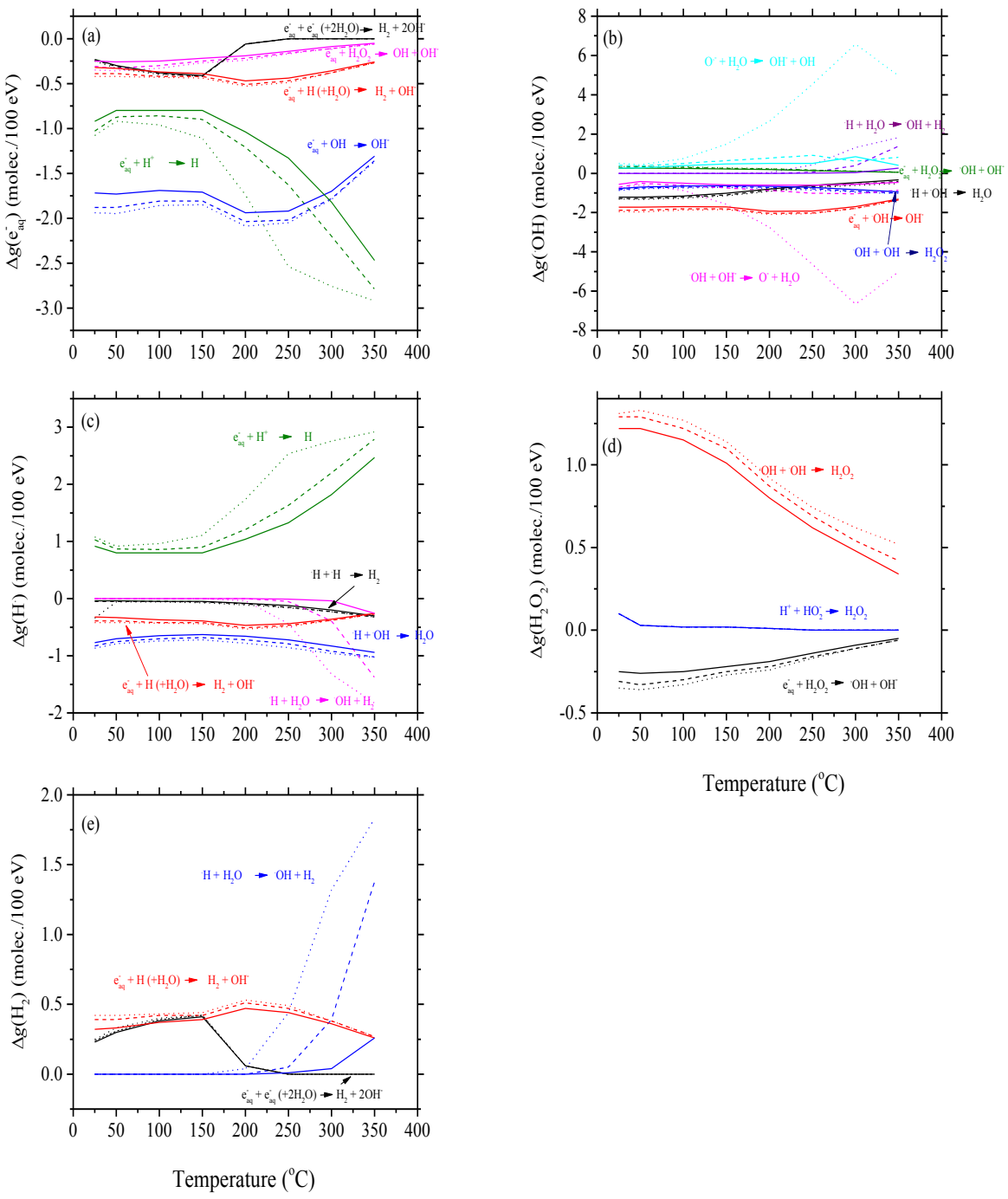

Figure 5.2 Variation of the calculated cumulative *G*-values (in molecule/100 eV) for the radiolysis of liquid water by 2 MeV neutrons as a function of temperature in the range of 25-350 °C: (a) $G(e^-_{aq})$, (b) $G(^{\bullet}OH)$, (c) $G(H^{\bullet})$, (d) $G(H_2O_2)$, and

(e) $G(H_2)$. Our simulated results, obtained at 10^{-7}, 10^{-6} and 10^{-5} s based on the radiation effects in 1.264, 0.465, 0.171, and 0.063 MeV recoil proton tracks, are shown as solid, dashed and dotted lines, respectively. To distinguish between one reaction and another reaction, we lead the eyes by matching the color of lines where the reactions equations belong to. The reactions are laid above zero value correspond to reactions that form species while under zero value correspond to the decay of species.

Pertinent to the calculation results, we should briefly emphasize the sharp discontinuity that is observed around 150 °C in the calculated yields of e^-_{aq}, which also can be seen in the yields of $H^\bullet$ and H_2 later on. This is due to the fact that the rate constant for the self-reaction of the hydrated electron, reaction (R5) drops abruptly above 150 °C (ELLIOT and BARTELS, 2009; PIMBLOT *et al.*,1991) and remain slightly constant up to 350 ^oC. We have discussed further about the uncertainty of the existence of discontinuity phenomenon in the rate constant of the reaction (R5) around 150 ^oC in near-neutral water, in section 3. As a consequence of reaction (R5), more and more hydrated electrons are available as the temperature increases, to either react in other intra-track reactions, such that competition between reactions (R1) and (R2) or escape into the bulk solution. Whilst at temperature 200 ^oC the curve of temperature dependence of $g(e^-_{aq})$ decreases slightly for all the obtaining time, this phenomena can be explained by the sharp continuous drop of reaction (R1) as seen in Figure 5.2a, where around this temperature the pH of water is slightly acidic ~5.7-6 (COHEN, 1980), therefore more H^+ ions react with hydrated electrons. For further explanation of this, we also provide in this present work the time profile of e^-_{aq} at 25 and 300 ^oC as shown in Figure 5.1a. From this figure, we investigate that the decay of hydrated electrons take place faster at higher temperature at factor 1.5 in magnitude near nanoseconds (ns). Concomitantly, the increased occurrence of reaction (R2) above 150 °C also leads to a (slight but nevertheless noticeable in Figure 1 in Chapter 4) downward discontinuity in the yields of $^\bullet OH$ and H_2O_2 (as H_2O_2 is formed mainly by the reaction of the $^\bullet OH$ radical with itself), where we will discuss more details in next sections.

5.4.2 Production and decay of hydroxyl radical (˙OH)

For ˙OH, as the main oxidizing radical formed in this 2 MeV fast neutron radiolysis, Figure 5.2b shows that the reactions to form this radical are (in order of decreasing importance):

$$H^{\bullet} + H_2O \rightarrow {}^{\bullet}OH + H_2 \qquad (R6)$$

$$e^-_{aq} + H_2O_2 \rightarrow {}^{\bullet}OH + OH^- \qquad (R4)$$

whereas its decay is dominated by reactions (in order of decreasing importance):

$$e^-_{aq} + {}^{\bullet}OH \rightarrow OH^- \qquad (R2)$$

$$H^{\bullet} + {}^{\bullet}OH \rightarrow H_2O \qquad (R7)$$

$${}^{\bullet}OH + {}^{\bullet}OH \rightarrow H_2O_2 \qquad (R8)$$

A very striking feature of our simulated results obtained at 10^{-5}s (red dotted lines in Figure 1b in Chapter 4) was the large increase with temperature, particularly above ~200 °C, of $G(^{\bullet}OH)$ and also for $G(H_2)$ and the corresponding decrease of $G(H^{\bullet})$ rather than results obtained at 10^{-6} and 10^{-7} s. The mechanism directly responsible for these behaviours is the oxidation of water by the hydrogen atom, as can be seen from Figure 5.2b:

$$H^{\bullet} + H_2O \rightarrow {}^{\bullet}OH + H_2 \qquad (R6)$$

We can highlight here that phenomenon of reaction (R6) plays important role at higher temperature and longer time. However, a controversy currently exists in the literature regarding the rate constant of reaction (R6), including estimates of 10^4 (ALCORN *et al.,* 2014) (value used in the present calculations), 3.18×10^4 (SWIATLA-WOJCIK and BUXTON, 2005), 2.2×10^3 (ELLIOT and BARTELS, 2009; BARTELS 2009), and 1.75×10^4 (SWIATLA-WOJCIK and BUXTON, 2010) M^{-1} s^{-1} at 300 °C, depending on the authors. As a result of this uncertainty, no clear conclusion has yet been obtained as to the real contribution of this potentially important reaction in the radiolysis of water at elevated temperatures. In the next section, we will see the existence of reaction (R6) gives the higher H_2 yield at longer time and higher temperatures. Contrary to the time profile of e^-_{aq} in Figure 5.1 where the decay take faster at higher temperature, the decay of ˙OH at 300 °C is lower than at room temperature, is again due to the reaction (R6) that produce ˙OH at high temperature, which is negligible at room temperature. However, the fact of reaction (R6) produce more H_2 than ˙OH is clearly seen from Figure 5.2b and e. The decay of the ˙OH

radicals is reduced as the temperature increases, that is, more $^{\bullet}OH$ radicals can escape the spur. In other words, the $^{\bullet}OH$ yield increases with temperature.

5.4.3 Production and decay of hydrogen ($H^{\bullet}$)

The $H^{\bullet}$ atom is one of the minor radical species in the radiolysis of water. It is relatively small, but is important for fundamental considerations. From Figure 5.2c, it is seen that the production of $H^{\bullet}$ atom is dominated by the rapidly converted e^{-}_{aq} into hydrogen atoms

$$e^{-}_{aq} + H^{+} \rightarrow H^{\bullet} \qquad (R1)$$

in the spur, while its decay is dominated by the reactions (R6), (R7), (R3) and (R9) (in order of decreasing importance): It clearly appears that reaction (16), which rapidly converted e^{-}_{aq} into hydrogen atoms, largely dominates all of the $H^{\bullet}$ decay reactions.

$$H^{\bullet} + H_2O \rightarrow {}^{\bullet}OH + H_2 \qquad (R6)$$

$$H^{\bullet} + {}^{\bullet}OH \rightarrow H_2O \qquad (R7)$$

$$e^{-}_{aq} + H^{\bullet} (+H_2O) \rightarrow H_2 + {}^{\bullet}OH \qquad (R3)$$

$$H^{\bullet} + H^{\bullet} \rightarrow H_2 \qquad (R9)$$

From Figure 5.2c, the available e^{-}_{aq} reacts rapidly with H^{+} in the spur mostly at longer obtaining time. However, as can be seen in Figure 1c (in Chapter 4), a switch from increasing to rapidly decreasing values is observed at 10^{-6} and 10^{-5} s especially around ~200-300 °C in our calculated $G(H^{\bullet})$ values (in contrast to the corresponding yields at 10^{-7} s, which increase monotonically with temperature).

5.4.4 Production and decay of hydrogen peroxide (H_2O_2)

Hydrogen peroxide is one of the main oxidizing species in the radiolysis of water. H_2O_2 formed in the radiolysis of water is found to be the main corrosion product, and it is involved in the oxidation damage of most alloy. It has long been established, both from the modeling and experimental results that the main precursor of H_2O_2 is the self-reaction of $^{\bullet}OH$:

$$^{\bullet}OH + {}^{\bullet}OH \rightarrow H_2O_2 \qquad (R8)$$

then less important (where it remains constant at different obtaining time) by

$$H^{+} + HO_2^{-} \rightarrow H_2O_2 \qquad (R10)$$

Figure 5.2d shows the clear evidence that the self-reaction of $^{\bullet}OH$ radicals is the major source of formation hydrogen peroxide. From the same figure it can be seen that the decay of H_2O_2 is given dominantly by reaction:

$$e^{-}_{aq} + H_2O_2 \rightarrow {}^{\bullet}OH + OH^{-} \qquad \text{(R4)}$$

There is also a large degree of uncertainty associated with the temperature dependence of the peroxide yields, which is difficult to obtain experimentally due to the thermal decomposition of H_2O_2 at high temperature start from ~100 °C (McCRACKEN *et al.* (1998); KENT and SIMS (1992)). SUNARYO et al. (1995) considered that H_2O_2 should be decomposed into H_2O and O_2 based on their experiment as below

$$H_2O_2 \rightarrow H_2O + \tfrac{1}{2}O_2 \qquad \text{(R11)}$$

This agreement between the experiment and model supports a posteriori the validity of the assumptions employed in the calculations.

5.4.5 Production and decay of molecular hydrogen (H_2)

One very important practical application of the radiolysis of water at high temperature is the use of molecular hydrogen dissolved in the cooling water of pressurized water reactors (PWRs) and boiling water reactors (BWRs) to mitigate corrosion. Hydrogen is known to reduce the concentration of oxidizing species such as O_2 and H_2O_2 and lower the electrochemical corrosion potential (ECP) of metal in the reactor's internal components, which is associated with cracking. The beneficial effect of molecular hydrogen has been known for many years and justification for its use has been based on the mechanism proposed by ALLEN *et al.* (1952).

Although H_2 is a molecular product, which expected to decrease as a function of temperature due to the diffusion of radical species out of the spur increases more rapidly than recombination (SANGUANMITH *et al.*, 2011), but as seen from Fig. 1e, it continues to increase particularly above 200 ^{o}C and the experimental data as well.

In neutral liquid water, the three main processes which result in significant production of H_2 are (in order of decreasing importance):

$$H^{\bullet} + H_2O \rightarrow {}^{\bullet}OH + H_2 \quad \text{(above ~200 } ^{o}\text{C)} \qquad \text{(R6)}$$

$$e^{-}_{aq} + H^{\bullet}\,(+H_2O) \rightarrow H_2 + {}^{\bullet}OH \qquad \text{(R3)}$$

$$e^{-}_{aq} + e^{-}_{aq}\,(+2H_2O) \rightarrow H_2 + 2OH^{-} \qquad \text{(R5)}$$

As already mentioned in earlier section, that discontinuity observed in $G(H_2)$ at 150 ^{o}C have been predicted as we incorporated the turnover of the rate constant for the self-reaction of e^{-}_{aq} (R5) that measured in alkaline water condition. Based on recent studies that have shown that a major fraction of the source of formation H_2 is due to the self-reactions of hydrated electron, therefore, further measurements of its rate constant in pure water are highly needed. A decrease in the yield of e^{-}_{aq} in high LET fast neutron as compared to low-LET γ-rays is accompanied by higher increase in molecular hydrogen yield.

The sharp increasing of H_2 yield is observed starting from 200 ^{o}C (for example at 10^{-5} s). The mechanism directly responsible for these behaviors is the oxidation of water by the hydrogen atom (R6), as can be seen from Figure 5.2e, however its rate constant is still in controversy. This reaction also was recently proposed to quantitatively explain the large, anomalous increase of the primary yield of H_2 observed experimentally in the low-LET radiolysis of water above 200-250 °C (McCRACKEN *et al.*, 1998; MEESUNGNOEN and JAY-GERIN, 2010; SWIATLA-WOJCIK and BUXTON, 2005; ELLIOT and BARTELS, 2009; BARTELS 2009; SWIATLA-WOJCIK and BUXTON, 2010). The effect of this reaction is more favorable for the formation of H_2 than $^{\bullet}$OH at high temperature. Judging from Figure 1 b, c and e (in Chapter 4), these fast neutron radiolysis yields for $^{\bullet}$OH, $H^{\bullet}$, and H_2 can hardly provide information about the value of the rate constant for reaction (R6), given the lack of experimental data above ~300 °C.

6. CONCLUSION

In this work, Monte-Carlo simulations were used to investigate the effect of temperature on the primary yields (*G*-values) of the radical and molecular products of the radiolysis of pure deaerated liquid water over the range 25-350 ^{o}C irradiated by 2 MeV fast neutrons. To reproduce the effects due to 2 MeV fast neutrons, we simulated short (~15-150 μm) track segments of each proton recoil released from neutron collisions.

The fast neutron *G*-values were obtained by assuming that the most significant contribution to the radiolysis comes from the first four elastically scattered recoil protons generated by the passage of the incident neutron and by neglecting the radiation effects due to oxygen ion recoils. The results of the simulations agreed reasonably well with existing experimental data. Our computed yields for fast neutrons showed essentially similar temperature dependences over the range of temperature studied with the data obtained for low-LET radiation, but with lower values for yields of free radicals and higher values for molecular yields; this result reflects the high-LET character of fast neutrons.

Finally, a striking feature of our simulated results was the marked increase, at long times and higher temperature (above 200 ^{o}C) of $G(H_2)$ and $G(^{\bullet}OH)$ and the corresponding decrease of $G(H^{\bullet})$, due to the occurrence of the reaction $H^{\bullet} + H_2O \rightarrow H_2 + {}^{\bullet}OH$ in the homogeneous chemical stage.

Even though H_2 is a molecular product, its "escape" yield $g(H_2)$ increases with increasing temperature. A main source of H_2 is the bimolecular reaction of two hydrated electrons (e^{-}_{aq}) which its rate constant, based on literature, drops abruptly above ~150 °C. However, when this drop in the e^{-}_{aq} self-reaction rate constant is included in low (isolated spurs) and high (cylindrical tracks) linear energy transfer (LET) modeling calculations, $g(H_2)$ shows a marked downward discontinuity at ~150 °C which is *not* observed experimentally. Considering the importance of the self-reaction of e^{-}_{aq} as a main source of molecular hydrogen in high-temperature water radiolysis, further measurements of its rate constant in pure water are obviously highly desirable. The applicability of the sudden drop

in k_1 observed at ~150 °C in alkaline water to near-neutral water is questionable and that further measurements of the rate constant in pure water are highly desirable.

7. ACKNOWLEDGMENTS

I would like to thank the Department of Nuclear Medicine and Radiobiology, Faculty of Medicine and Health Sciences, *Université de Sherbrooke*.

I would like to thank Prof. J.-P. Jay-Gerin, my supervisor, for the opportunity he gave to join his group, his advices, number of discussions, and encouragement.

I appreciated the help and support of Dr. J. Meesungnoen, Sunuchakan Sanguanmith and Leila Mirsaleh Kohan. Also I would like to thank my colleagues in our laboratory, Shayla Mustaree and Vanaja Kanike and also all my colleagues in the department.

Special thanks for Professor Prof. Y. Katsumura, Dr. Yusa Muroya, Dr. D.A. Guzonas, and Dr. C.R. Stuart for useful discussions and correspondence, and for kindly sending us their experimental data prior to publication. The financial assistance from the Atomic Energy of Canada Limited, the Natural Sciences and Engineering Research Council of Canada, and Natural Resources Canada is gratefully acknowledged.

I would like to thank Dr. Geni Rina Sunaryo for giving me the chance to pursue my dream. I would like to thank my institution in Indonesia, BATAN, for letting me disappear for almost two and a half years.

Finally, I would like to extend my deepest gratitude to my family and friends in Oasis Christian Center. To my husband, Junsun Nainggolan and our three cheerful children, Jeremy, Rachael and Pieter, I would like to offer my appreciation of the love and support they have given me through my graduate career.

8. REFERENCES

ALLEN, A.O., 1952. Decompositon of water and aqueous solutions under mixed fast neutron and gamma radiation. *J. Phys. Chem.* **56,** 575-586.

ALLEN, A.O., 1961. *The Radiation Chemistry of Water and Aqueous Solutions*. D. Van Nostrand Co., Princeton, N.J.

AMICHAI, O. and TREININ, A., 1969. Chemical reactivity of $O(^3P)$ atoms in aqueous solution. *Chem. Phys. Lett.* **3**, 611-613.

ANDERSON, D.W., 1984. *Absorption of Ionizing Radiation*. University Park Press, Baltimore, MD.

AUTSAVAPROMPORN, N., 2006. *The effects of pH and radiation quality (LET) on the radiolysis of liquid water and aqueous solutions: A study by using Monte-Carlo simulations*. M.Sc. Thesis, Burapha University, Bangsaen (Thailand).

AUTSAVAPROMPORN, N., MEESUNGNOEN, J., PLANTE, I., and JAY-GERIN, J.-P., 2007. Monte-Carlo simulation study of the effects of acidity and LET on the primary free-radical and molecular yields of water radiolysis – Application to the Fricke dosimeter. *Can. J. Chem.* **85**, 214-229.

AUXIER, J.A., SNYDER, W.S., and JONES T.D.,1968. Neutron interactions and penetration in tissue.*In* Radiation dosimetry. Vol. I. *Edited by* F.H. Attix, W.C. Roesch, and E. Tochilin. Academic Press, New York. 275.

BALLARINI, F., BIAGGI, M., MERZAGORA, M., OTTOLENGHI, A., DINGFELDER, M., FRIEDLAND, W., JACOB, P., and PARETZKE, H.G., 2000. Stochastic aspects and uncertainties in the prechemical and chemical stages of electron tracks in liquid water: A quantitative analysis based on Monte Carlo simulations. *Radiat. Environ. Biophys.* **39**, 179-188.

BARTELS, D.M., 2009. Comment on the possible role of the reaction $H^{\bullet} + H_2O \rightarrow H_2 + {}^{\bullet}OH$ in the radiolysis of water at high temperatures. *Radiat. Phys. Chem.* **78**, 191-194.

BASS, A.D. and SANCHE, L., 2003. Dissociative electron attachment and charge transfer in condensed matter. *Radiat. Phys. Chem.* **68**, 3-13.

BERNAS, A., FERRADINI, C., and JAY-GERIN, J.-P., 1996.Électrons en excès dans les milieux polaires homogènes et hétérogènes. *Can. J. Chem.***74**, 1-23.

BIEDENKAPP, D., HARTSHORN, L.G., and BAIR, E.J., 1970. The O(^1D) + H_2O reaction. *Chem. Phys. Lett.* **5**, 379-380.

BURNS, W.G. and MOORE, P.B., 1976. Water radiolysis and its effect upon in reactor zircaloy corrosion. *Radiat. Eff.* **30**, 233-242.

BUXTON, G.V., 2001. High temperature water radiolysis. In: Jonah, C.D. and Rao, B.S.M. (Eds.), *Radiation Chemistry - Present Status and Future Trends*. Elsevier, Amsterdam, 145-162.

CEMBER, H., and JOHNSON, T.E., 2009. Introduction to health physics. 4th ed. McGraw-Hill, New York.

CHATTERJEE, A. and SCHAEFER, H.J., 1976. Microdosimetric structure of heavy ion tracks in tissue. *Radiat. Environ. Biophys.***13**, 215-227.

CHATTERJEE, A. and HOLLEY, W.R., 1993. Computer simulation of initial events in the biochemical mechanisms of DNA damage. *Adv. Radiat. Biol.* **17**, 181-226.

CHRISTENSEN, C.J., NIELSEN, A., BAHNSEN, A., BROWN, W.K., RUSTAD, B.M., 1972. Free-neutron beta-decay half-life. *Phys. Rev. D***. 5**, 1628-1640.

CHRISTENSEN, H. and SEHESTED, K., 1986. The hydrated electron and its reactions at high temperatures. *J. Phys. Chem.* **90**, 186-190.

CHRISTENSEN, H., 2006. Fundamental aspects of water coolant radiolysis. SKI Report 2006:16. Swedish Nuclear Power Inspectorate, Stockholm, Sweden.

CHRISTOPHOROU, L.G., McCORKLE, D.L., and CHRISTODOULIDES, A.A., 1984. Electron attachment processes. In: Christophorou, L.G. (Ed.), *Electron-Molecule Interactions and their Applications*, vol. 1. Academic Press, Orlando, FL, 477-617.

CLIFFORD, P., GREEN, N.J.B., OLDFIELD, M.J., PILLING, M.J., and PIMBLOTT, S.M., 1986. Stochastic models of multi-species kinetics in radiation-induced spurs. *J. Chem. Soc., Faraday Trans. 1*, **82**, 2673-2689.

COBUT, V., 1993. *Simulation Monte-Carlo du transport d'électrons non relativistes dans l'eau liquide pure et de l'évolution du milieu irradié: rendements des espèces créées de 10^{-15} à 10^{-7} s*. Ph.D. Thesis, Université de Sherbrooke.

COBUT, V., FRONGILLO, Y., JAY-GERIN, J.-P., and PATAU, J.P., 1994. Calculs

des rendements des produits de la radiolyse de l'eau en fonction du temps par une méthode Monte-Carlo. *J. Chim. Phys.* **91**, 1018-1024.

COBUT, V., JAY-GERIN, J.-P., FRONGILLO, Y., and PATAU, J.P., 1996. On the dissociative electron attachment as a potential source of molecular hydrogen in irradiated liquid water, *Radiat. Phys. Chem.* **47**, 247-250.

COBUT, V., FRONGILLO, Y., PATAU, J.P., GOULET, T., FRASER, M.-J., and JAY-GERIN, J.-P., 1998. Monte Carlo simulation of fast electron and proton tracks in liquid water. I. Physical and physicochemical aspects. *Radiat. Phys. Chem.* **51**, 229-243.

COHEN, P., 1980. *Water Coolant Technology of Power Reactors*. American Nuclear Society, La Grange Park, IL.

CZAPSKI, G. and SCHWARZ, H.A., 1962. The nature of the reducing radical in water radiolysis. *J. Phys. Chem.* **66**, 471-474.

DEGROOT, M.H. and SCHERVISH, M.J., 2002. Probability and statistics. 3rd ed. Addison-Wesley, Boston, MA.

DINGFELDER, M. and FRIEDLAND, W., 2001. Basic data for track structure simulations: Electron interaction cross-sections in liquid water. In: Kling, A., Barão, F., Nakagawa, M., Távora, L., and Vaz, P. (Eds.), *Advanced Monte Carlo for Radiation Physics, Particle Transport Simulation and Applications*. Springer-Verlag, Berlin, 267-272.

DINGFELDER, M., RITCHIE, R.H., TURNER, J.E., FRIEDLAND, W., PARETZKE, H.G., and HAMM, R.N., 2008. Comparisons of calculations with PARTRAC and NOREC: Transport of electrons in liquid water. *Radiat. Res.***169**, 584-594.

EDWARDS, E.J., WILSON, P.P.H., ANDERSON, M.H., MEZYK, S.P., PIMBLOTT, S.M., and BARTELS, D.M., 2007. An apparatus for the study of high temperature water radiolysis in a nuclear reactor: Calibration of dose in a mixed neutron/gamma radiation field. *Rev. Sci. Instrum.* **78**, 124101.

ELLIOT, A.J., McCRACKEN, D.R., BUXTON, G.V., and WOOD, N.D., 1990. Estimation of rate constants for near-diffusion-controlled reactions in water at high temperatures. *J. Chem. Soc. Faraday Trans.* **86**, 1539-1547.

ELLIOT, A.J., CHENIER, M.P., and OUELLETTE, D.C., 1993. Temperature

dependence of *g* values for H_2O and D_2O irradiated with low linear energy transfer radiation. *J. Chem. Soc. Faraday Trans.***89**, 1193-1197.

ELLIOT, A.J., 1994. Rate constants and *G*-values for the simulation of the radiolysis of light water over the range 0-300 ºC. Report AECL-11073. Atomic Energy of Canada Ltd., Chalk River, ON.

ELLIOT, A.J. and OUELLETTE, D.C., 1994. Temperature dependence of the rate constant for the reaction e^-_{aq}+ OH in water up to 150 °C. *J. Chem. Soc. Faraday Trans.* **90**, 837-841.

ELLIOT, A.J., OUELLETTE, D.C., and STUART, C.R., 1996*a*. The temperature dependence of the rate constants and yields for the simulation of the radiolysis of heavy water. Report AECL-11658. Atomic Energy of Canada Ltd., Chalk River, ON.

ELLIOT, A.J., CHENIER, M.P., OUELLETTE, D.C., and KOSLOWSKY, V.T., 1996*b*. Temperature dependence of *g* values for aqueous solutions irradiated with 23 MeV $^2H^+$ and 157 MeV $^7Li^{3+}$ ion beams. *J. Phys. Chem.***100**, 9014-9020.

ELLIOT, A.J. and BARTELS, D.M., 2009. The reaction set, rate constants and *g*-values for the simulation of the radiolysis of light water over the range 20° to 350°C based on information available in 2008. Report AECL No. 153-127160-450-001. Atomic Energy of Canada Limited, Chalk River, Ontario, Canada.

EVANS, R.D., 1955. *The Atomic Nucleus*. Krieger Publ. Co., Malabar, FL.

FARAGGI, M. and DÉSALOS, J., 1969. Effect of positively charged ions on the "molecular" hydrogen yield in the radiolysis of aqueous solutions. *Int. J. Radiat. Phys. Chem.* **1**, 335-344.

FERRADINI, C., 1979. Actions chimiques des radiations ionisantes. *J. Phys. Chim.* **76**, 636-644.

FERRADINI, C. and JAY-GERIN, J.-P., 1999.La radiolyse de l'eau et des solutions aqueuses: historique et actualité. *Can. J. Chem.***77**, 1542-1575.

FRIEDLANDER, G., KENNEDY, J.W., MACIAS, E.S., and MILLER J.M., 1981. Nuclear and radiochemistry. 3rd ed. Wiley, New York.

FRONGILLO, Y., FRASER, M.J., COBUT, V., GOULET, T., JAY-GERIN, J.-P., and PATAU, J.P., 1996. Évolution des espèces produites par le ralentissement de

protons rapides dans l'eau liquid : simulation fondée sur l'approximation des temps de réaction indépendants. *J. Chim. Phys.* **93**, 93-102.

FRONGILLO, Y., GOULET, T., FRASER, M.-J., COBUT, V., PATAU, J.P., and JAY-GERIN, J.-P., 1998. Monte Carlo simulation of fast electron and proton tracks in liquid water. II. Nonhomogeneous chemistry. *Radiat. Phys. Chem.* **51**, 245-254.

GOULET, T. and JAY-GERIN, J.-P., 1989.Thermalization of subexcitation electrons in solid water. *Radiat. Res.***118**, 46-62.

GOULET, T., PATAU, J.P., and JAY-GERIN, J.-P., 1990. Influence of the parent cation on the thermalization of subexcitation electrons in solid water. J. Phys. Chem. **94**, 7312-7316.

GOULET, T. and JAY-GERIN, J.-P., 1992. On the reactions of hydrated electrons With $^{\bullet}OH$ and H_3O^+. Analysis of photoionization experiments. *J.Chem. Phys.* **96**, 5076-5087.

GOULET, T., JAY-GERIN, J.-P., FRONGILLO, Y., COBUT, V., and FRASER, M.-J., 1996. Rôle des distances de thermalisation des électrons dans la radiolyse de l'eau liquide. *J. Chim. Phys.* **93**, 111-116.

GOULET, T., FRASER, M.-J., FRONGILLO, Y., and JAY-GERIN, J.-P., 1998. On the validity of the independent reaction times approximation for the description of the nonhomogeneous kinetics of liquid water radiolysis. *Radiat. Phys. Chem.* **51**, 85-91.

GREEN, N.J.B., PILLING, M.J., PIMBLOTT, S.M., and CLIFFORD, P., 1990. Stochastic modeling of fast kinetics in a radiation track. *J. Phys. Chem.* **94**, 251-258.

HELLER, J.M., Jr., HAMM, R.N., BIRKHOFF, R.D., and PAINTER, L.R., 1974. Collective oscillation in liquid water. *J. Chem. Phys.* **60**, 3483-3486.

HERVÉ DU PENHOAT, M.-A., GOULET, T., FRONGILLO, Y., FRASER, M.-J., BERNAT, Ph., and JAY-GERIN, J.-P., 2000. Radiolysis of liquid water at temperatures up to 300 ^{o}C: A Monte Carlo simulation study. *J. Phys. Chem. A.* **104**, 11757-11770.

HERVÉ DU PENHOAT, M.-A., MEESUNGNOEN, J., GOULET, T., FILALI-

MOUHIM, A., MANKHETKORN, S., and JAY-GERIN, J.-P., 2001. Linear-energy-transfer effects on the radiolysis of liquid water at temperatures up to 300 ºC - A Monte-Carlo study. *Chem. Phys. Lett.* **341**, 135-143.

HICKEL, B., 1991. Quelques problèmes concernant la radiolyse de l'eau liquide à haute température : application aux réacteurs nucléaires. *J. Chim. Phys.* **88**, 1177-1193.

HOCHANADEL, C.J. and GHORMLEY, J.A., 1962. Effect of temperature on the decomposition of water by gamma rays. *Radiat. Res.***16**, 653-660.

IAEA-TECDOC-799, 1995. *Atomic and Molecular Data for Radiotherapy and Radiation Research*. International Atomic Energy Agency, Vienna.

ICRU REPORT 31, 1979. *Average Energy Required to Produce an Ion Pair*. International Commission on Radiation Units and Measurements, Washington, DC.

INOKUTI, M., 1971. Inelastic collisions of fast charged particles with atoms and molecules—the Bethe theory revisited. *Rev. Mod. Phys.* **43**, 297-347.

ISHIGURE, K., KATSUMURA, Y., SUNARYO, G.R., and HIROISHI, D., 1995. Radiolysis of high temperature water. *Radiat. Phys. Chem.* **46**, 557-560.

JANIK, D., JANIK, I., and BARTELS, D.M., 2007. Neutron and β/γ radiolysis of water up to supercritical conditions. 1. β/γ yields for H_2, $H^{\bullet}$ atom, and hydrated electron. *J. Phys. Chem. A.* **111**, 7777-7786.

KABAKCHI, S.A. and BUGAENKO, V.L., 1992. Mathematical modeling of radiolysis of liquid water at high temperatures. *High Energy Chem.* **26**, 319-323.

KAPLAN, I.G. and MITEREV, A.M., 1987. Interaction of charged particles with molecular medium and track effects in radiation chemistry. *Adv. Chem. Phys.* **68**, 255-386.

KARA-MICHAILOVA, E. and LEA, D.E., 1940. The interpretation of ionization measurements in gases at high pressures. *Proc. Cambridge Phil. Soc.* **36**, 101-126.

KATZ, R., 1970. RBE, LET and z/β^{α}. *Health Phys*. **18**, 175

KATZ, R., 1978. Track structure theory in radiobiology and in radiation detection. *Nucl. Track Detect*. **2**, 1-28.

KATSUMURA, Y., SUNARYO, G., HIROISHI, D., and ISHIGURE, K., 1998. Fast

neutron radiolysis of water at elevated temperatures relevant to water chemistry. *Prog.Nucl. Energy* **32**, 113-121.

KATSUMURA, Y., 2004. Application of radiation chemistry to nuclear technology. In: Mozumder, A. and Hatano, Y. (Eds.), *Charged Particle and Photon Interactions with Matter. Chemical, Physicochemical, and Biological Consequences with Applications*. Marcel Dekker, New York, 697-727.

KENT, M.C. and SIMS, H.E., 1992*a*. The yield of γ-radiolysis products from water at temperatures up to 300 ºC.*Proceedings of the 6th International Conference on Water Chemistry of Nuclear Reactor Systems*. British Nuclear Energy Society, London, 153-158.

KENT, M.C. and SIMS, H.E., 1992*b*. The yield of γ-radiolysis products from water at temperatures up to 270 ºC. Report AEA-RS-2302. Atomic Energy Authority, Didcot, Oxfordshire, U.K.

KIMMEL, G.A., ORLANDO, T.M., VÉZINA, C., and SANCHE, L., 1994. Low-energy electron-stimulated production of molecular hydrogen from amorphous water ice. *J. Chem. Phys.* **101**, 3282-3286.

KNUTH, D.E., 1998. The art of computer programming. 3rd ed. Vol. 2. Addison-Wesley, Reading, MA.

KRAFT, G. and KRÄMER, M., 1993. Linear energy transfer and track structure. *Adv. Radiat. Biol.* **17**, 1-52.

KRANE, K.S., 1988. Introductory nuclear physics. Wiley, New York.

KUPPERMANN, A., 1959. Theoretical foundations of radiation chemistry.*J.Chem. Educ.* **36**, 279-285.

LAVERNE, J.A., 2000. Track effects of heavy ions in liquid water. *Radiat. Res.* **153**, 487-496.

LAVERNE, J.A., 2004. Radiation chemical effects of heavy ions. In: Mozumder, A. and Hatano, Y. (Eds.), *Charged Particle and Photon Interactions with Matter.Chemical, Physicochemical, and Biological Consequences with Applications*. Marcel Dekker, New York, pp. 403-429.

LAVERNE, J.A. and PIMBLOTT, S.M., 1993. Diffusion-kinetic modeling of the

electron radiolysis of water at elevated temperatures. *J. Phys. Chem.* **97**, 3291-3297.

LAVERNE, J.A. and PIMBLOTT, S.M., 1995. Electron energy-loss distributions in solid, dry DNA. *Radiat. Res.* **141**, 208-215.

LAVERNE, J.A. and SCHULER, R.H., 1987*a*. Radiation chemical studies with heavy ions: Oxidation of ferrous ion in the Fricke dosimeter. *J. Phys. Chem.* **91**, 5770-5776.

LINSTROM, P.J. and MALLARD, W.G. (Eds.), 2005. NIST Chemistry WebBook, NIST Standard Reference Database No. 69. National Institute of Standards and Technology, Gaithersburg, M.D. Available from http://webbook.nist.gov.

MAGEE, J.L., 1953. Radiation chemistry. *Annu. Rev. Nucl. Sci.* **3**, 171-192.

MAGEE, J.L. and CHATTERJEE, A., 1980. Radiation chemistry of heavy-particle tracks. 1. General considerations. *J. Phys. Chem.* **84**, 3529-3536.

MAGEE, J.L. and CHATTERJEE, A., 1987. In: Freeman, G.R. (Ed.), *Kinetics of Nonhomogeneous Processes*. Wiley, New York, pp. 171-214.

McCRACKEN, D.R., TSANG, K.T., and LAUGHTON, P.J., 1998. Aspects of the physics and chemistry of water radiolysis by fast neutrons and fast electrons in nuclear reactors. Report AECL-11895. Atomic Energy of Canada Ltd., Chalk River, ON.

MEESUNGNOEN, J., BENRAHMOUNE, M., FILALI-MOUHIM, A., MANKHETKORN, S., and JAY-GERIN, J.-P., 2001. Monte Carlo calculation of the primary radical and molecular yields of liquid water radiolysis in the linear energy transfer range 0.3-6.5 keV/μm: Application to ^{137}Cs gamma rays. *Radiat. Res.* **155**, 269-278.

MEESUNGNOEN, J., JAY-GERIN, J.-P., FILALI-MOUHIM, A., and MANKHETKORN, S., 2002*a*. On the temperature dependence of the primary yield and the product $G\varepsilon_{max}$ of hydrated electrons in the low-LET radiolysis of liquid water. *Can. J. Chem.* **80**, 767-773.

MEESUNGNOEN, J., JAY-GERIN, J.-P., FILALI-MOUHIM, A., and MANKHETKORN, S., 2002*b*. Low-energy electron penetration range in liquid water. *Radiat. Res.* **158**, 657-660.

MEESUNGNOEN, J., FILALI-MOUHIM, A., SNITWONGSE NA AYUDHYA, N.,

MANKHETKORN, S., and JAY-GERIN, J.-P., 2003. Multiple ionization effects on the yields of $HO_2^{\bullet}/O_2^{\bullet-}$ and H_2O_2 produced in the radiolysis of liquid water with high-LET $^{12}C^{6+}$ ions: A Monte-Carlo simulation study. *Chem. Phys. Lett.* **377**, 419-425.

MEESUNGNOEN, J. and JAY-GERIN, J.-P., 2005*a*. High-LET radiolysis of liquid water with $^{1}H^{+}$, $^{4}He^{2+}$, $^{12}C^{6+}$, and $^{20}Ne^{9+}$. *J. Phys. Chem. A.* **109**, 6406-6419.

MEESUNGNOEN, J. and JAY-GERIN, J.-P., 2005*b*. Effect of multiple ionization on the yield of H_2O_2 produced in the radiolysis of aqueous 0.4 *M* H_2SO_4 solutions by high-LET $^{12}C^{6+}$ and $^{20}Ne^{9+}$ ions. *Radiat. Res.* **164**, 688-694.

MEESUNGNOEN, J., 2007. *Effect of multiple ionization on the radiolysis of liquid water irradiated with heavy ions: A theoretical study using Monte-Carlo simulations*. Ph.D. Thesis, Université de Sherbrooke.

MEESUNGNOEN, J., JAY-GERIN, J.-P., 2010. Radiation chemistry of liquid water with heavy ions: Monte-Carlo simulation studies, in: Hatano, Y., Katsumura, Y., Mozumder, A. (Eds.), Charged Particle and Photon Interactions with Matter. Recent Advances, Applications, and Interfaces. Taylor & Francis, Boca Raton, Florida, pp. 355-400.

MICHAUD, M., CLOUTIER, P., and SANCHE, L., 1991. Low-energy electron-energy-loss spectroscopy of amorphous ice: Electronic excitations. *Phys. Rev. A.* **44**, 5624-5627.

MICHAUD, M., WEN, A., and SANCHE, L., 2003. Cross sections for low-energy (1-100 eV) electron elastic and inelastic scattering in amorphous ice. *Radiat. Res.* **159**, 3-22.

MICHAUD, M. and SANCHE, L., 1987. Absolute vibrational excitation cross section for slow-electron (1-18 eV) scattering in solid H_2O. *Phys. ReV. A.* **36**, 4684-4699.

MOZUMDER, A., CHATTERJEE, A., and MAGEE, J.L., 1968. Theory of radiation chemistry. IX. Model and structure of heavy particle tracks in water. *Adv. Chem. Series* 81, 27-48.

MOZUMDER, A. and MAGEE, J.L., 1975. The early events of radiation chemistry. *Int. J. Radiat. Phys. Chem.***7**, 83-93.

MOZUMDER, A., 1999. *Fundamentals of Radiation Chemistry*. Academic Press,

San Diego, CA.

MUROYA, Y., MEESUNGNOEN, J., JAY-GERIN, J.-P., FILALI-MOUHIM, A., GOULET, T., KATSUMURA, Y., and MANKHETKORN, S., 2002. Radiolysis of liquid water: An attempt to reconcile Monte-Carlo calculations with new experimental hydrated electron yield data at early times. *Can. J. Chem.* **80**, 1367-1374.

MUROYA, Y., PLANTE, I., AZZAM, E.I., MEESUNGNOEN, J., KATSUMURA, Y., and JAY-GERIN, J.-P., 2006. High-LET ion radiolysis of water: Visualization of the formation and evolution of ion tracks and relevance to the radiation-induced bystander effect. *Radiat. Res.* **165**, 485-491.

MUROYA, Y., LIN, M., DE WAELE, V., HATANO, Y., KATSUMURA, Y., and MOSTAFAVI, M., 2010. First observation of picosecond kinetics of hydrated electrons in supercritical water. *J. Phys. Chem. Lett.* **1**, 331-335.

NETA, P., HUIE, R.E., and ROSS, A.B., 1988. Rate constants for reactions of inorganic radicals in aqueous solution. *J. Phys. Chem. Ref. Data* **17**, 1027-1284.

NIKJOO, H., UEHARA, S., EMFIETZOGLOU, D., and CUCINOTTA, F.A., 2006. Track-structure codes in radiation research. *Radiat. Meas.* **41**, 1052-1074.

NOYES, R.M., 1961. Effects of diffusion rates on chemical kinetics. In: Porter, G. and Stevens, B. (Eds.), *Progress in Reaction Kinetics*, vol. 1. Pergamon Press, Oxford, pp. 129-160.

OGURA, H. and HAMILL, W.H., 1973. Positive hole migration in pulse-irradiated water and heavy water. *J. Phys. Chem.* 77, 2952-2954.

PARETZKE, H.G., 1987. Radiation track structure theory. In: Freeman, G.R. (Ed.), *Kinetics of Nonhomogeneous Processes*. Wiley, New York, pp. 89-170.

PARETZKE, H.G., GOODHEAD, D.T., KAPLAN, I.G., and TERRISSOL, M., 1995. Track structure quantities. In: *Atomic and Molecular Data for Radiotherapy and Radiation Research*, IAEA-TECDOC-799. International Atomic Energy Agency, Vienna, pp. 633-721.

PASTINA, B., LAVERNE, J.A., and PIMBLOTT, S.M., 1999. Dependence of molecular hydrogen formation in water on scavengers of the precursor to the hydrated electron. *J. Phys. Chem. A.* **103**, 5841-5846.

PASTINA, B. and LAVERNE, J.A., 2001. Effect of molecular hydrogen on hydrogen peroxide in water radiolysis. *J. Phys. Chem. A.* **105**, 9316-9322.

PERALTA, L., 2002. Monte Carlo simulation of neutron thermalization in matter. *Eur. J. Phys.* **23**, 307-314.

PIMBLOTT, S.M., and LAVERNE, J.A., 2002. Effects of track structure on the ion radiolysis of the Fricke dosimeter. *J. Phys. Chem.* **106**, 9420-9427.

PIMBLOTT, S.M. and MOZUMDER, A., 1991. Structure of electron tracks in water. 2. Distribution of primary ionizations and excitations in water radiolysis. *J. Phys. Chem.* **95**, 7291-7300.

PIMBLOTT, S.M., PILLING, M.J., and GREEN, N.J.B., 1991. Stochastic models of spur kinetics in water. *Radiat. Phys. Chem.* **37**, 377-388.

PIMBLOTT, S.M. and GREEN, N.J.B., 1995. Recent advances in the kinetics of radiolytic processes. In: Compton, R.G. and Hancock, G. (Eds.), *Research in Chemical Kinetics*, vol. 3. Elsevier, Amsterdam, pp. 117-174.

PLANTE, I.L., FILALI-MOUHIM, A., and JAY-GERIN, J.-P., 2005. SimulRad: A Java interface for a Monte-Carlo simulation code to visualize in 3D the early stages of water radiolysis. *Radiat. Phys. Chem.* **72**, 173-180.

PLANTE, I., 2009. Développement de codes de simulation Monte-Carlo de la radiolyse de l'eau et de solutions aqueuses par des électrons, ions lourds, photons et neutrons : Application à divers sujets d'intérêt expérimental. Ph.D. Thesis, Université de Sherbrooke.

PLATZMAN, R.L., 1955. Subexcitationelectrons. *Radiat. Res.* **2**, 1-7.

PLATZMAN, R.L., 1958. The physical and chemical basis of mechanisms in radiation biology. In: Claus, W.D. (Ed.), *Radiation Biology and Medicine. Selected Reviews in the Life Sciences*. Addison-Wesley, Reading, MA, pp. 15-72.

PLATZMAN, R.L., 1962*a*. Superexcited states of molecules. *Radiat. Res.***17**, 419-425.

PODGORSAK, E.B., 2006. *Radiation Physics for Medical Physicists,* Springer-Verlag Berlin Heidelberg, Germany.

RINARD, P., 1991. *Passive nondestructive assay of nuclear materials*. *Edited by* D. Reilly, N. Ensslin, H. Smith, Jr., and S. Kreiner. NUREG/CR-5550. U.S. Nuclear Regulatory Commission, Washington, D.C.

ROWNTREE, P., PARENTEAU, L., and SANCHE, L., 1991. Electron stimulated desorption via dissociative attachment in amorphous H_2O. *J. Chem. Phys.* **94**, 8570-8576.

RUDD, M.E., KIM, MADISON, D.H. and GAY, T.J., 1992. Electron production in proton collisions with atoms and molecules: energy distributions. *Rev. Mod. Phys.* **64**, 441-490.

SAMUEL, A.H. and MAGEE, J.L., 1953. Theory of radiation chemistry. II. Track effects in radiolysis of water. *J. Chem. Phys.***21**, 1080-1087.

SANCHE, L., 2002. Nanoscopic aspects of radiobiological damage: Fragmentation induced by secondary low-energy electrons. *Mass Spectrom. Rev.* **21**, 349-369.

SANGUANMITH, S., MUROYA, Y., MEESUNGNOEN, J., LIN, M., KATSUMURA, Y., MIRSALEH KOHAN, L., GUZONAS, D.A., STUART, C.R., and JAY-GERIN, J.-P., 2011*a*. Low-linear energy transfer radiolysis of liquid water at elevated temperatures up to 350°C: Monte-Carlo simulations. *Chem. Phys. Lett*. **508**, 224-230.

SAUER, M.C., Jr., SCHMIDT, K.H., HART, E.J., NALEWAY, C.A., and JONAH, C.D., 1977. LET dependence of transient yields in the pulse radiolysis of aqueous systems with deuterons and αparticles. *Radiat. Res.* **70**, 91-106.

SCHRÖDER, W.U., 2009. Personal communication.

SCHULER, R.H. and ALLEN, A.O., 1957. Radiation chemistry studies with cyclotron beams of variable energy: Yields in aerated ferrous sulfate solution. *J. Am. Chem. Soc.* **79**, 1565-1572.

SHULTIS, J.K., and FAW, R.E., 2008. Fundamentals of nuclear science and engineering. 2nd ed. Taylor & Francis Group, Boca Raton, FL.

ŠTEFANIĆ, I. and LAVERNE, J.A., 2002. Temperature dependence of the hydrogen peroxide production in the γ-radiolysis of water. *J. Phys. Chem. A.* **106**, 447-452.

STUART, C.R., OUELLETTE, D.C., and ELLIOT, A.J., 2002. Pulse radiolysis studies of liquid heavy water at temperatures up to 250 ºC. Report AECL-12107. Atomic Energy of Canada Ltd., Chalk River, ON.

SUNARYO, G.R., KATSUMURA, Y., and ISHIGURE, K., 1995*a*. Radiolysis of water at elevated temperatures–III.Simulation of radiolytic products at 25 and 250°C under the irradiation with γ-rays and fast neutrons. Radiat. Phys. Chem. **45**, 703-714.

SUNARYO, G.R., KATSUMURA, Y., HIROISHI, D., and ISHIGURE, K., 1995*b*. Radiolysis of water at elevated temperatures–II.Irradiation with γ-rays and fast neutrons up to 250°C. *Radiat. Phys. Chem*. **45**, 131-139.

SWIATLA-WOJCIK, D. and BUXTON, G.V., 1995. Modeling of radiation spur processes in water at temperatures up to 300 ºC. *J. Phys. Chem.* **99**, 11464-11471.

SWIATLA-WOJCIK, D. and BUXTON, G.V., 1998.Modelling of linear energy transfer effects on track core processes in the radiolysis of water up to 300 ºC. *J. Chem. Soc., Faraday Trans.* **94**, 2135-2141.

SWIATLA-WOJCIK, D. and BUXTON, G.V., 2000. Diffusion-kinetic modelling of the effect of temperature on the radiation chemistry of heavy water. *Phys. Chem. Chem. Phys.* **2**, 5113-5119.

SWIATLA-WOJCIK, D. and BUXTON, G.V., 2001. Isotopic effect in the radiolysis of water. Diffusion-kinetic modelling up to 300°C. Res. Chem. Intermed. **27**, 875-889.

SWIATLA-WOJCIK, D. and BUXTON, G.V., 2005. On the possible role of the reaction $H^{\bullet} + H_2O \rightarrow H_2 + {}^{\bullet}OH$ in the radiolysis of water at high temperatures. *Radiat. Phys. Chem.***74**, 210-219.

SWIATLA-WOJCIK, D. and BUXTON, G.V., 2010. Reply to comment on the possible role of the reaction $H^{\bullet} + H_2O \rightarrow H_2 + {}^{\bullet}OH$ in the radiolysis of water at high temperatures. Radiat. Phys. Chem. **79**, 52-56.

TIPPAYAMONTRI, T., SANGUANMITH, S., MEESUNGNOEN, J., SUNARYO, G.R., and JAY-GERIN, J.-P., 2009. Fast neutron radiolysis of the ferrous sulfate (Fricke) dosimeter: Monte-Carlo simulations. *Recent Res. Devel. Physical Chem.* **10**, 143-211.

TAUBE, H., 1957. Photochemical reactions of ozone in solution. *Trans. Faraday Soc.* **53**, 656-665.

TOBUREN, L.H., 2004. Ionization and secondary electron production by fast charged particles. In: Mozumder, A. and Hatano, Y. (Eds.), *Charged Particle and Photon*

Interactions with Matter: Chemical, Physicochemical, and Biological Consequences with Applications. Marcel Dekker, New York, pp. 31-74.

TURNER, J.E., MAGEE, J.L., HAMM, R.N., CHATTERJEE, A., WRIGHT, H.A., and RITCHIE, R.H., 1981. Early events in irradiated water. In: Booz, J., Ebert, H.G., and Hartfiel, H.D. (Eds.), *Seventh Symposium on Microdosimetry*, Oxford, U.K., Sept. 8-12, 1980. Harwood Academic Publ., London, pp. 507-520.

TURNER, J.E., MAGEE, J.L., WRIGHT, H.A., CHATTERJEE, A., HAMM, R.N., and RITCHIE, 1983. Physical and chemical development of electron tracks in liquid water. *Radiat. Res.* **96**, 437-449.

TURNER, J.E., WRIGHT, H.A., HAMM, R.N., 1985. A Monte Carlo primer for health physicists. *Health Phys.* **48**, 717-733.

TURNER, J.E., HAMM, R.N., SOULEYRETTE, M.L., MARTZ, D.E., RHEA, T.A., and SCHMIDT, D.W., 1988*a*. Calculations for β dosimetry using Monte Carlo code (OREC) for electron transport in water. *Health Phys.* **55**, 741-750.

TURNER, J.E., HAMM, R.N., WRIGHT, H.A., RITCHIE, R.H., MAGEE, J.L., CHATTERJEE, A., and BOLCH, W.E., 1988b. Studies to link the basic radiation physics and chemistry of liquid water. *Radiat. Phys. Chem.* **32**, 503-510.

UEHARA, S. and NIKJOO, H., 2006. Monte Carlo simulation of water radiolysis for low-energy charged particles. *J. Radiat. Res.* **47**, 69-81.

WATT, D.E., 1996. *Quantities for Dosimetry of Ionizing Radiations in Liquid Water*. Taylor and Francis, London, U.K.

ZAIDER, M., and BRENNER, D.J., 1984. The Applications of Track Calculations to Radiobiology I. Monte Carlo Simulation of Proton Tracks. *Radiat. Res*. **100**, 231-247.

9. APPENDIX

LIST OF ABSTRACTS OF COMMUNICATIONS PRESENTED IN INTERNATIONAL/NATIONAL CONFERENCES

1. The 6th International Symposium on Supercritical Water-Cooled Reactors (ISSCWR-6)

March 03-07, 2013, Kingkey Palace Hotel, Shenzhen, Guangdong, China

Calculation of the Yields for the Primary Species Produced in Liquid Water by Fast Neutron Radiolysis at Temperatures between 25 and 350 °C

Sofia Loren Butarbutar, Sunuchakan Sanguanmith, Jintana Meesungnoen, Geni Rina Sunaryo, Jean-Paul Jay-Gerin

Abstract

Controlling the water chemistry in a water-cooled nuclear power reactor requires understanding and mitigating the effects of water radiolysis to limit the corrosion and degradation of materials by oxidizing radiolysis products. However, direct measurement of the chemistry in reactor cores is extremely difficult due to the extreme conditions of high temperature, pressure, and mixed neutron/γ-radiation fields, which are not compatible with normal chemical instrumentation. For these reasons, theoretical models and computer simulations are essential for predicting the detailed radiation chemistry of the cooling water in the core and the impact on materials.

In this work, Monte Carlo simulations were used to calculate the g-values for the primary species (e^-_{aq}, $H^\bullet$, H_2, $^\bullet OH$, and H_2O_2) formed from the radiolysis of neutral liquid water by 2 MeV monoenergetic neutrons at temperatures between 25 and 350 °C. The 2 MeV neutron was considered representative of a fission-neutron flux in a reactor. For light water, the moderation of these neutrons generated elastically scattered recoil protons of 1.264, 0.465, 0.171, and 0.063 MeV, which had, at 25 °C, linear energy transfers (LETs) of 22, 43,

69, and 76 keV/μm, respectively. Neglecting the radiation effects due to oxygen ion recoils and assuming that the most significant contribution to the radiolysis came from these first four recoil protons, the fast neutron yields could be estimated as the sum of the g-values for these protons after allowance was made for the appropriate weightings according to their energy.

The g-values were calculated at 10^{-7} and 10^{-6} s after the ionization event at all temperatures, in accordance with the time range associated with the scavenging capacities generally used for fast neutron radiolysis experiments. The results of the simulations agreed reasonably well with the experimental g-values, taking into account the relatively large uncertainties in the experimental measurements, the relatively small number of reported radiolysis yields, and the simplifications included in the model. Compared with data obtained for low-LET radiation (^{60}Co γ-rays or fast electrons), our computed yields for fast neutron radiation showed essentially similar temperature dependences over the range of temperature studied, but with lower values for yields of free radicals and higher values for molecular yields. This general trend is a reflection of the high-LET character of fast neutrons. Although the results of the simulations were consistent with the experiment, more experimental data are required to better describe the dependence of radiolytic yields on temperature and to test more thoroughly our modeling calculations.

2. 96th Canadian Chemistry Conference and Exhibition, QUÉBEC, QUEBEC

May 26-30, 2013

Fast Neutron Radiolysis of Liquid Water at Temperatures Between 25 and 350 °C: Monte Carlo Simulations

Sofia Loren Butarbutar, Sunuchakan Sanguanmith, Jintana Meesungnoen, Geni Rina Sunaryo, Jean-Paul Jay-Gerin

Abstract

Controlling the water chemistry in a water-cooled nuclear power reactor requires understanding the effects of water radiolysis to limit the degradation of materials. However, direct measurement of the chemistry in the reactor core region is difficult due to the extreme conditions of high temperature, pressure, and mixed neutron/γ-radiation fields. Therefore, theoretical calculations are essential for predicting the detailed radiation chemistry of the cooling water in the reactor core. Rather surprisingly, only limited information exists on the fast neutron radiolysis of water, and fast neutron *g*-values at high temperatures are not well established. In this work, Monte-Carlo simulations are used to calculate the *g*-values for the primary species (e^{-}_{aq}, $H^{\bullet}$, H_2, $^{\bullet}OH$, and H_2O_2) formed from the radiolysis of neutral water by 2 MeV neutrons over the range 25 to 350 °C. The 2 MeV neutrons is considered representative of a fission-neutron flux in a reactor. For light water, the most significant contribution to the radiolysis comes from the first four neutron collisions that generate mostly recoil protons. Neglecting oxygen ion recoils, the fast neutron yields are estimated as the sum of the *g*-values for the four recoil protons after appropriate weightings are applied according to their energy. The simulation results are tested against available experimental *g*-values and compared with data for γ-radiolysis.